Effects of thermal stratification and hydraulic retention on carbon flux in shallow subtropical lakes

林，浩之

(Degree)
博士（学術）

(Date of Degree)
2022-03-25

(Date of Publication)
2023-03-01

(Resource Type)
doctoral thesis

(Report Number)
甲第8350号

(URL)
https://hdl.handle.net/20.500.14094/D1008350

Doctoral Dissertation

Effects of thermal stratification and hydraulic retention on carbon flux in shallow subtropical lakes

亜熱帯地域の小面積湖沼における水温成層と滞留時間が炭素フラックスに与える影響評価

February 1, 2022

Department of Civil Engineering

Graduate School of Engineering

Kobe University

林浩之

LIN, HAO-CHIH

177T752T

Abstract

Thermal stratification and typhoon-induced mixing are critical processes impacting vertical distributions of carbon (C) in subtropical lakes. Notably, the shallow lakes are well-mixing easily during extreme weather events than deep lakes. However, the influences of these physical processes on C fluxes in shallow subtropical lakes during the typhoon period remained uncertain, contributing to understanding the fates of C fluxes in lake ecosystems under climate change. This study was conducted in two shallow subtropical mountain lakes with different nutrient levels. To know the relationship between seasonal thermal stratification and inorganic C fluxes, the vertical profiles of water temperature and dissolved inorganic carbon (DIC) were investigated in Yuan-Yang Lake (YYL) from 2004 to 2017 for each month. Additionally, to compare the C fluxes with different nutrient levels under the typhoon periods, the water quality variables such as DIC, dissolved organic carbon (DOC), and Chlorophyll *a* (Chl. *a*) were measured in YYL (oligotrophic lake) and Tsui-Fong Lake (TFL, mesotrophic lake) from 2007 to 2017 for each month. A three-dimensional hydraulic model was employed to accurately simulate the hydraulic retention time (t_r) and obtain the net ecosystem production (NEP). Our results showed that the DIC inhibited the vertical mixing of bottom DIC into the water surface due to stratification from spring to summer (March to August) in YYL. A substantial amount of sediment DIC was released from September to November under the typhoon-induced mixing and fall overturn. Significantly, the river flows rapidly flushed to the outflow during typhoons, resulting in that t_r was 4.4 days during the typhoon in YYL. The NEP in YYL was decreased 107% from the post-typhoon to typhoon period. In contrast, the relatively long t_r of 39 days induced that the NEP decreased 87% during the typhoon period in TFL. These results demonstrated that the thermal stratification and hydraulic retention time during typhoons control the seasonal patterns of C fluxes in subtropical shallow lakes.

Contents

1. Introduction

The marine and freshwater ecosystems sequestrated approximately 30-50 % of carbon (C) from the atmosphere into the earth's surface (Intergovernmental Panel on Climate Change (IPCC), 2013). The air-sea C exchange captured around 50-60 % (2.3 ± 0.7 Pg C yr^{-1}) of total C on the earth (IPCC, 2013) by photosynthesis such as macroalgae and seagrass meadows (Duarte and Cebrián, 1996; Duarte and Krause-Jensen, 2017; Ortega et al., 2019), known as "blue carbon" (Nellemann, 2009). On the other hand, the freshwater ecosystems not only release around 0.3-1.9 Pg C yr^{-1} into the atmosphere (Aufdenkampe et al., 2011; Lauerwald et al., 2015; Raymond et al., 2013) but also deliver 0.9 Pg C yr^{-1} into the ocean (Cole et al., 2007). As a fraction of the land to the marine ecosystems, freshwater ecosystems regulate the C fluxes into the ocean due to climate change (Tranvik et al., 2009). Thus, freshwater ecosystems, particularly lake ecosystems, are essential to understanding the influences of hydrological mechanisms and processes on C fluxes (Macreadie et al., 2019).

Practical pressure of CO_2 (pCO_2) is vital to estimate the CO_2 emission across the air-water interface (Cole et al., 1994). pCO_2 can be directly measured on the water surface by using a floating chamber (Belanger and Korzun, 1991; Raymond et al., 1997), or if we ignore the calcification, the pCO_2 be estimated from dissolved inorganic C (DIC) and pH based on assumed the conditions rely on the carbonate (CO_3^{2-}), and hydrogen carbonates (HCO_3^-) concentration (Smith, 1985). Additionally, water temperature, wind speed, salinity, and total alkalinity (TA) are essential parameters to calculate the CO_2 flux (Smith, 1985; Cole and Caraco, 1998; MacIntyre et al., 2002). On the other hand, dissolved organic carbon (DOC) was a critical modifier to facilitate the CO_2 emission from water to the atmosphere (Tranvik, 1988; del Giorgio et al., 1999). Some studies revealed that the air temperature controls the pCO_2 due to the thermal stratification and biological activity in lakes (Sobek et al., 2005; Gudasz et al., 2010). The bio-photochemical degradation and mineralization play vital roles in shaping the CO_2 flux in lakes because colored DOC reduced the ultraviolet radiation (UVR) and active photosynthetic radiation (400–700 nm, PAR) (Scully et al., 1996; Williamson et al., 1999; Lapierre et al., 2013). Therefore, DOC and DIC are principally associated with the pCO_2 in lakes (Smith, 1985; Hope et al., 1996; Bade et al., 2004).

Physical and hydrological processes are vital to know the responses of C fluxes in lake ecosystems under climate change-induced extreme weather events (Woolway et al., 2018; Doubek et al., 2021). Climate change affects the strength of thermal stratification within not only stratified lakes (Kraemer et al., 2015) but also the intensity and frequency of extreme storm events, inducing the frequency of vertical

mixing in different climate zones (Woolway et al., 2020). Storm-induced mixing is a critical way to upwell the C from sediment into the water surface (Jennings et al., 2012; Hanson et al., 2015). Notably, the responses of C fluxes in small-size lakes (lake area < 1 km^2) are sensitive under climate change due to physical processes such as mixing, turbulences, and water temperatures (Winslow et al., 2015; Doubek et al., 2021; MacIntyre et al., 2021). Some studies revealed that the river inflows and wind turbulences mix the allochthonous C from sediments into the water column after storm events in small stratified lakes (Vachon and del Giorgio, 2014; Bartosiewicz et al., 2015; Czikowsky et al., 2018). Hence, vertical mixing is an essential physical process in small stratified lakes because it controls C fluxes (Imberger, 1985; MacIntyre, 1993; Boehrer and Schultze, 2008; Gudasz et al., 2010). However, despite the small lakes and ponds were occupied 25-35 % of the total lakes area on earth (Downing et al., 2006; Verpoorter et al., 2014), the small lakes were ignored for estimating the global C emission (Cole et al., 2007; Raymond et al., 2013). Hence, the C flux in previous studies might be underestimated on the earth scale if these did not concern the C flux in small (shallow) lakes. Holgerson and Raymond (2016) also demonstrated that a substantial amount of carbon dioxide (CO_2) and methane (CH_4) (0.58 Pg C yr^{-1}) were released in small lakes and ponds from water to the atmosphere. Therefore, the C fluxes' responses in lake ecosystems based on physical and hydrological processes under climate change are uncertain and not clarified in small (shallow) lakes.

Some studies suggested that the precipitation and hydraulic retention regimes may be significant for structuring lake ecosystem function, especially C fluxes (Ojala et al., 2011; Vachon and del Giorgio, 2014; Bartosiewicz et al., 2015; Zwart et al., 2017). The strong storm events (> 40 mm d^{-1}) induced the lake trophic state from autotrophic to heterotrophic and released large amounts (around 150 to 300 mg C m^2 d^{-1}) of CO_2 and CH_4 from lakes to the atmosphere (Ojala et al., 2011; Vachon and del Giorgio, 2014; Bartosiewicz et al., 2015). Zwart et al. (2017) showed that increased annual precipitation would alter water level, organic C flux and reduce hydrologic residence time (or hydraulic retention time) from watersheds to lakes. In addition, the residence time is an essential parameter for calculating the seasonal net ecosystem production (NEP) (Nakayama et al., 2020a). However, lake sizes (Read et al., 2012), thermal stratification (Åberg et al., 2010; Bartosiewicz et al., 2015), internal seiche dynamic (Woolway et al., 2018; MacIntyre et al., 2021), and the ratio of the watershed area to lake surface area (WA:LA) (den Heyer and Kalff, 1998; Vachon and del Giorgio, 2014) impact on the C fluxes and residence time. In addition, the allochthonous inflow or groundwater and autochthonous (sediment) C determine the C fluxes in lakes due to the remineralization, sedimentation, and C burial within lakes

(den Heyer and Kalff, 1998; Striegl and Michmerhuizen, 1998; Einsele, 2001; Hope et al., 2004). Thus, thermal stratification and hydraulic retention are also critical factors controlling the fate of C fluxes. To clarify how lake mixing regimes and hydraulic retention affect NEP in a small lake, the three-dimensional numerical model is one of the robust tools to accurately calculate the residence time and seasonal NEP (Nakayama et al., 2020a).

Extreme storm events, such as typhoons and cyclones, almost pass in the tropical and subtropical regions (Kossin et al., 2013). Some shallow lakes (water depth < 5 m) have been found that water surface temperatures decrease by 3 to 6 °C and well-mixing in water columns after tropical cyclones (Klug et al., 2012). On the other hand, the typhoon events can contribute 200-1,000 mm d^{-1} into a shallow subtropical lake and contribute 10-35 % of annual precipitation, resulting in the seasonal patterns of metabolism and CO_2 flux were dramatically changed (Jones et al., 2009; Tsai et al., 2011). Chiu et al. (2020) revealed that typhoon precipitation brings a large amount of terrestrial organic C into the shallow subtropical lakes. Typhoon events and thermal stratification may control C distribution's temporal and spatial variability (Jones et al., 2009; Chiu et al., 2020). Therefore, shallow subtropical lakes are the ideal sites to monitor storm-induced mixing and represent climate change impacts on the C fluxes in lake ecosystems. However, long-term investigations of shallow subtropical lakes, such as those at seasonal and annual scales, are rare but valuable. Yuang-Yang Lake (YYL) and Tsui-Fong lake (TFL) are small, shallow lakes in Taiwan and experience multiple typhoon events each year (Tsai et al., 2011; Chiu et al., 2020). Some studies investigated the water columns in YYL and TFL; the lakes are stratified from early April to October and are usually mixed in winter from December to February (Kimura et al., 2012; Tsai et al., 2016; Chiu et al., 2020). Additionally, typhoon-induced mixing can contribute 2,200 kg C yr^{-1} in YYL (Jones et al., 2009) because typhoon disturbances alter water level and rapidly dilute the water quality (Tsai et al., 2011; Chiu et al., 2020). Thus, further research on small shallow subtropical lakes is essential to clarify the physical structures and estimate NEP accurately.

Here, we hypothesize that temporal and spatial variations in DOC and DIC are affected by physical factors such as thermal stratification, water flushing, and residence time, resulting in seasonal NEP changes in shallow subtropical lakes. These factors might influence lakes' primary production and nutrient levels under changing precipitation patterns (Kortelainen et al., 2006; Woolway et al., 2018; Chiu et al., 2020; Nakayama et al., 2020a). Therefore, this study aimed to (i) clarify how the effect of thermal stratification on the seasonal DIC in a subtropical shallow lake (ii) estimate the seasonal NEP using a three-dimensional numerical model to simulate hydraulic retention effects. Furthermore, (iii) investigate the vertical profiles of water

temperature, DIC, DOC, and Chlorophyll a (Chl. *a*) in shallow subtropical lakes with different trophic levels, and (iv) clarify how typhoon disturbance impacts C flux, focusing on the effects of inflow and thermal stratification on DIC, DOC, and CO_2 fluxes. This study provides a physical environment on C flux interacting with biological processes in shallow subtropical lakes.

2. Material and methods

First, to quantify the seasonal mixing regime in a subtropical shallow lake (Yuang-Yang Lake), we investigated water temperature and DIC vertical profile from July 2004 to December 2017 (not including 2012 and 2013, ten years total). Next, to clarify how typhoon disturbances impact C flux in two lakes with different trophic levels, Yuan-Yang Lake (oligotrophic lake) and Tsui-Fong Lake (mesotrophic lake), the vertical profiles of water temperature and water quality variables (DIC, DOC, Chl. *a*) were investigated five typical years from 2009 to 2010 and 2015 to 2017. Furthermore, we calculated the NEP and simulated the hydraulic retention effect using Fantom during a strong typhoon event and different seasonal periods. Additionally, we utilized structural equation modeling (SEM) to analyze how water quality changes with CO_2 flux between different seasonal periods.

2.1. Study sites

This study was conducted in two subtropical mountain lakes of northeastern Taiwan (**Figure 1**). Yuang-Yang Lake (YYL) is located in the Chilan mountain region with an altitude of 1650 m, a cloud forest in Yilan county (24.58° N, 121.40° E). YYL is a polymictic lake and ice-free year-round due to typhoon disturbance and fall overturn (Tsai et al., 2008; Kimura et al., 2012), which has six inflows and one outflow (**Figure 1**), the surface area was 3.5 ha, and average water depth was around 4.3 to 4.5 m (Tsai et al., 2008; Chiu et al., 2020). The daily average water temperature was around 5-25 °C on the water surface (Chiu et al., 2020). The annual precipitation approximately ranged from 3300 to 4500 mm that induced the abundance of water resources to play an essential role in soil C fluxes and water retention in YYL, such as fog and typhoon events (Lai et al., 2006; Chang et al., 2007). The watercolor of YYL is brown and humic, with a pH of approximately 5.4 (Wu et al., 2001; Tsai et al., 2008). The total nitrogen (TN) was ranged from 20 to 50 μg-N L^{-1}, total phosphate (TP) was ranged from 10 to 20 μg-P L^{-1}, and seasonal variation of lake metabolism ranges from -11.4 to -74.9 μmol of O_2 m^{-3} d^{-1}, indicating YYL is considered to be an oligotrophic lake (Tsai et al., 2008; Chiu et al., 2020).

On the other hand, Tsui-Fong Lake (TFL) is located around 21 km from the YYL in the Taiping mountain region, surrounded by cypress forest (*Chamaecyparis formosensis*) with an altitude of 1850 m (24.52° N, 121.60° E). TFL has 11 inflows (one primary and ten minor flows) and one outflow (**Figure 1**). The lake surface area varies from 8.0 to 25 ha, and the total water depth ranges from 3.0 m during the dry period to 12 m during typhoon season (Tsai et al., 2016; Chiu et al., 2020). The

watercolor is green during the dry period due to algal blooms during March and June, with the high Chl. *a* around 30 to 100 μg L^{-1} (Tsai et al., 2016; Chiu et al., 2020). TN, TP, and seasonal variation of lake metabolism are ranged from 20 to 70 μg-N L^{-1}, 30 to 60 μg-N L^{-1}, and -25.4 to 57.4 μmol of O_2 m^{-3} d^{-1}, respectively, indicating that TFL is considered to be a mesotrophic lake (Tsai et al., 2016; Chiu et al., 2020).

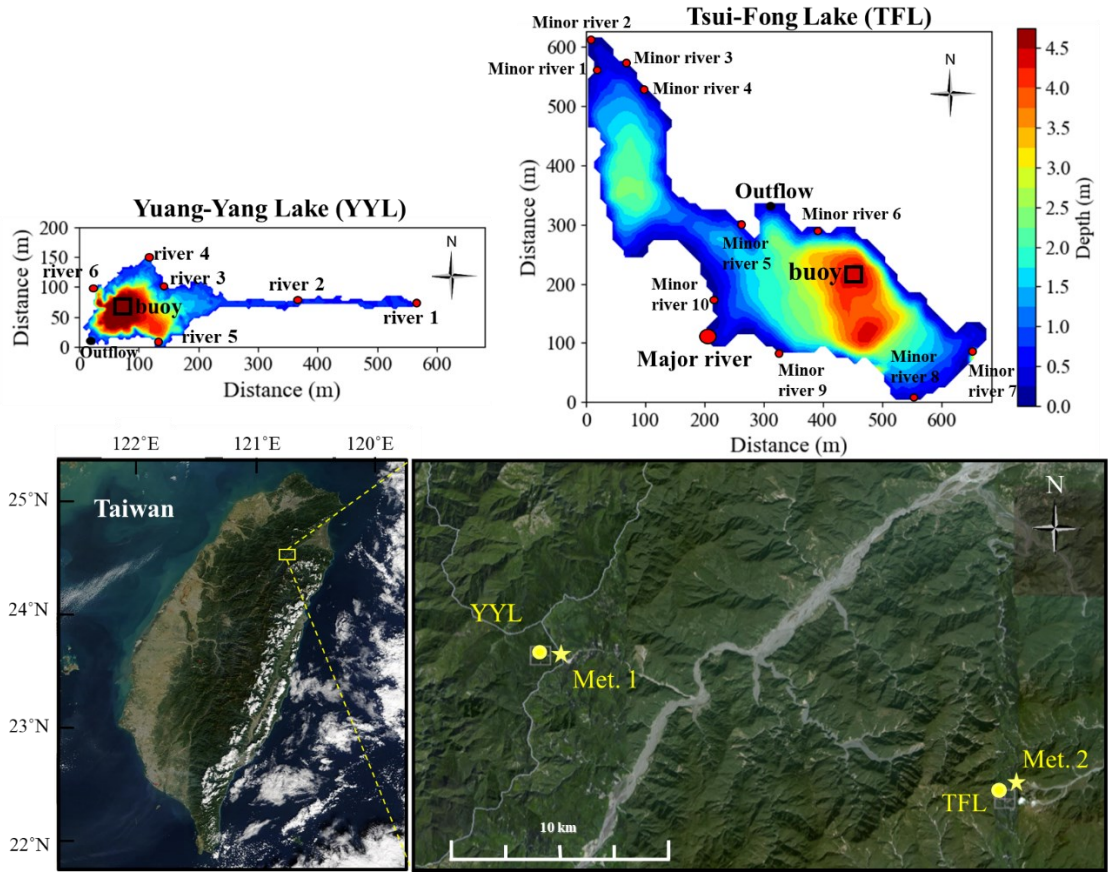

Figure 1. Location of sites with an enlarged bathymetric map of Yuan-Yang Lake (YYL) and Tsui Fong Lake (TFL) with water depths contour. Buoy (Black rectangles), weather station (Stars, Met. 1 and Met. 2), river inflow (Red circles), and outflow (Black dots) deployment sites. The satellite images from MODIS Rapid Response Team, NASA (Left), and Google Earth (Right).

2.2 Data collection and measurements

We investigated the vertical profile of water temperature and DIC once or twice a month in YYL, categorizing spring (March to May), summer (June to August), autumn (September to November), and winter (December to February) in four seasons for ten years. Furthermore, since the mean duration of typhoon events was less than five days, we added summer typhoons (June to August) and autumn typhoons (September to November) periods to know how the water columns of water temperature and DIC differ between four seasons and typhoons.

Next, to determine how water quality factors (DOC, DIC, Chl. *a*) differ between before and after typhoons in two lakes, we categorized seasonal pattern into three periods for five years: "pre-typhoon" (April to July), "during-typhoon" (August to November), and "post-typhoon" (December to March).

2.2.1 Meteorological and limnological data

The water temperature was measured at water depths of 0.04, 0.25, 0.5, 0.75, 1.0, 1.5, 2, 2.5, 3.0, 3.5, and 4.0 m using thermistor chains (Templine, Apprise Technologies, Inc., Duluth, Minnesota, USA) at the buoys of both lakes (Figure 1), and the wind monitors (model 03001, R.M. Young, Traverse, MI, USA) measured the wind speed and wind direction at 2.0 m above the water surface. The water depths were measured at the deepest spots (buoy) through the water column using a water depth meter (model HOBO U20; Onset computer company, MA, USA). Additionally, we measured air pressure (model 090D; Met One Ins., NW, USA), active photosynthetic radiation (PAR, model LI-190; LI-COR, Lincoln, NE, USA), and precipitation (model N-68; Nippon Electric Instrument, Japan) at weather stations located around 1.0 km from the buoys (Figure 1). The recorded data were automatically saved every 10 min in a data logger (model CR1000, Campbell Sci. Inc., USA) at each buoy and weather station. In addition, to know how the water quality changed during typhoons, we used a Submersible Fluorometer (model C3, Turner designs, CA, USA) to measure Chl. *a* and colored dissolved organic matter (CDOM) at 0.25 m deep and recorded automatically every 10 min.

2.2.2 Water chemical samples (DIC, DOC, pH, and Chl. *a*)

The water samples were collected at water depths of 0.04, 0.50, 1.00, 2.00, and 3.50 m at the buoy sites, and surface water (0.04 m) from river inflows and outflows, using a horizontal Van Dorn bottle (2.20 L, acrylic) (Figure 1). The pH was measured using a water quality probe (model Hydrolab 4α; Hach, CO, USA) at the water surface (0.04 m). We used a portable hand pump (Hand Vacuum pump, One Lincoln

Way, MO, USA) filtered (47 mm GF／F, nominal pore size 0.70 μm, Whatman, Maidstone, Kent, UK) the water samples. The filter paper opaque bottles and filtrate samples were kept in airtight vials (Vial glass 40 ml, K60958A-912) at around four °C until the sample was measured. These samples were analyzed less than 72 hours after sampling. The Chl. *a* was extracted from the filter papers with methanol and measured using a portable fluorometer (model 10-AU-005-CE; Turner Designs, CA, USA). On the other hand, DIC and DOC concentrations were measured using an infrared gas detector that detected DOC and DIC with persulfate digestion (model 1030W/1088, Xylem, TX, USA).

2.3 Data analysis

We used the Brunt–Väisälä frequency, mixing depth, and intrusion depth to quantify the strength of stratification, estimated where the river intruded and defined the water layers in YYL (section 2.3.1). Next, the epilimnion DIC (water depth of 0.04 to 0.25 m), meteorological (wind speed, air pressure), and limnological data (water temperature, pH) were used to calculate CO_2 flux (section 2.3.2) and NEP using a residence time and DIC data sets (section 2.3.3) in YYL and TFL. Finally, we performed hydrological model simulations to evaluate the effect of typhoon disturbance on DIC residence time within lakes (section 2.3.4). Additionally, we applied the SEM analysis to know the effects of meteorological and water quality data on DIC flux (section 2.3.5).

2.3.1. Brunt–Väisälä frequency, mixing depth, and intrusion depth

The stratification induces water particle oscillations due to density perturbation. The oscillation frequency is denoted as “Brunt-Väisälä Frequency” or “buoyancy frequency” (Imboden and Wüest, 1995). Brunt–Väisälä frequency (N, s^{-1}) is often used to quantify the strength of stratification in the previous studies because of that associated with the vertical mixing in lakes (Imboden and Wüest, 1995; von Rohden and Ilmberger, 2001). The equation was followed as:

$$N = \sqrt{-\frac{g}{\rho}\frac{d\rho}{dz}} \quad (1)$$

where g is the gravity acceleration, ρ is the density of water, and z is the vertical coordinate of water depth (m). We calculated the vertical average of N^2-for the water column from 0.04 to 4.0 m deep, and most of the cases were $N^2 > 0$.

As **Figure 2**, we referred from Staehr and Sand-Jensen (2007) to define the depth of vertical mixing depth (Z_m, m) and Epilimnion

$$Z_m = Z|_{T = T_s - 1} \quad (2)$$

where Z_m is the mixing water depth, and T_s is the water surface temperature at 0.04 m deep. We defined an intrusion depth to know where the river flow intrudes (Z_i, m) and defined the Hypolimnion

$$Z_i = Z|_{T = T_R} \quad (3)$$

where T_R is the water surface temperature of a river (Figure 2).

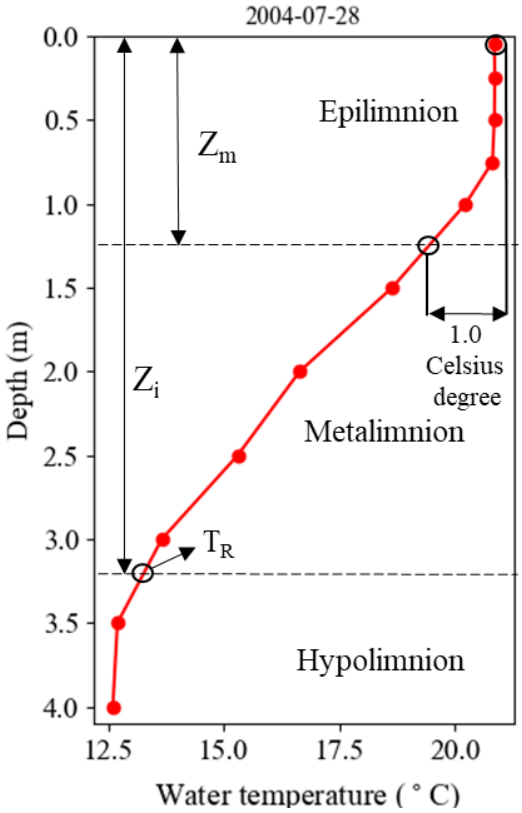

Figure 2. Definition of the layers (Epilimnion, Metalimnion, and Hypolimnion), mixing depth (Z_m), and intrusion depth (Z_i). Vertical profile of water temperature on July 28, 2004.

2.3.2. CO_2 flux across the air-water interface (F_{CO2})

To quantify how much C was exchanged between lake and atmosphere, we not only calculated the partial pressure of the air-water CO_2 ($pCO2$) by applying Fick's law (Table 1) but also considered the CO_2 transfer velocity due to the wind speed (Wanninkhof, 1992; MacIntyre et al., 2002) and dissociation rate in lakes by using empirical equations (Plummer and Busenberg, 1982). When CO_2 is absorbed from the atmosphere into the lakes, F_{CO2} is a negative value.

Table 1. Equations and references for CO_2 flux (F_{CO2}) across the air-water interface.

Variables	Equation	References & equipment
F_{CO2} (mg C m^{-2} d^{-1})	$k_{CO2} \cdot K_H(pCO2_{water} - pCO2_{air})$	Fick's law diffusion
$pCO2_{air}$ (CO_2 partial pressure in the atmosphere, µatm)	Measured data · 390 (ppm)	Air pressure sensor (section 2.2.1)
$pCO2_{water}$ (µatm)	$\frac{DIC(10^{-pH})^2}{[(10^{-pH})^2 + (10^{-pH})K_1 + K_1K_2]K_H}$	Cai and Wang, 1998
pH	Measured data	Water quality probe (section 2.2.2)
DIC (µmol C kg^{-1})	Measured data (DIC concentration, 0.04 m)	
k_{CO2} (Gas transfer velocity, cm h^{-1})	$k_{600}\left(\frac{Sc_{CO_2}}{600}\right)^{-0.5}$	Jähne et al., 1987
k_{600} (Gas exchange coefficient)	$2.07 + 0.215\ U_{10}^{1.7}$	Cole and Caraco, 1998
Sc_{CO_2} (Schmidt number)	$1911.1 - 118.11\ T + 3.4527\ T^2 - 0.04132\ T^3$	Wanninkhof, 1992
U_{10} (Wind speed above 10 m water surface)	$U_2 \cdot (\frac{10_{(m)}}{2_{(m)}})^{0.15}$	Smith, 1985
U_2 (Wind speed above 2.0 m water surface)	Measured data	Wind monitor (section 2.2.1)
K_H (Henry's coefficient)	$\exp(108.39 + 0.0199\mathrm{T} - \frac{6920}{\mathrm{T}} - 40.452\log \mathrm{T} + \frac{669365}{T^2})$	Plummer and Busenberg, 1982
K_1 (1st dissociation constant)	$\exp(-356.31 - 0.0609\mathrm{T} + \frac{21834}{\mathrm{T}} + 126.83\log \mathrm{T} - \frac{1684915}{\mathrm{T}^2})$	Plummer and Busenberg, 1982
K_2 (2nd dissociation constant)	$\exp(-107.8 - 0.0325\mathrm{T} + \frac{5152}{\mathrm{T}} + 38.926\log \mathrm{T} - \frac{56371}{T^2})$	Plummer and Busenberg, 1982
T (K degree)	Measured data	Water temperature at 0.04 m deep

2.3.3. Net Primary Production (NEP) estimated using a conceptual model

The change in DIC (mg C m^{-3}) was modeled by applying a conceptual model to obtain NEP (mg C m^{-3} d^{-1}) (Nakayama et al., 2020a) as follows:

$$\mathrm{V_{total}} C_U \frac{\partial \mathrm{DIC}}{\partial \mathrm{t}} = -\mathrm{V_{total}} \mathrm{NEP} + Q_{Re} C_U (\mathrm{DIC}_R - \mathrm{DIC}_L) - A_L F_{CO2} \quad (4)$$

where $\mathrm{V_{total}}$ is the total volume of the lake (m^3), C_U is the coefficient that converts the unit from mg C L^{-1} to mg C m^{-3}, Q_{Re} is the effective exchange flux (m^3 d^{-1}) by using a three-dimensional hydrological model, DIC_R is the mean DIC of rivers, DIC_L is the mean DIC of lakes (mg C L^{-1}), and A_L is the lake surface area (m^2). F_{CO2} is the DIC flux across the air-water interface (mg C m^{-2} d^{-1}) (section 2.3.2). Because the phytoplankton and planktonic bacteria are the dominant DIC sink in two lakes (Tsai et al., 2008; Shade et al., 2010), the F_{CO2} cannot be negligible in equation (5).

To know the seasonal change in NEP, we assumed the DIC_R was under the steady-state condition for DIC. Despite the DIC_R may dramatically change during the typhoon period, some previous studies demonstrated the vertical profile of water temperature and metabolism turned back to original level just a few days after a flood (Tsai et al., 2011; Kimura et al., 2012) in YYL. Thus, the fluctuation in DIC_R due to flooding is negligible when analyzing the seasonal change in NEP. Therefore, under the steady-state condition for DIC, NEP was obtained as:

$$\mathrm{NEP} = \frac{Q_{Re}}{\mathrm{V_{total}}} C_U (\mathrm{DIC}_R - \mathrm{DIC}_L) - \frac{A_L}{\mathrm{V_{total}}} F_{CO2} \quad (5)$$

When DIC_L is smaller than DIC_R and the CO_2 is absorbed in water, resulting in that C is accumulated within the lake, which leads to a positive NEP. Conversely, when DIC_L is larger than DIC_R and CO_2 released into the air, resulting inorganic C being produced within the lake, which leads to a negative NEP.

Because the stratification affects a three-dimensional flow and mass transport, the residence time is not equal to $\mathrm{V_{total}} / Q_{Re}$ (Nakayama et al., 2020a). Hence, we attempted to estimate residence time using a three-dimensional numerical simulation (section 2.3.4). Finally, when $\Delta\mathrm{DIC} = \mathrm{DIC}_R - \mathrm{DIC}_L$, we obtain the conceptual model of NEP was followed as:

$$\mathrm{NEP} = -C_U \frac{\Delta \mathrm{DIC}}{t_r} - \frac{A_L}{\mathrm{V_{total}}} F_{CO2} = -C_U \frac{\Delta \mathrm{DIC}}{t_r} - F_C \quad (6)$$

where t_r is the residence time (d^{-1}) (section 2.3.4). We obtained ΔDIC using DIC at water depths as followed

$$\Delta\mathrm{DIC} = (\Delta\mathrm{DIC}_{0.04\mathrm{m}}\mathrm{V}_{0.04\mathrm{m}} + \Delta\mathrm{DIC}_{0.5\,\mathrm{m}}\mathrm{V}_{0.5\mathrm{m}} + \Delta\mathrm{DIC}_{1\,\mathrm{m}}\mathrm{V}_{1\mathrm{m}} + \Delta\mathrm{DIC}_{2\,\mathrm{m}}\mathrm{V}_{2\mathrm{m}} + \Delta\mathrm{DIC}_{3.5\mathrm{m}}\mathrm{V}_{3.5\mathrm{m}})/\mathrm{V_{total}} \quad (7)$$

where $\Delta\mathrm{DIC_{dep}}$ is the value of DIC at a depth of dep, and $\mathrm{V_{dep}}$ is the volume (m^3) at a

depth of dep.

However, since equation (6) uses the upper layer variables only but not in the lower layer, we needed to confirm the validity of equation (6) to estimate NEP in an entire stratified lake. Thus, to know how stratification inhibits the vertical C flux between the upper and lower layers, we attempted to clarify whether applying equation (6) to a stratified lake is possible. Therefore, DIC in the upper and lower layers is modeled (Nakayama and Imberger, 2010; Nakayama et al., 2012) and considered phytoplankton's effect on DIC flux from the lake bottom the model as follows (**Figure 3**).

The upper layer:

$$V_U \frac{d\mathrm{DIC}_U}{dt} = C_U Q_U \mathrm{DIC}_R - C_U Q_{out} \mathrm{DIC}_U - V_U \alpha_{PU} Chl_U + A_I w_I (\mathrm{DIC}_L - \mathrm{DIC}_U) - A_L F_{CO2} \quad (8)$$

The lower layer:

$$V_L \frac{d\mathrm{DIC}_L}{dt} = C_U Q_L \mathrm{DIC}_R - V_L \alpha_{PL} Chl_L + A_I w_I (\mathrm{DIC}_U - \mathrm{DIC}_L) + A_B D_B \quad (9)$$

$$V_{total} = V_U + V_L \quad (10)$$

$$Q_{in} = Q_U + Q_L \quad (11)$$

where DIC_U is DIC in the upper layer, and DIC_L is the DIC in the lower layers (mg C L^{-1}), total volume area (V_{total}) was the sum of upper (V_U) and lower (V_L) layers volumes (m^3) of a lake; Q_{in} and Q_{out} are the river inflow and outflow (m^3 s^{-1}), respectively ; Q_{in} is the river inflow into the upper (Q_U) and lower layers (Q_L) (m^3 s^{-1}); α_{PU} and α_{PL} are the absorption rate of DIC by phytoplankton (mg C mg^{-1} s^{-1}); Chl_U and Chl_L are the Chl. a in the upper and lower layers (mg L^{-1}), respectively; A_I is the density interface area between the upper and lower layers (m^2); A_B is the bottom area; w_I is the entrainment velocity between the upper and lower layers (m s^{-1}); and D_B is the DIC flux from the lake bottom.

Since we assumed the rive inflow and outflow were a steady-state ($Q_{in} = Q_{out}$), equations (8) to (11) yield the equation as follows:

$$0 = C_U Q_U \mathrm{DIC}_R - C_U Q_{out} \mathrm{DIC}_U - V_U \alpha_{PU} Chl_U + C_U Q_L \mathrm{DIC}_R - V_L \alpha_{PL} Chl_L + A_B D_B - A_L F_{CO2} \quad (12)$$

Finally, we obtained equation (13) as below, similar to equation (6).

$$NEP = \frac{V_U \alpha_{PU} Chl_U + V_L \alpha_{PL} Chl_L - A_B D_B}{V_{total}} \tag{13}$$

$$= \frac{C_U(\mathrm{DIC}_R - \mathrm{DIC}_U)}{t_r{}'} - \frac{A_L}{V_{total}} F_{CO2}$$

where $t_r{}'$ is the theoretical residence time by Equation (14) as follows:

$$t_r{}' = \frac{V_{total}}{Q_{in}} \tag{14}$$

Equation (13) considers the effect of photosynthesis on DIC in the whole lake, comparing equation (6). When the DIC flux should be suppressed between the upper and lower layers due to the stratification effect (Imboden and Wüest, 1995), the Q_{in} may be underestimated when the $t_r{}'$ assumes that inflow is mixed quickly (equation (14)). Thus, the t_r of equation (11) is applied by using a three-dimensional model that should be considered the stratification effect to estimate NEP in the entire lake rather than the theoretical residence time ($t_r{}'$).

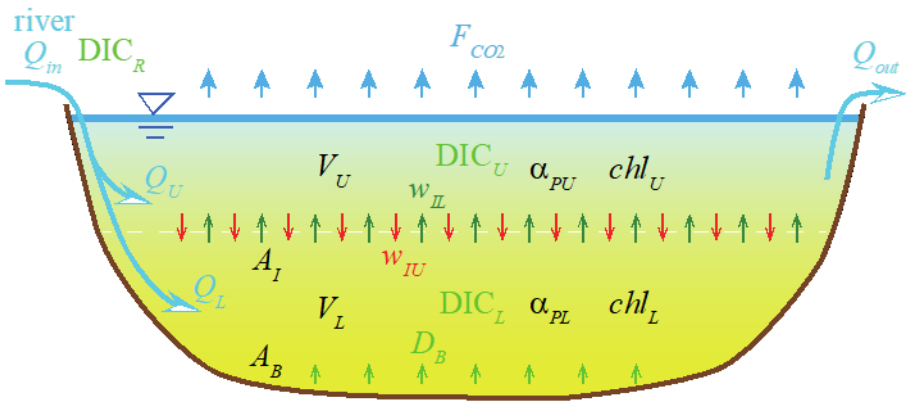

Figure 3. The schematic diagram for the NEP model. A two-layer fluid is assumed to exist.

2.3.4. Simulating the hydraulic retention and residence time

To estimate the residence time (t_r), we performed a three-dimensional environmental model, Fantom (Nakayama et al., 2020a). Fantom is performed the water mass and energy by using the generic length-scale equation model to transport calculations (Jones and Launder, 1972; Umlauf and Burchard, 2003), which based on the object-oriented programming methods (Laniak et al., 2013; Nakamoto et al., 2013; Nakayama et al., 2014). In addition, Fantom is considered bathymetry data to simulate the bottom slopes from a z-coordinate system with partial cells (Adcroft et al., 1997). We used sonar to measure the bathymetry data of lakes (model LMS-332c GPS Receiver and Sonar, Lowrance, USA) in August 2007 every 1.00 m in depth. For numerical simulations, the vertical grid size was 0.20 m, and the time step was 0.50 s in both lakes. The horizontal grid sizes were 4.0, 10.0 m in YYL and TFL, respectively. We computed the time series of the mean tracer concentration in the entire available computational domain, which was used to estimate residual time using:

$$T_r = (Tr_0 - Tr_L) \exp\left(-\frac{t}{t_r}\right) + Tr_L \tag{15}$$

where T_r is the mean tracer concentration, and t is the time (d^{-1}). We used a uniform tracer concentration of 1.0 in the initial condition (Tr_0) for the entire domain of lakes. Tr_L is the quasi-steady-state tracer concentration, which indicates the effect of stratification on hydraulic retention time. Since Tr_L tends to be zero, the water column is no stratification in a stratified lake.

To know the residence time for each season in YYL, we applied vertical profiles of mean water temperature and DIC as the initial stratified conditions (**Table 2**). The initial river discharges (Q_{in}) were 0.072, 0.009, 0.027, 0.018, 0.036, and 0.018 $m^3\ s^{-1}$ from river 1 to river 6 in YYL, respectively (**Figure 1**). Thus, the initial water depths were 4.35 for each season.

Next, to estimate the t_r during typhoon periods, we used the base flow to be the initial discharge, which was 0.048 (pre-typhoon), 0.107 (during-typhoon), 0.028 (post-typhoon) $m^3\ s^{-1}$, and initial water depths were 4.38, 4.46, 4.35 m in YYL, respectively. On the other hand, the base inflows were 0.185 (pre-typhoon), 0.411 (during-typhoon), 0.067 $m^3\ s^{-1}$ (post-typhoon), and initial water depths were 3.27, 7.01, 4.08 m in TFL, respectively.

Table 2. Variables of simulation scenario for estimate simulated residence time for each season. WT is water temperature.

Variables	Spring	Summer	Autumn	Winter	Unit
Sampling date	2008/05/17	2004/07/28	2009/11/11	2007/10/20	yyyy/mm/dd
Water depth	4.10	4.15	4.30	4.31	m
Vertical profiles					
DIC (0.04 m)	3.76	3.38	3.27	2.75	mg L^{-1}
DIC (0.50 m)	3.96	3.52	3.25	2.83	mg L^{-1}
DIC (1.00 m)	4.08	4.16	3.60	2.82	mg L^{-1}
DIC (2.00 m)	4.39	4.89	3.02	2.51	mg L^{-1}
DIC (3.5 m)	6.03	14.72	3.60	2.99	mg L^{-1}
WT (0.04 m)	18.62	20.85	14.34	12.17	°C
WT (0.25 m)	18.21	20.86	14.34	12.05	°C
WT (0.50 m)	18.09	20.85	14.34	12.08	°C
WT (0.75 m)	17.82	20.81	14.28	12.01	°C
WT (1.00 m)	16.89	20.23	14.23	11.94	°C
WT (1.50 m)	15.62	18.64	13.12	11.87	°C
WT (2.00 m)	14.86	16.64	12.12	11.87	°C
WT (2.50 m)	13.86	15.30	11.83	11.80	°C
WT (3.00 m)	12.37	13.66	11.67	11.78	°C
WT (3.50 m)	11.14	12.70	11.49	11.67	°C
WT (4.00 m)	11.08	12.60	11.52	11.65	°C
Horizontal input and output					
DIC (inlet 1)	9.47	5.54	3.41	1.97	mg L^{-1}
DIC (inlet 2)	2.48	1.09	0.92	0.45	mg L^{-1}
DIC (inlet 3)	0.66	0.57	1.62	0.58	mg L^{-1}
DIC (inlet 4)	1.11	0.88	0.90	0.50	mg L^{-1}
DIC (inlet 5)	4.53	2.97	3.38	1.60	mg L^{-1}
DIC (inlet 6)	0.53	0.39	0.61	0.35	mg L^{-1}
DIC (Outlet)	3.80	2.76	3.11	2.68	mg L^{-1}
T_{river}	12.40	14.47	12.78	12.94	°C

2.3.5 Structure equation model (SEM)

We developed the SEM based on previous studies (den Heyer and Kalff, 1998; Tranvik et al., 2009; Groeneveld et al., 2016; Wang et al., 2018; Aarnos et al., 2018; Dodds and Whiles, 2019). We not only considered the physical factors such as hydrological transportation and wind speed but also biochemical factors such as biological and photo-mineralization in this SEM (**Figure 4**). To quantify the objective function for paths and parameters, we used the Wishart likelihood function and applied Z-test to obtain p-values. To fit and validate the SEM's reliabilities, we calculated root mean square error (RMSE) of approximation and adjusted goodness of fit index (AGFI) (Igolkina and Meshcheryakov, 2020).

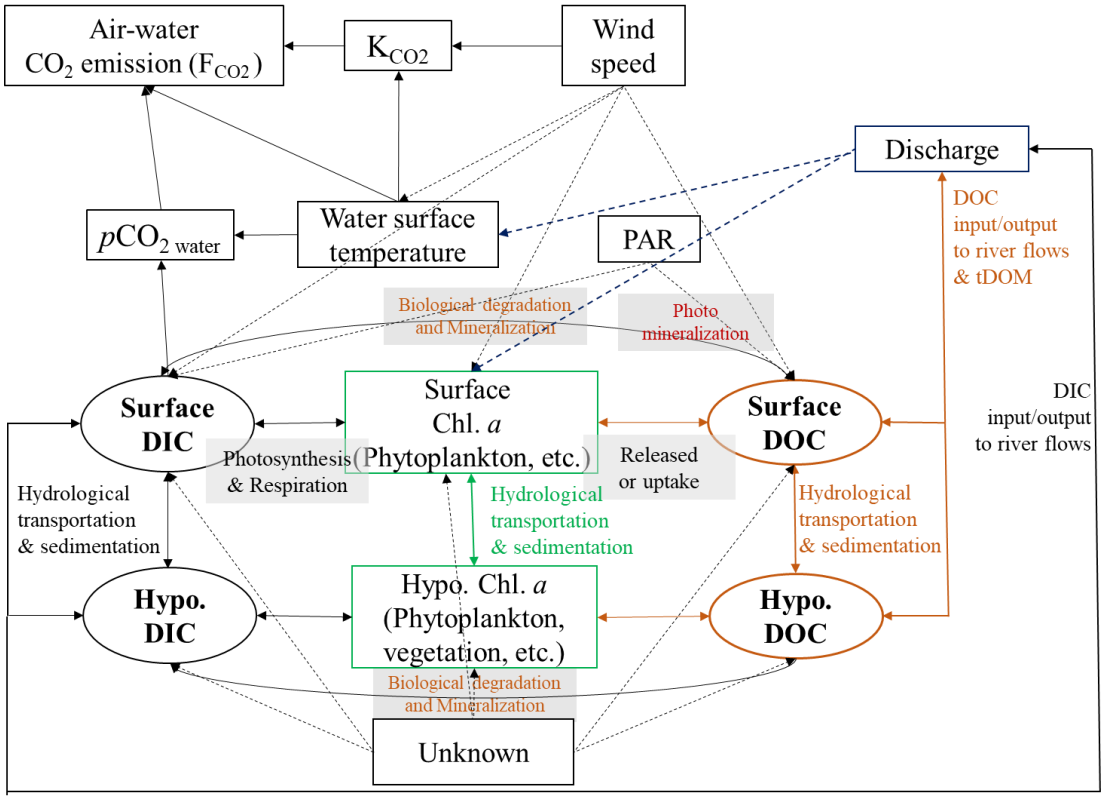

Figure 4. Conception diagram of carbon fluxes for SEM.

3. Results

We showed the three parts in the results from section 3.1 to section 3.3. First, in section 3.1, to clarify the effect of thermal stratification on the seasonal DIC in a subtropical shallow lake, we showed the vertical profiles of water temperature and DIC and estimated the residence time and NEP for each season (spring, summer, autumn, and winter). Next (section 3.2) shows the vertical profiles of water temperature, DIC, DOC, and Chl. *a* in shallow subtropical lakes with different trophic levels. Finally, section 3.3 is compared the detailed impacts of typhoon disturbance on C flux between pre- and post-typhoon periods by SEM analysis and the simulation results of Fantom.

3.1. The effect of thermal stratification on vertical profiles of DIC and NEP

3.1.1. Water temperature and DIC in YYL

Overall, mean water surface temperatures (0.04 m) were 14.6, 20.4, 15.4, and 11.3 °C from spring, summer, autumn, and spring, respectively (**Figure 5 a–d**). At the bottom (4.0 m), mean water temperatures were 8.5, 12.7, 12.9, and 8.7°C from spring to winter, respectively (**Figure 5 a–d**). Significantly, the highest difference in mean water temperature between the surface and bottom was 7.7 °C in summer (**Figure 5 b**), and the lowest difference was 2.5 °C in autumn and winter (**Figure 5 c–d**). Thus, substantial DIC was stored in the bottom from spring to autumn (**Figure 5 a–c**). Mean surface water DIC was about 3.0 mg C L^{-1} from spring to summer and about 2.5 mg C L^{-1} from autumn to winter (**Figure 5 a–d**). Mean DIC was highest in summer (7.5 mg C L^{-1}) and lowest in winter (2.8 mg C L^{-1}) at 3.5 m deep (**Figure 5 a–d**).

During typhoons, the mean surface water temperatures were lower, around 3.0 °C than typical summer, and mean DIC during the summer typhoons were vertically uniform and only about 2.5 mg C L^{-1} (**Figure 5 b** and **e**). However, the mean surface water temperatures were higher, around 1.6 °C than typical autumn, and mean surface water DIC was lowest, around 2.0 mg C L^{-1} during the autumn typhoons (Figure 3f).

Mean river temperatures were the highest in summer (15.1 °C) and lowest in winter (10.7 °C) (**Figure 6 a**). As a result, the difference in water temperature between lake surface water and the rivers was the highest (5.3 °C) in summer (Figure 4a), resulting in that mean DIC declined about 40% after summer typhoons (red rectangles in Figure 4b).

The mean river DIC was the highest in summer (3.7 mg C L^{-1}) and the lowest (1.8 mg C L^{-1}) during autumn typhoons (**Figure 6 b**).

In the upper layer, the ΔDIC were negative values from spring to summer (**Figure 7 a** and **b**). The absolute mean of ΔDIC was lower in spring (around 0.3 mg C L^{-1}) and summer (around 0.5 mg C L^{-1}) than in autumn (about 1.0 mg C L^{-1}), and was the lowest in winter (around 0.06 mg C L^{-1}) (Figure 5a–5d). Mean upper layer ΔDIC was smaller in typical summer than during the typhoons about 0.2 mg C L^{-1} (**Figure 7 b** and **e**). In contrast, mean ΔDIC in typical autumn was larger than during the typhoons (Figure 5c and 5f).

In the lower layer, the ΔDIC were all positive values for each season. The mean ΔDIC was 0.83, 3.82, 1.86, and 0.32 mg C L^{-1} for spring, summer, autumn, winter, respectively **Figure 7 a–d**). The lower layer ΔDIC was smaller during summer typhoons (0.69 mg C L^{-1}) than autumn typhoons (0.77 mg C L^{-1}) (**Figure 7 e–f**).

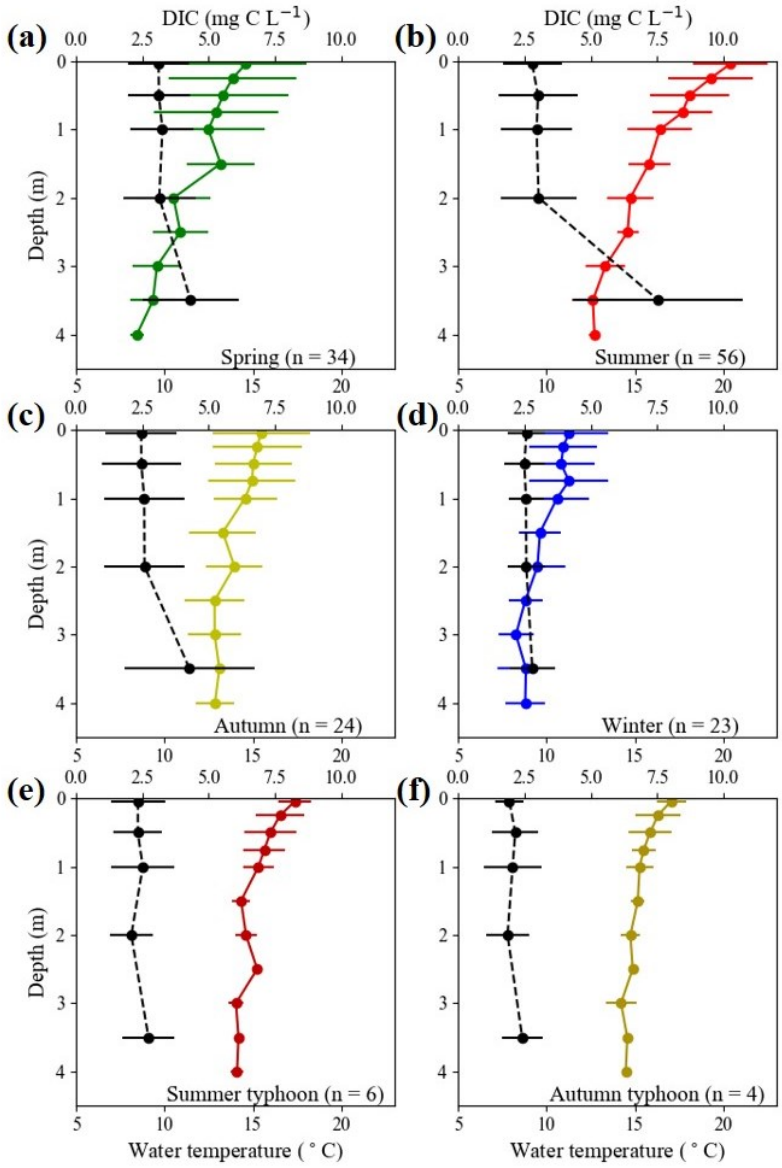

Figure 5. Vertical profiles of mean water temperature (colors solid lines) and DIC (black dashes) in **(a)** spring, **(b)** summer, **(c)** autumn, and **(d)** winter, and during the **(e)** summer typhoons and **(f)** autumn typhoons from July 2004 to December 2017. The dots show the mean value, and the horizontal lines indicate the standard deviation (n is the number of samples).

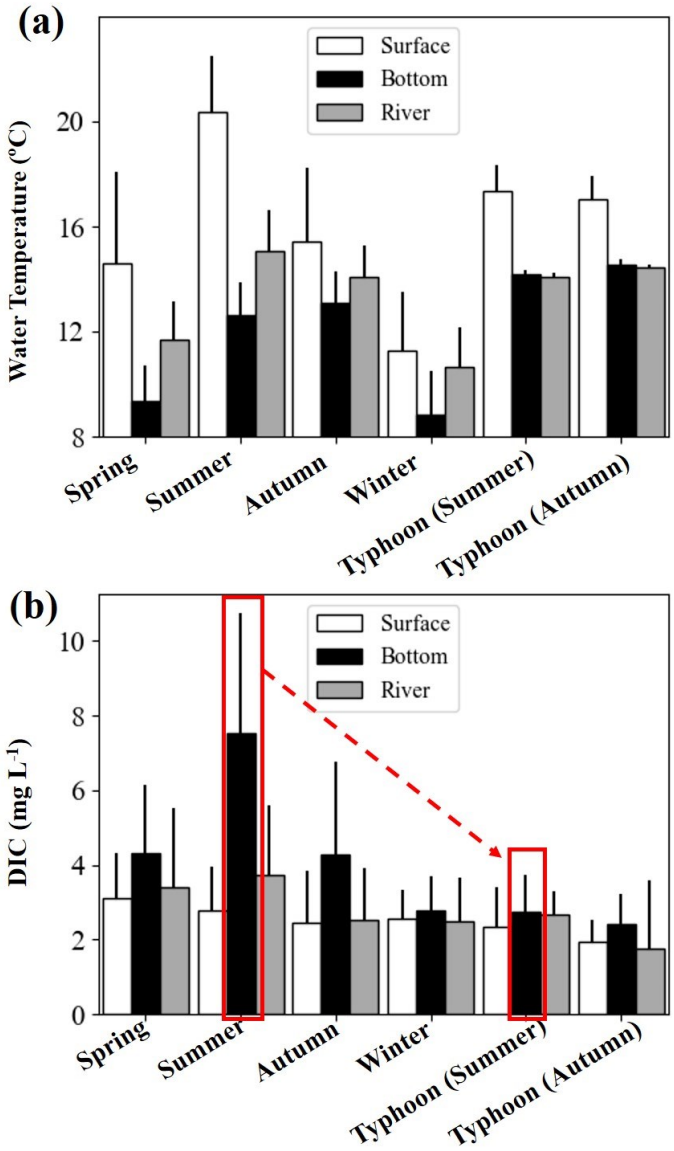

Figure 6. Comparison of **(a)** water temperatures and **(b)** DIC of the water surface (0.04 m, white bars), water bottom (3.5 m, black bars), and river water (T_R and DIC_R, gray bars). The bars represent the mean values, the solid black lines indicate the standard deviations, and red rectangles indicate the change in surface DIC concentration due to dilution after typhoons in summer.

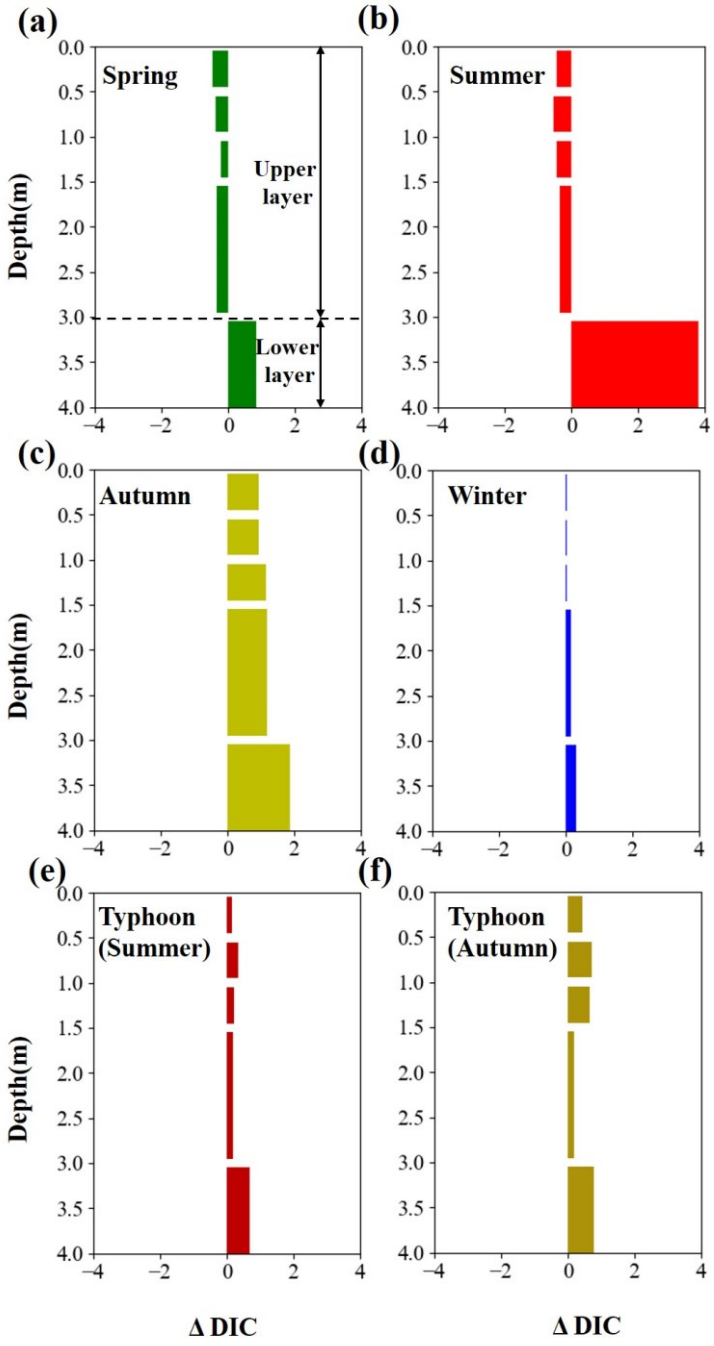

Figure 7. Mean vertical profiles of ΔDIC (mg C L^{-1}) in **(a)** spring, **(b)** summer, **(c)** autumn, **(d)** and winter, and during the **(e)** summer typhoons, and **(f)** autumn typhoons.

3.1.2. Mixing depth, Brunt-Väisälä frequency, and intrusion depth

Mean mixing depth was the largest in winter (25 % of the water depth) and smallest in summer (7.50 %; **Figure 8 a**). The stratifications from spring to summer were stronger than in autumn and winter because mean Brunt-Väisälä frequency was the highest in spring and summer ranged from around 6.00×10^{-3} to 1.30×10^{-2} s^{-1}(**Figure 8 b**). In addition, the Brunt-Väisälä frequency after typhoons was higher than in autumn and winter (**Figure 8 b**). As a result, mean intrusion depth was about 50% of the total water column from spring to autumn and 100% of the whole water column after the typhoons (**Figure 8 c**). In contrast, intrusion depth in winter was small, approximately 10% of the total water column (**Figure 8 c**).

We used the Spearman correlation to quantify the correlation coefficient (rs) and represent the statistical significance (**Table 3**). As a result, the water surface DIC was not associated with water temperature or Brunt-Väisälä frequency (Figure 7a and 7d). (**Table 3** and **Figure 9 a**). However, hypolimnion DIC and water temperature showed a significant positive correlation ($rs = 0.61$, $p < 0.001$) (Figure 7b). Hypolimnion DIC and river DIC had the strongest positive correlation ($rs = 0.69$, $p < 0.001$) (**Figure 9** c). Hypolimnion DIC and river DIC showed a positive correlation with Brunt-Väisälä frequency ($rs = 0.43$ and 0.32, $p < 0.001$) (Figure 7e and 7f). The Brunt-Väisälä frequency and mixing depth were associated with surface water temperatures (**Figure 9 g–h**) with high Spearman correlation coefficients ($rs = 0.64$ & 0.40, $p < 0.001$). Although Brunt-Väisälä frequency and mixing depth had the strongest correlation ($rs = - 0.88$, $p < 0.001$) (**Figure 9 i**), mixing depth was not strongly correlated with hypolimnion DIC or river DIC (**Table 3**). Intrusion depth had significant positive correlations with water surface temperature, Brunt-Väisälä frequency, and hypolimnion DIC ($rs = 0.58$, 0.32, and 0.32, respectively, $p < 0.001$). In contrast, intrusion depth was not associated with mixing depth, water surface DIC, or river DIC.

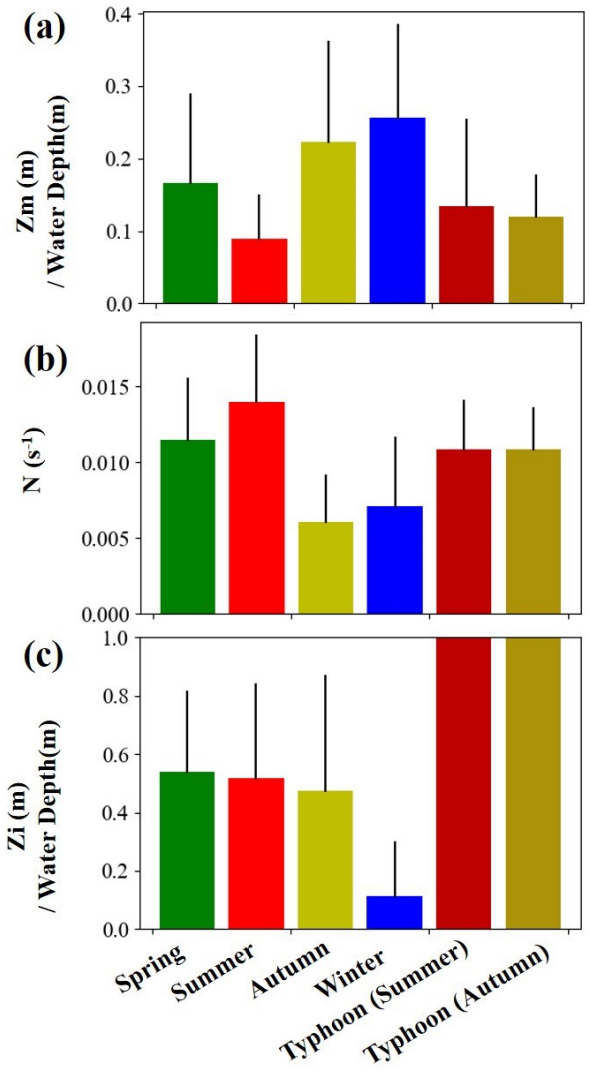

Figure 8. Comparison of the **(a)** mixing depth (Z_m), **(b)** Brunt–Väisälä frequency (N), and **(c)** intrusion depth (Z_i) for each category in YYL. The bars represent the mean values, and the solid black lines indicate the standard deviations. The total water depths were used to normalize the intrusion and mixing depths.

Table 3. Spearman correlation coefficients for DIC, water surface temperature, Brunt-Väisälä frequency, mixing depth, and intrusion depth. * represents the statistical significance at p-value ≤ 0.05; ** represents the statistical significance at p-value ≤ 0.01; *** represents the statistical significance at p-value ≤ 0.001.

Variables	*Mixing depth*	*Brunt-Väisälä frequency*	*Water surface DIC*	*Hypolimnion DIC*	*River DIC*	*Intrusion depth*
Water surface temperature	-0.398***	0.643***	0.029	0.611***	0.310**	0.581***
	(122)	(142)	(142)	(142)	(76)	(66)
Mixing depth		-0.879***	0.115	-0.221	-0.158	-0.155
		(122)	(122)	(122)	(66)	(52)
Brunt-Väisälä frequency			0.017	0.427***	0.324***	0.324***
			(142)	(142)	(76)	(66)
Water surface DIC				0.438***	0.320***	0.162
				(152)	(84)	(66)
Hypolimnion DIC					0.686***	0.321***
					(84)	(66)
River DIC						-0.005
						(31)

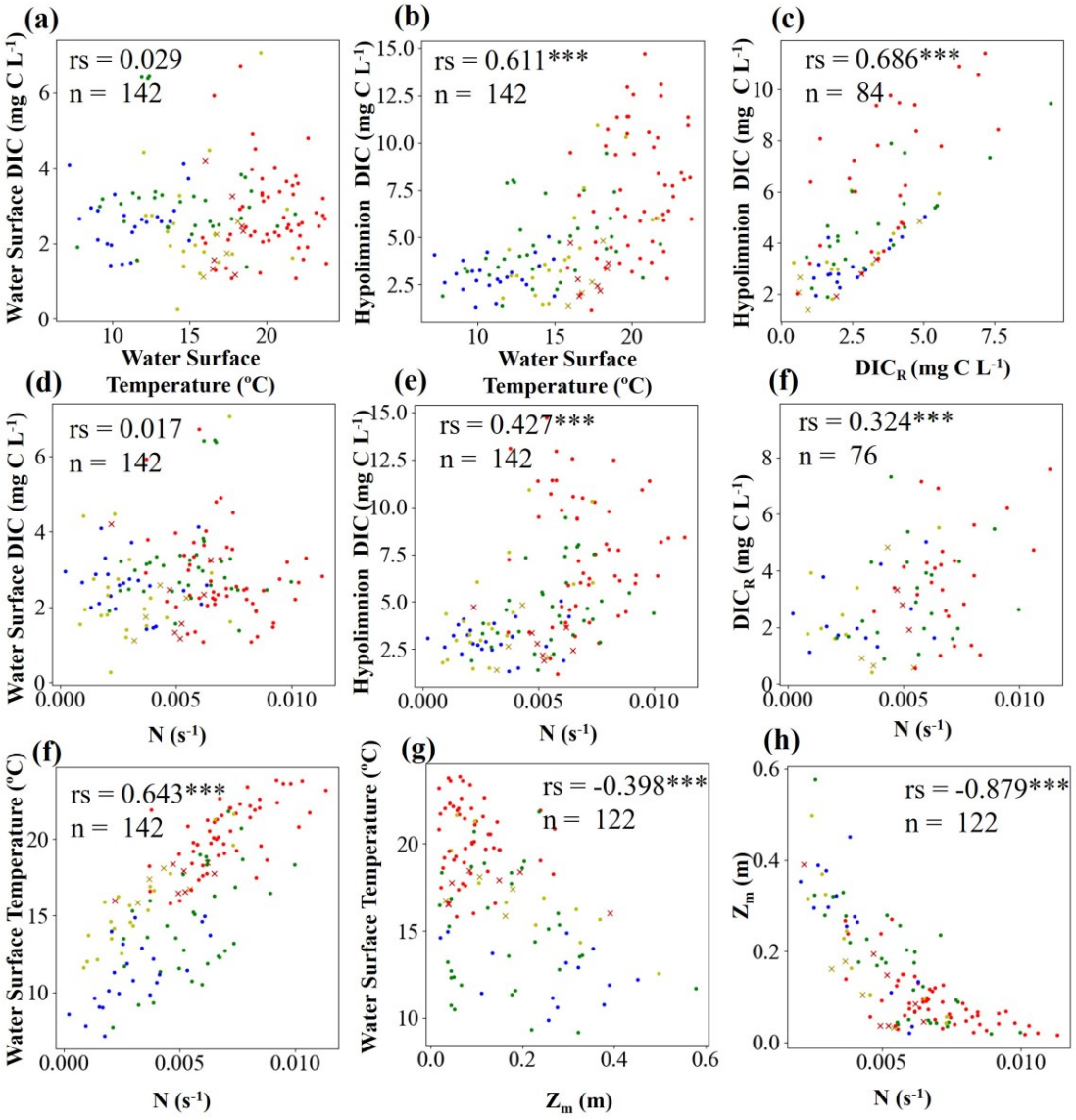

Figure 9. Relationships between **(a)** water surface temperature and water surface DIC, **(b)** water surface temperature and hypolimnion DIC, **(c)** river DIC (DIC_R) and hypolimnion DIC, **(d)** Brunt–Väisälä frequency (N) and water surface DIC, **(e)** N and hypolimnion DIC, **(f)** N and DIC_R, **(g)** N and water surface temperature, **(h)** mixing depth (Z_m) and water surface temperature, and **(i)** N and Z_m. The green, red, yellow, and blue points represent spring, summer, autumn, and winter data. The dark red and dark yellow crosses represent the summer and autumn typhoon data. rs is the Spearman correlation coefficients. *** indicates statistical significance at p-value ≤ 0.001.

3.1.3. NEP and F_{CO2} in YYL

We showed the effect of stratification and river intrusion on the vertical distribution of tracers under summer conditions (**Figure 10**). We found that the upper layer is well-mixed on the second day after the initial condition (**Figure 10 a–b**). However, the river flow cannot intrude into the lower layer because the water temperature of the river inflow is almost the same as the middle layer, resulting in the slow descent of the thermocline from the second to the third day (**Figure 10 c**). In contrast, the tracer was confirmed to be well-mixed in the entire domain in winter because of weak stratification. As a result, the residence times were 2.6, 2.6, 1.7, and 1.3 days for spring, summer, autumn, and winter, respectively. The residence time was longer-ranged from 1.3 to 0.9 days in spring and summer than autumn and winter due to the stronger stratification.

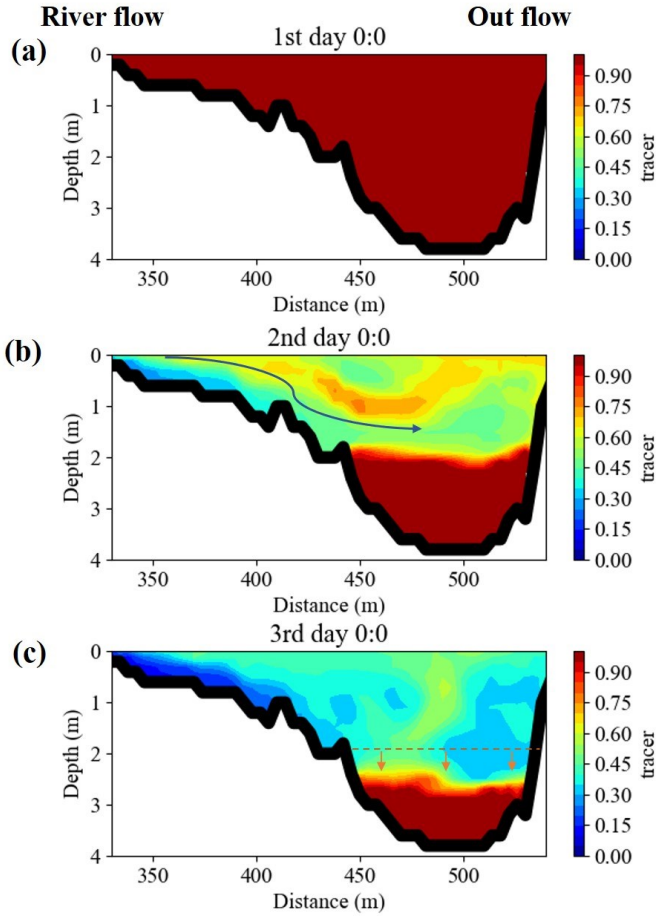

Figure 10. Vertical distribution of the tracer in summer. **(a)** Day 1, 00:00 a.m.; **(b)** day 2, 00:00 a.m.; **(c)** day 3, 00:00 a.m. The horizontal coordinate shows the distance from the northernmost end of YYL (m); the vertical coordinate shows the depth (m) from the water surface to the bottom. Contour shows the concentration of the tracer.

Mean F_{CO2} was the lowest in summer (131.2 mg C m^{-2} d^{-1}) and highest in autumn (207.2 mg C m^{-2} d^{-1}) (**Table 4**). The standard deviations of DIC and F_{CO2} were higher in summer and autumn than spring and winter (**Table 4**). Water temperatures (11.1 ± 1.9 °C), DIC (2.20 ± 0.43 mg L^{-1}), and k_{CO2} (1.85 ± 0.42 cm h^{-1}) were lowest in winter, which led to a lower mean F_{CO2} than in spring and autumn.

NEP was positive only in spring in the entire YYL (**Figure 11**). We followed equation (6) to obtain NEP in the upper layer using the ΔDIC, because the upper layer plays a major role in CO_2 emissions. As the results, NEP in the upper layer was 114.1 (spring), 144.0 (summer), -644.8 (autumn), and -69.7 (winter) mg C m^{-3} d^{-1} (**Figure 11**). The contribution of F_C to NEP in the upper layer was 24.9%, 15.5%, 5.5%, and 33.5% in spring, summer, autumn, and winter, respectively (**Table 4**). Therefore, CO2 emissions were confirmed to not be negligible in (6). On the other hand, NEP in the lower layer was -319.6, -1470.3, -1282.6, -374.5 mg C m^{-3} d^{-1} from spring to winter. The effect of stratification on the suppression of vertical mixing between the upper and lower layers enhanced positive total NEP in spring. A large amount of C was stored in the lower layer, resulting in the negative total NEP in summer.

Table 4. CO_2 flux in YYL from July 2011 to December 2017 (not including 2012 and 2013). F_C is CO_2 emission.

Variables	Unit	Spring	Summer	Autumn	Winter
n		12	18	12	12
WT	(°C)	15.59 ± 2.96	20.58 ± 1.87	15.72 ± 2.18	11.05 ± 1.92
k_{CO2}	(cm h^{-1})	2.23 ± 0.55	2.42 ± 0.33	2.35 ± 0.26	1.85 ± 0.42
pH		6.10 ± 0.84	5.78 ± 0.85	6.05 ± 0.58	6.25 ± 0.66
DIC	(mg L^{-1})	2.44 ± 0.54	2.31 ± 1.32	2.56 ± 1.70	2.20 ± 0.43
$pCO2_{air}$	(μatm)	331.6 ± 1.30	331.6 ± 1.05	332.4 ± 0.79	332.0 ± 0.52
$pCO2_{water}$	(μatm)	782.3 ± 172.2	792.3 ± 512.4	823.1 ± 557.6	664.3 ± 140.9
F_{CO2}	(mg C m^{-2} d^{-1})	255.0 ± 103.9	265.1 ± 292.0	309.7 ± 389.1	169.8 ± 85.1
F_C	(mg C m^{-3} d^{-1})	92.7 ± 37.8	96.4 ± 106.2	112.6 ± 147.6	61.74 ± 31.0

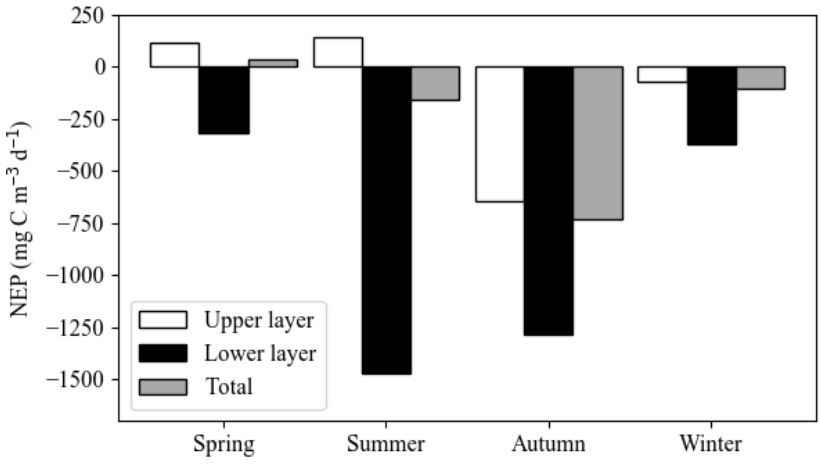

Figure 11. NEP in YYL from July 2004 to December 2017. C is absorbed when NEP > 0 and C is released when NEP < 0. White bars represent NEP in the upper layer (0.04 to 2.5 m water depth), black bars represent NEP in the lower layer (2.5 to 4.0 m water depth), and gray bars represent the whole-lake mean NEP.

3.2 Comparison of the limnological and meteorological data between before and after typhoons with subtropical shallow lakes

3.2.1 Seasonal dynamics of metrological and limnological data

In YYL, the mean wind speed was 1.07 m s^{-1}, and the maximum wind speeds exceeded 8.0 m s^{-1} during typhoons from 2009 to 2017 (**Figure 12 a**). The mean water depth was 4.40 m (**Figure 12 a**). The vertical profile of the water temperature showed stratification from April to September and a well-mixed water column from December to February (**Figure 12 b**). The daily surface temperatures (at 0.04 to 0.5 m water depth) are around 5.60 to 23.9°C (**Figure 12 b**). The average surface DIC was 2.42 mg C L^{-1}, ranging from 0.50 to 7.06 mg C L^{-1} (**Figure 12 c**). In June, the maximum bottom DIC (at 3.5 m water depth) was 10.3 mg C L^{-1}, about ten times higher than the maximum surface DIC. The DIC was not significantly different between the surface and bottom from December to January. The average surface and bottom DOC were 5.63 and 7.26 mg C L^{-1}, respectively (**Figure 12 d**), which the DOC was approximately two times higher than the DIC concentration (**Figure 12 c–d**). Especially, DOC and DIC were approximately two to ten times higher during typhoon periods (August to November) than the other periods (**Figure 12 c–d**). The average surface Chl. *a* was 2.92 μg L^{-1}. Hypolimnion Chl. *a* was two to ten times higher (around 30.0–150 μg L^{-1}) than epilimnion Chl. *a* due to algal bloom from April to August (**Figure 12 e**). The mean F_{CO2} was 165 mg C m^{-2} d^{-1}, ranging from -163 to 1018 mg C m^{-2} d^{-1} (**Figure 12 f**). Overall, YYL was found to release C into the atmosphere (**Figure 12 f**).

In TFL, the mean wind speed was 1.89 m s^{-1} and was more significant than YYL, and the maximum wind speed was 14.7 m s^{-1} during the typhoon (**Figure 13 a**). Because TFL only had seepage flow and no significant river outflow, the average and the total water depth variation were higher than YYL. In addition, the watershed flowing into TFL was larger than YYL, and the maximum water depth was more than 10.0 m, resulting in the total water depth returning to the average value of 30.0 days or more after a typhoon (**Figure 13 a**). The average surface temperature was 15.8°C, and the maximum water temperature was 25.5°C, with a difference of 8.0°C between the surface and bottom in TFL (**Figure 13 b**). However, measuring the bottom water temperature from the thermistor chain after rains was impossible because the total water depth was greater than the thermistor's length (3.50 m). Surface DIC was around 0.50 to 7.00 mg C L^{-1} (**Figure 13 c**). The average surface DOC and bottom DOC were 4.40 and 4.62 mg C L^{-1}, respectively (**Figure 13 d**). The mean surface Chl. *a* in TFL was 43.9 μg L^{-1}, which was higher than YYL, and the maximum Chl. *a* was 153 μg L^{-1} (**Figure 13** e). F_{CO2} was around -0.17 to -361 mg C m^{-2} d^{-1} (excluding July

to October 2015 and August 2016), which showed that TFL is a C sink lake (**Figure 13 f**).

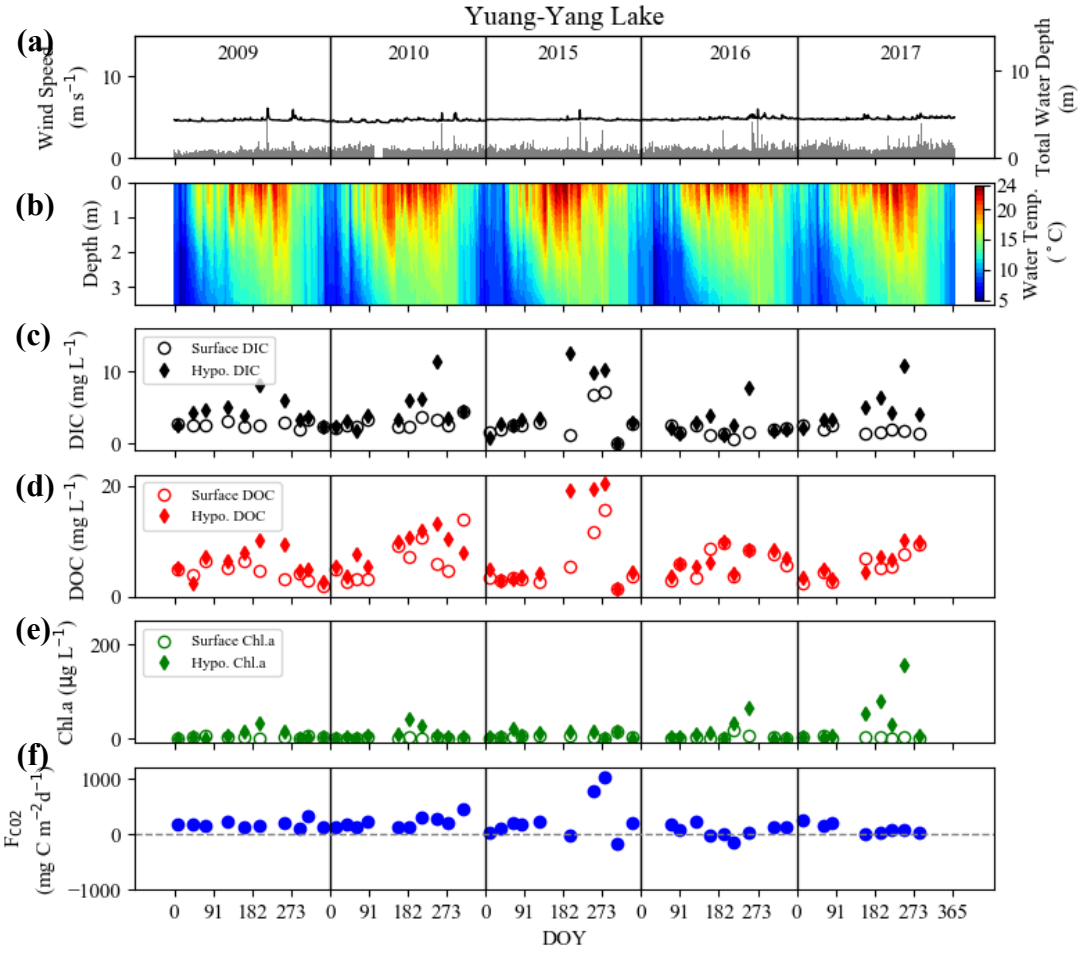

Figure 12. Five years of temporal data on **(a)** wind speed (U_{10}, grey bars) and total water depth (solid black line), **(b)** water temperature, **(c)** epilimnion (hollow black circles) and hypolimnion (black diamonds) DIC, **(d)** epilimnion (red hollow circles) and hypolimnion (red diamonds) DOC, **(e)** epilimnion (hollow green circles) and hypolimnion (green diamonds) Chl. *a*, and **(f)** C emission across the air-water interface (F_{CO2}) in YYL. **(a–b)** are daily averages and **(c–f)** are water samplings per month.

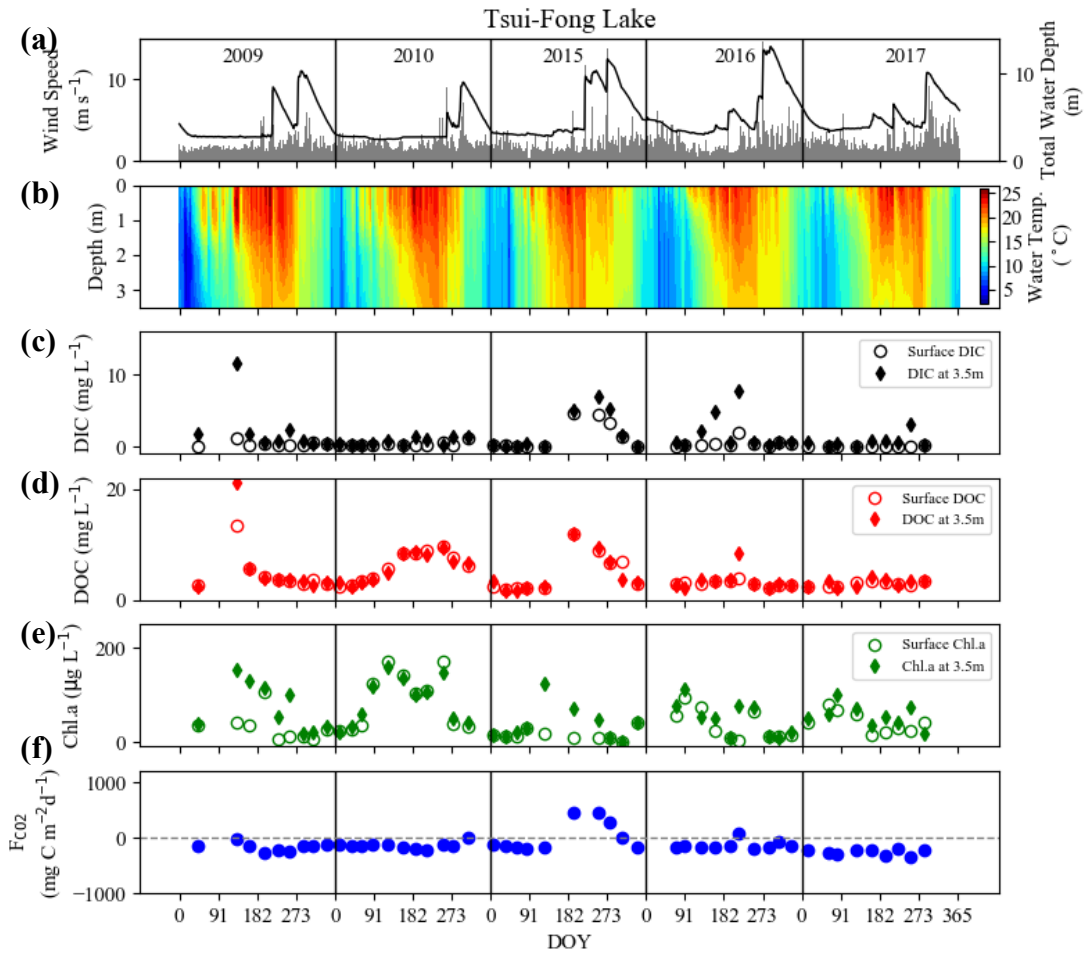

Figure 13. Five years of temporal data on **(a)** wind speed (U_{10}, grey bars) and total water depth (solid black line), **(b)** water temperature, **(c)** DIC at epilimnion (hollow black circles) and 3.50 m water depth (black diamonds), **(d)** DOC at epilimnion (red hollow circles) and 3.50 m water depth (red diamonds) DOC, **(e)** Chl. *a* at epilimnion (hollow green circles) and 3.50 m water depth (green diamonds), and **(f)** C emission across the air-water interface (F_{CO2}) in TFL. **(a–b)** are daily average and **(c–f)** are water samplings per month.

3.2.2 Variation in water temperature, DIC, Chl. *a*, and NEP during pre- and post-typhoon periods

Overall, the mean surface temperatures during the pre- and during-typhoon periods were 18.0°C and 17.9°C in YYL, and 19.5 and 19.2°C in TFL (**Figure 14 a–b**). In the post-typhoon period, the mean surface temperature was 12.7°C in YYL and 12.6°C in TFL (**Figure 14 a–b**). The surface DIC was higher in the during-typhoon period than the pre- and post-typhoon ones in both lakes, which was2.91 and 6.01 mg C L^{-1} in YYL at 3.50 m water depth (**Figure 14 c–d**) and 0.71(average pre- and post-typhoon) and 0.88 (during-typhoon) mg C L^{-1} in TFL, respectively. The mean Chl. *a* was relatively constant at the surface water in YYL (**Figure 14 a**). However, the average Chl. *a* changed from 63.5 (pre-typhoon) to 34.8 μg L^{-1} (during-typhoon) at the water surface (**Figure 14 e–f**) in TFL. The Chl. *a* decreased from 90.9 (pre-typhoon) to 34.2 (during-typhoon) μg L^{-1} at 3.50 m water depth in TFL (**Figure 14 e–f**). The variance patterns of DOC were similar to DIC **(Figure 14 c–d** and **h–i**). Mean DOC was the highest in the during-typhoon period than the other period in YYL (**Figure 14 h**); the DOC diluted vertically in the during-typhoon and post-typhoon period in TFL (**Figure 14 i**).

As the results of numerical simulation, the residence times (t_r) were 5.80 d (pre-typhoon), 4.40 d (during-typhoon), 5.70 d (post-typhoon) in YYL. On the other hand, the residence times of TFL were longer than YYL, which were 10.0 days (pre-typhoon), 18.0 days (during-typhoon), and 39.0 days (post-typhoon) (**Table 5**). The results showed the NEP was 230 mg C m^{-3} d^{-1} in TFL and 118 mg C m^{-3} d^{-1} in YYL, meaning that C was absorbed into both lakes during the pre-typhoon period (**Figure 15**). However, high Chl. *a* content might lead to the higher C absorption t (**Figure 15**). The NEP in YYL was negative: -8.70 and -42.1 mg C m^{-3} d^{-1} in the during- and post-typhoon periods, respectively. The NEP was 97.3 mg in the during-typhoon period and 40.5 mg C m^{-3} d^{-1} in the post-typhoon period in TFL.

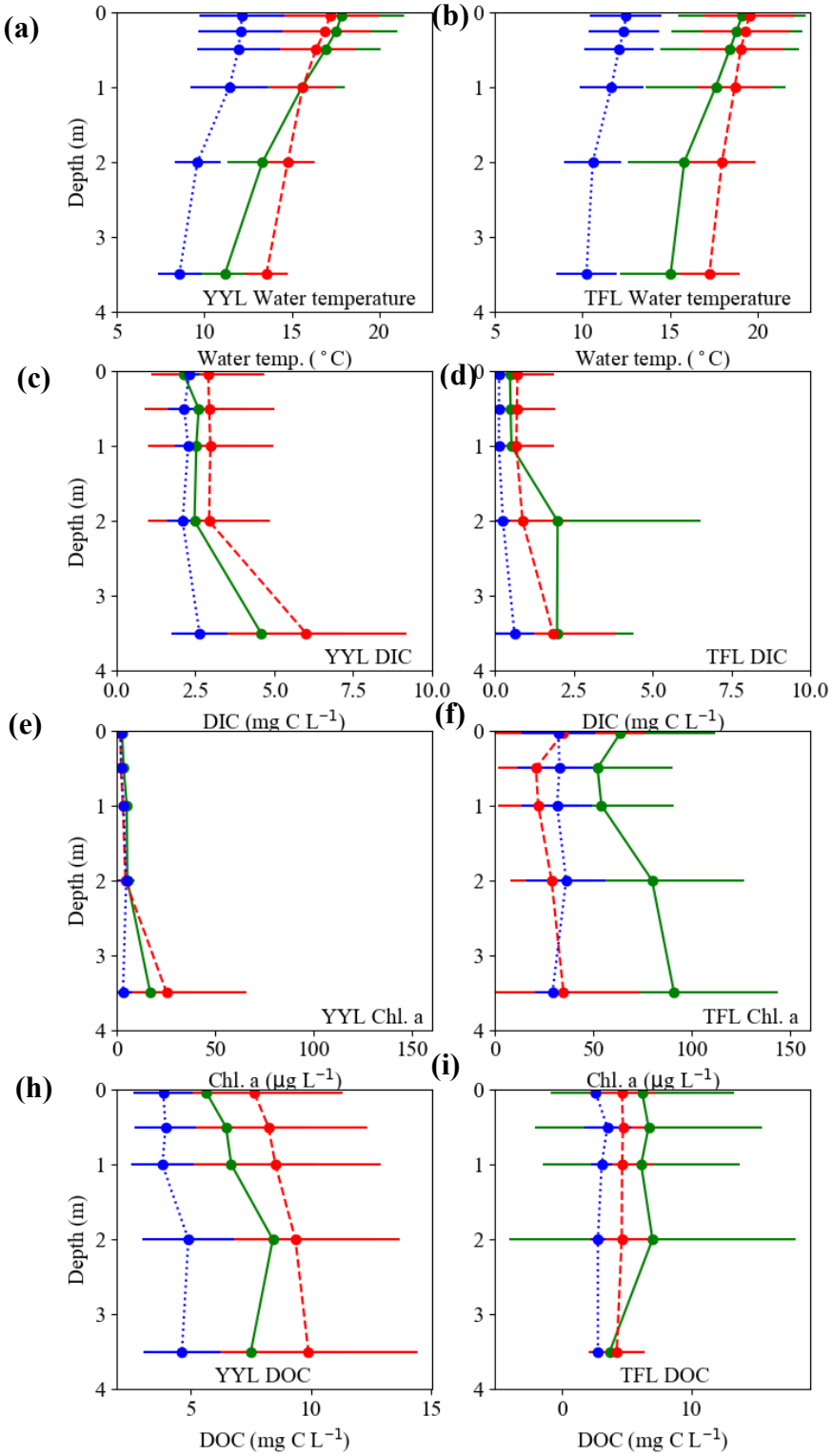

Figure 14. Vertical profiles of average **(a, b)** water temperature, **(c, d)** DIC, and **(e, f)** Chl. *a* and **(h, i)** DOC in the pre-typhoon period (solid green lines), during-typhoon period (red dashes), and post-typhoon period (blue dotted lines) from January 2009 to December 2017 within the lakes. The dots and crosses show the average value, and the horizontal lines indicate the standard deviation (SD).

Table 5. Results of residence times (t_r) during different periods.

Site		**Period**		
Parameters		**Before typhoon**	**During typhoon**	**After typhoon**
YYL				
Volume	(m^3)	4.10×10^4	4.29×10^4	4.02×10^4
Discharge	($m^3\ s^{-1}$)	0.048	0.107	0.028
Water depth	(m)	4.38	4.46	4.35
t_r'*	(d)	9.86	4.64	16.6
t_r	(d)	5.8	4.4	5.7
Overestimate (by t_r')	(%)	70.1	5.45	191
TFL				
Volume	(m^3)	2.19×10^5	8.32×10^5	3.39×10^5
Discharge	($m^3\ s^{-1}$)	0.185	0.411	0.067
Water depth	(m)	3.27	7.01	4.08
t_r' *	(d)	13.7	23.4	58.6
t_r	(d)	10	18	39
Overestimate (by t_r')	(%)	37	30.2	50.2

* t_r' was determined with equation (15)

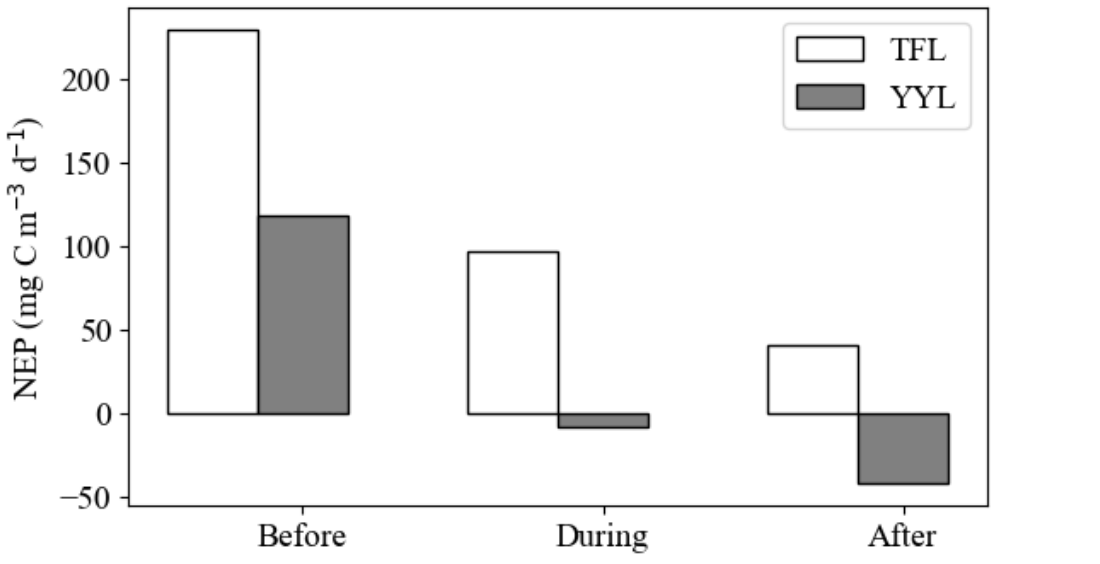

Figure 15. The average NEP (mg C m^{-3} d^{-1}) between YYL (grey bars) and TFL (white bars) for each period (before, during, and after typhoons).

3.3 The detailed impacts of typhoons on DIC and DOC flux

3.3.1 Analysis of C flux using SEM

Overall, results showed that F_{CO2} is strongly correlated with wind speed, water surface temperature, and $pCO2_{water}$. The $pCO2_{water}$ was the most critical factor in F_{CO2} due to Fick's law. The influence of water surface DIC on F_{CO2} was much more than water surface temperature and wind speed (**Figure 16** and **Figure 17**). We also analyzed for each season in two lakes; please see **Supplement figure 1-8**.

In YYL, PAR, water surface DOC, and bottom DOC affected surface DIC during the pre-typhoon period in YYL (**Figure 16 a**). However, only bottom DIC was strongly associated with water surface DIC in the during-typhoon period (**Figure 16 b**). Moreover, the river discharge, PAR, water surface DOC and bottom DIC were more closely correlated to surface DIC in the post-typhoon than the pre-typhoon period (**Figure 16 c**).

In TFL, bottom DIC and water surface DOC were positively correlated with water surface DIC during the pre-typhoon period (**Figure 17 a**). In contrast, river inflow, PAR, and Chl. a were negatively associated with water surface DIC (**Figure 17 a**). During the typhoon period, water surface DOC and inflows discharge were strongly correlated with water surface DIC (**Figure 17 b**). However, during the post-typhoon period, the influences of water surface DOC and inflows discharge on water surface DIC were smaller than those of the pre- and during-typhoon periods (**Figure 17 c**). Therefore, epilimnion DOC and Chl. *a* may play a critical role in mediating water surface DIC, $pCO2_{water}$, and F_{CO2} dynamics in TFL. It should be noted that Chl. *a* was associated with epilimnion DIC in TFL, but not in YYL, suggesting that Chl. a contributes to biological processes involving the epilimnion DIC and F_{CO2} in TFL. Therefore, DOC input from inflows is considered the most significant factor controlling DIC, $pCO2_{water}$, and F_{CO2} in the oligotrophic YYL.

YYL (a) before (pre-typhoon)

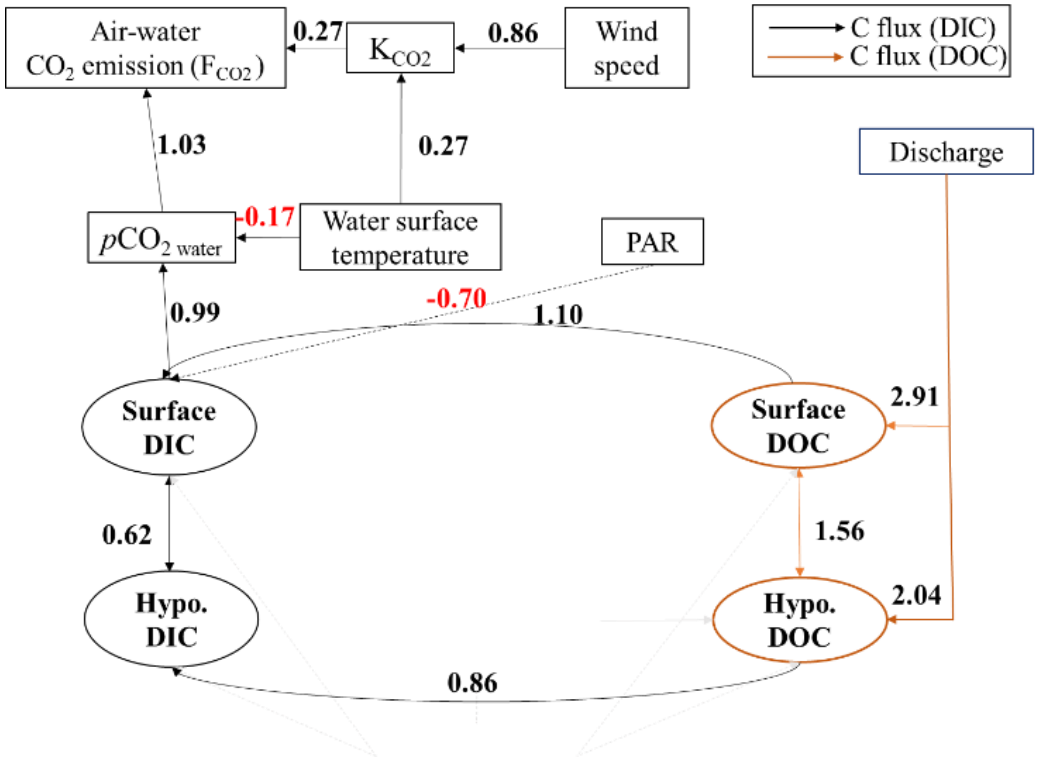

(b) during typhoon

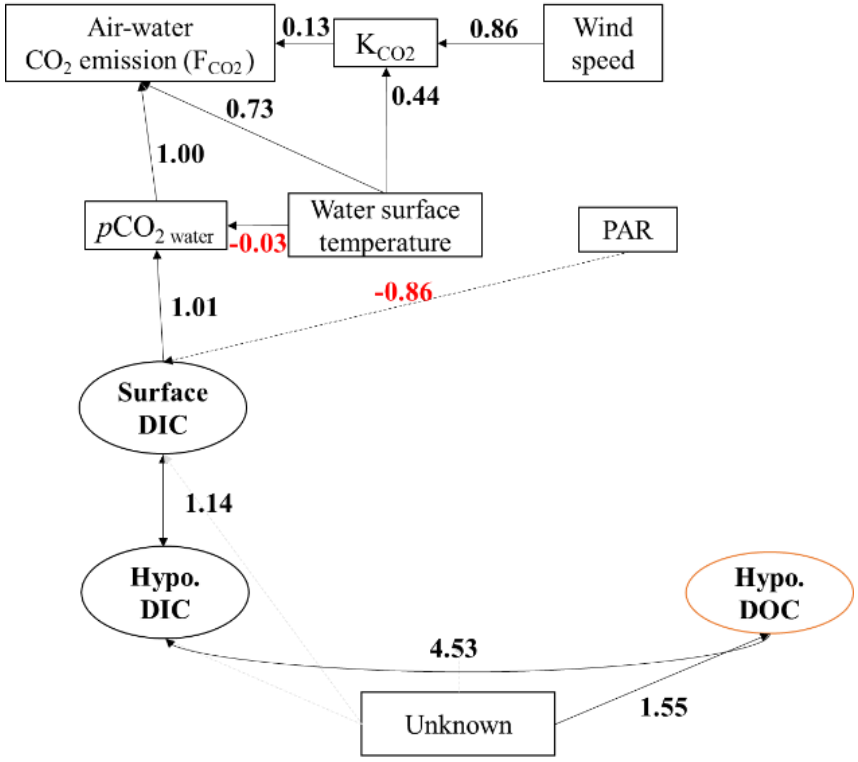

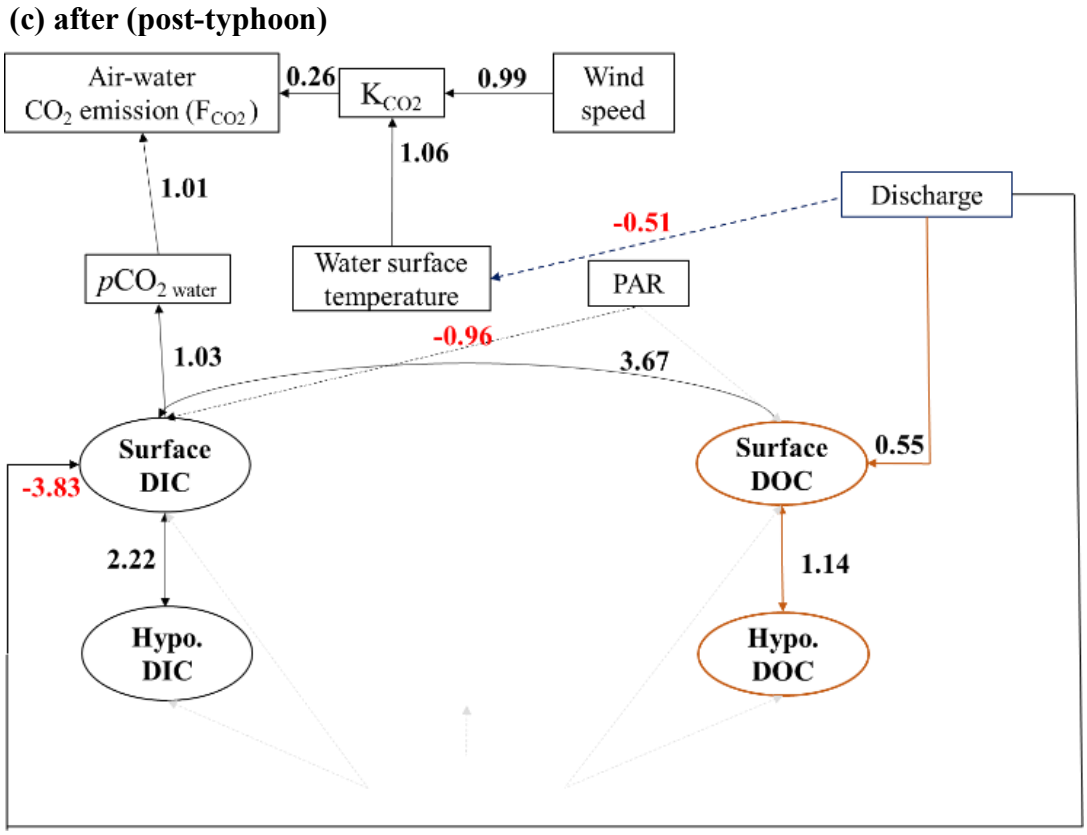

Figure 16. SEM analysis showing DIC fluxes (black arrows) and DOC fluxes (brown arrows) **(a)** before, **(b)** during, and **(c)** after typhoons in YYL. The coefficient values are calculated from the Wishart likelihood function. The value of a coefficient indicates the relative influence of the path. The path coefficients (black and brown arrows) show statistical significance (p-value < 0.05). Standardized RMSE is less than 0.10; AGFI is more than 0.95 for each period.

TFL (a) before (pre-typhoon)

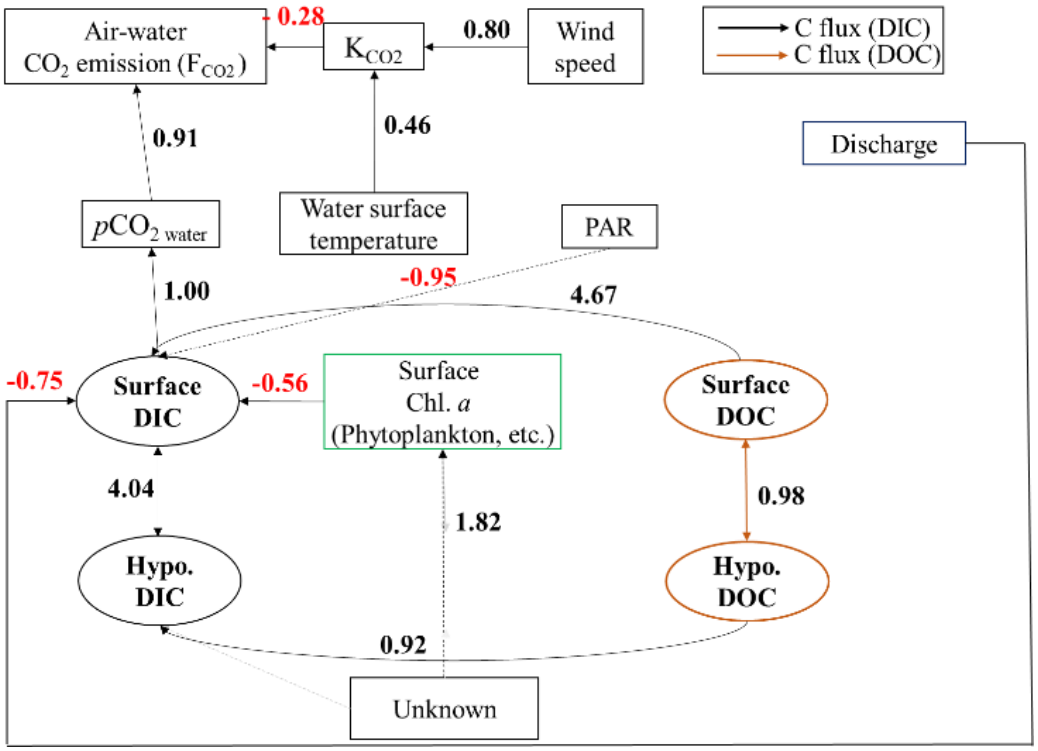

(b) during typhoon

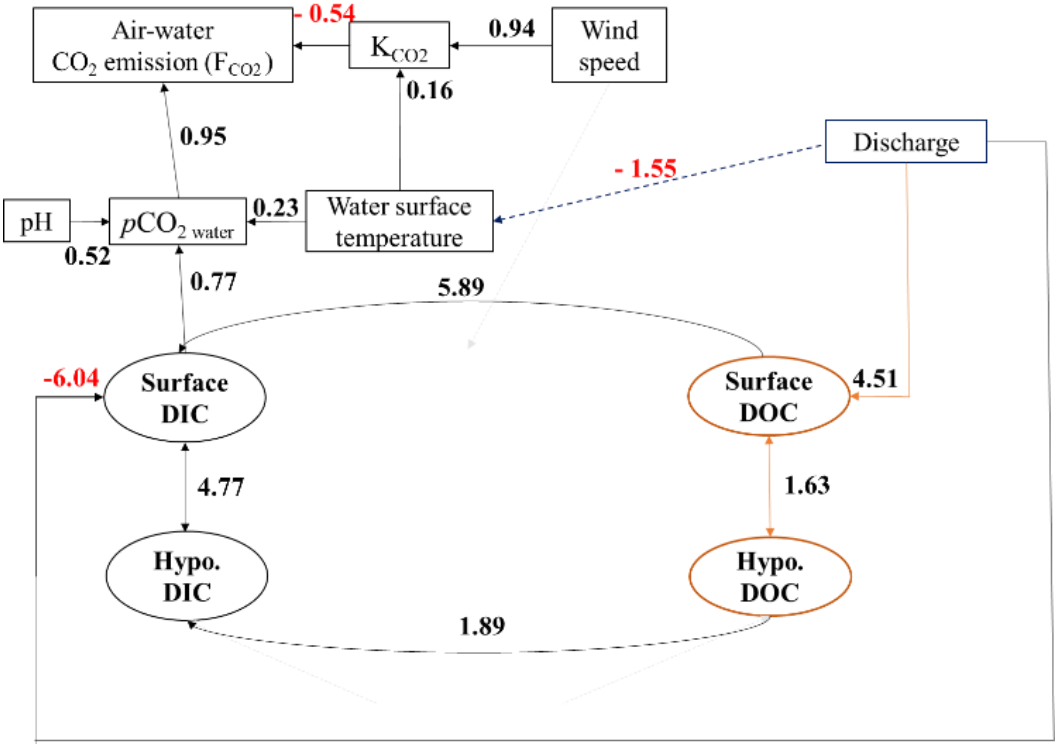

(c) after (post-typhoon)

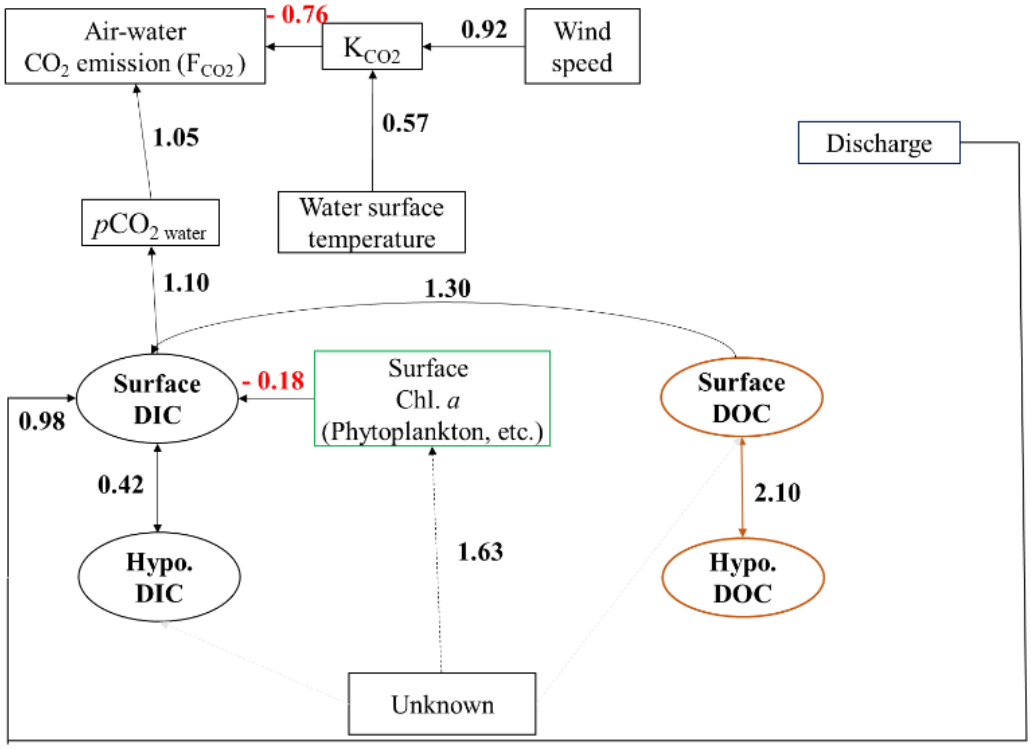

Figure 17. SEM analysis showing DIC fluxes (black arrows) and DOC fluxes (brown arrows) **(a)** before, **(b)** during, and **(c)** after typhoons in TFL. The coefficient values are calculated from the Wishart likelihood function. The value of a coefficient indicates the relative influence of the path. The path coefficients (black and brown arrows) show statistical significance (p-value < 0.05). Standardized RMSE is less than 0.10; AGFI is more than 0.95 for each period.

3.3.2 Linear relationship between F_{CO2} and limnological data

Overall, F_{CO2} was significantly correlated with DIC in the during-typhoon period ($R^2 > 0.9$, p-values < 0.001) in TFL and YYL. DOC and F_{CO2} were positively correlated in both lakes in the during-typhoon period but not in the YYL during pre-typhoon or post-typhoon periods (
Figure 18 c–d). Additionally, Chl. *a* had a slightly negative correlation with F_{CO2} in TFL ($R^2 < 0.25$, p-values < 0.05) in pre- or post-typhoon, but not in YYL (
Figure 18 e–f). Wind speed was negatively correlated with F_{CO2} in TFL (
Figure 18 h). However, the wind speed was not associated with $\boldsymbol{F_{CO2}}$ in YYL because it (0.11–2.72 m s^{-1}) was less than half of the wind speed in TFL (0.58–3.89 m s^{-1}) (
Figure 18 g–h).

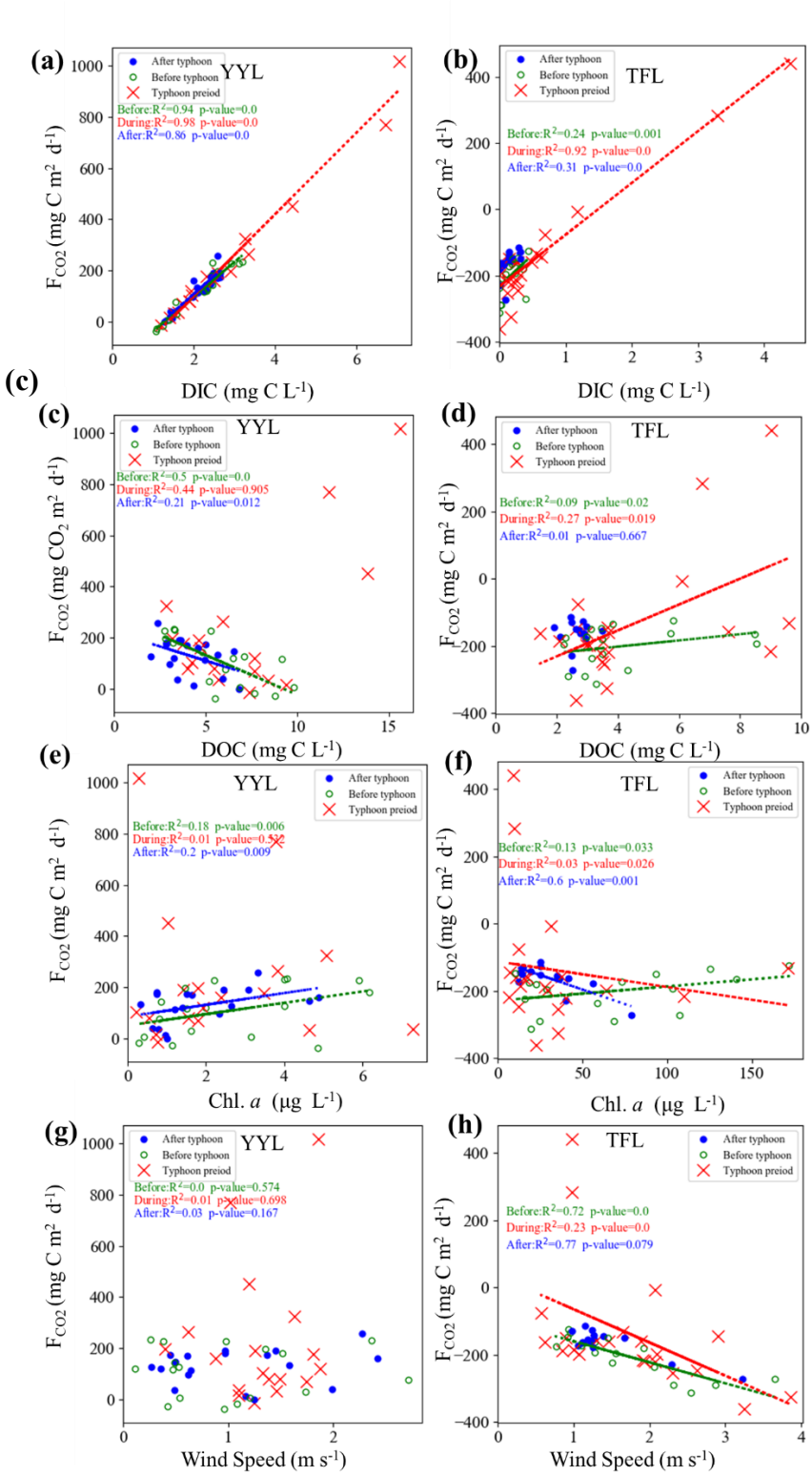

Figure 18 Relationship between F_{CO2} and limnological data (Wind speed (U_{10}), DIC, DOC, and Chl. *a* at the epilimnion **(a, c, e, g)** in YYL and **(b, d, f, h)** in TFL. Green circles show the before-typhoon period, red crosses show the during typhoon period, and blue dots show the after-typhoon period. The dotted lines show a linear regression line for each period.

3.3.3 Effects of a typhoon on C

We found that typhoons impacted the vertical mixing of lake waters and thus temporarily decreased the DIC level (section 3.1). To clarify how typhoon events affect DIC, we investigated the influence of Typhoon Megi (Number 1617), which is the strongest in YYL and TFL from September 26 to 29, 2016. We also showed the other strong typhoon (Typhoon Dujuan, Number 1521) during 2015 in YYL; please see **Supplement figure 9-10**.

The maximum PAR reaches 2,000 μmol photons m^{-2} s^{-1} on average days, but during Typhoon Megi, it decreased to 300–500 μmol photons m^{-2} s^{-1} (**Figure 19 a–b**). The PAR even got close to zero in the middle of the typhoon (September 28). The water columns were well-mixed during the two days of the typhoon (**Figure 19 c–d**). After Typhoon, the vertical gradient of water temperature was approximately 1.50°C m^{-1} in YYL and 0.50°C m^{-1} in TFL from September 29 to October 1, 2016 (**Figure 19 c–d**), until the stratification recovered to the original level (> 2.0°C m^{-1}) after October 2. Chl. *a* gradually increased due to the nutrient inflow from rivers after the typhoon passed (**Figure 19 e–f**). CDOM was diluted by 50.0% in YYL and approached 0.0 ppb (QSE) in TFL after Typhoon Megi (**Figure 19 e–f**). Wind speed and precipitation dramatically increased from September 26–28 (**Figure 19 g–h**), and the precipitation was around 369–583 mm d-1 (**Figure 19 i–j**), which contributed 10.0, and 11.1% of the annual precipitation at the YYL and TFL, respectively.

In YYL, the total water depth of the tracer was rapidly flushed, resulting water columns were well-mixed on days 2–3 in YYL (**Figure 20 b–d**). The water was renewed within the entire lake until day 4 in YYL (**Figure 20 e**). In TFL, the total water depth increased about 1.65 m from September 27 to 29 because TFL only has a seepage flow. The tracer was diluted by 25.0–35.0% in the entire lake on days 3 to 4 in TFL (**Figure 20 i–j**). The average t_r in TFL (22.3 days) was four times longer than YYL (5.3 days) (**Table 5**). Even during typhoon Megi, the results of numerical simulation showed that TFL had a longer t_r than YYL. We conjecture that C adjacent to the water surface remains high during the typhoon period. Due to the weaker stratification, typhoons significantly affect C by diluting high-concentration C from the bottom to the upper layer (**Figure 20**).

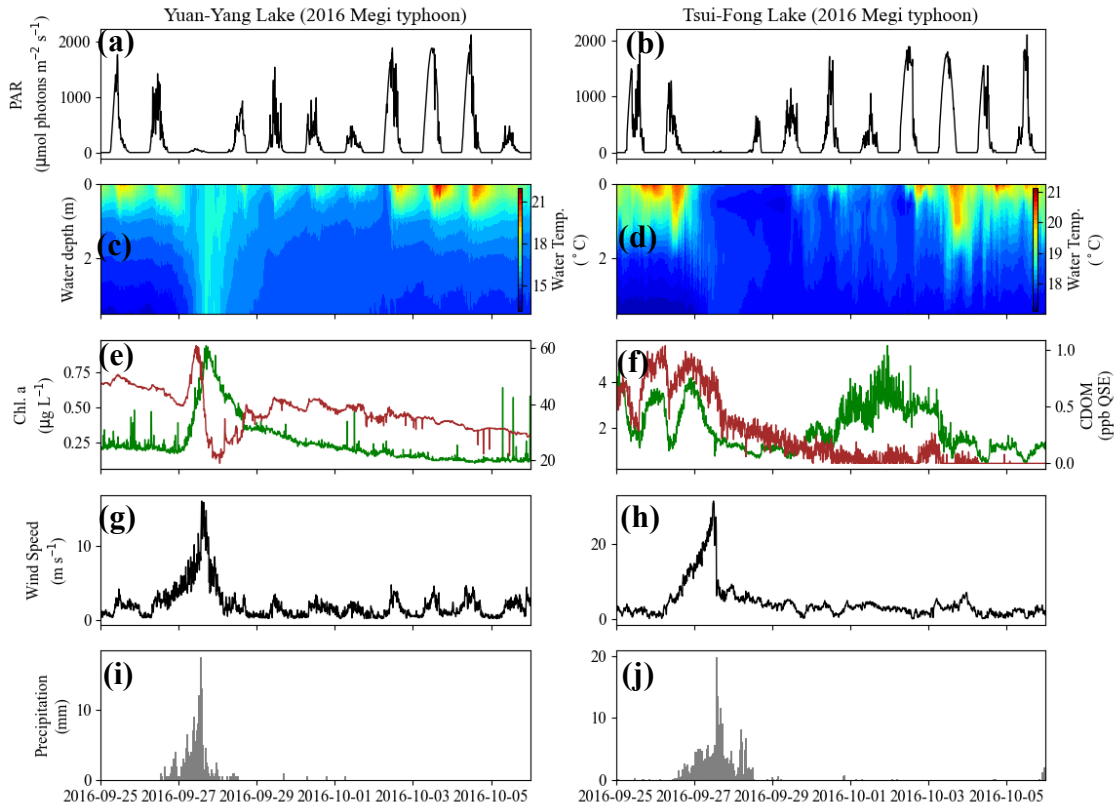

Figure 19. Data profile of **(a–b)** PAR, **(c–d)** water temperature, **(e–f)** Chl. *a* (green line), and CDOM (brown line) at 0.25 m water depth. **(g–h)** Wind speed at 10 m high (U_{10}), **(i-j)** precipitation in YYL and TFL during Typhoon Megi (September 25 to October 5, 2016). Data were captured every 10 min.

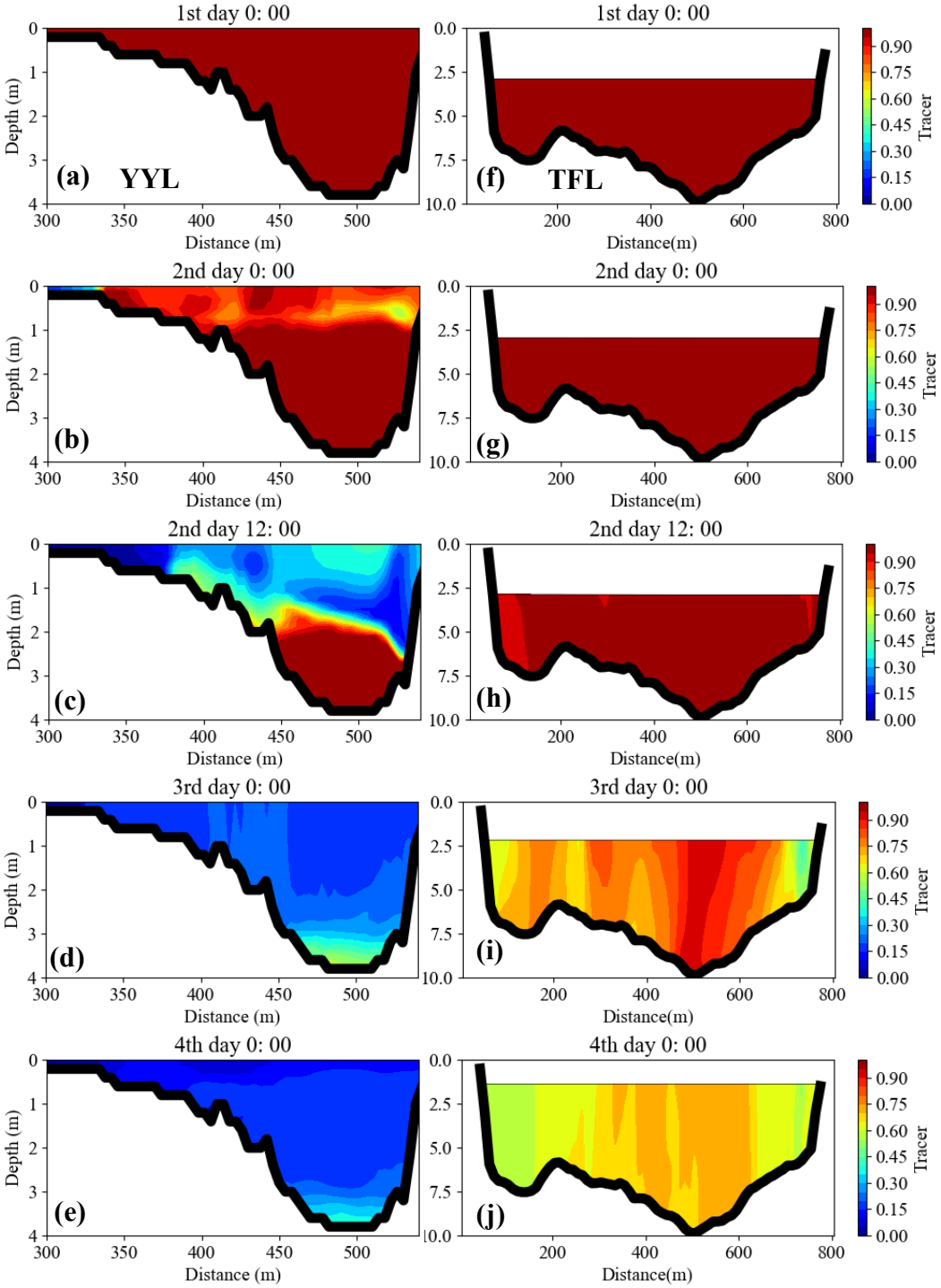

Figure 20. Vertical distribution of the tracer on **(a)** day 1 (1 d) 00:00 a.m., **(b)** 2 d 00:00 a.m., **(c)** 2 d 12:00 p.m., **(d)** 3 d 00:00 a.m., and **(e)** 4 d 00:00 a.m. in YYL, and **(f)** 1 d 00:00 a.m., **(g)** 2 d 00:00 a.m., **(h)** 2 d 12:00 p.m., **(i)** 3 d 00:00 a.m., and **(j)** 4 d 00:00 a.m. in TFL during Typhoon Megi from September 26–29, 2016. The horizontal coordinate shows the distance (m); the vertical coordinate shows the depth (m) from the water surface. Contour shows the concentration of the tracer

4. Discussion

This section shows the discussion and concludes the results. In the first part, we discussed the effect of thermal stratification on DIC and NEP in YYL (section 4.1). In the other part, we discussed the effects of typhoon disturbances and hydraulic retention on C flux in YYL and TFL (section 4.2).

4.1 Effect of thermal stratification on DIC and C fluxes in YYL

In YYL, the stratification was stable from spring to summer (mean N: 0.011 s^{-1} & 0.013 s^{-1}, respectively) than autumn to winter (mean N: 6.00×10^{-3} s^{-1} & 7.00×10^{-3} s^{-1}, respectively) (**Figure 8**). Even though the average irradiance (solar radiation) intensity was similar between spring and autumn, the stratification in autumn tended to be weaker than in spring due to the vertical mixing induced by the typhoons (**Figure 6** and **Figure 8**). In summer, irradiance was the strongest, resulting in the strong stratification, despite the typhoons (**Figure 8**). The significant density difference between the upper and lower layers inhibited the penetration of river inflow into the hypolimnion. Therefore, in spring and summer, water exchange between the upper and deeper layers was suppressed.

The DIC data showed that stable stratification inhibited the vertical transport from the lower to the upper layer, resulting in the upper layer ΔDIC being negative from spring to summer due to the predominance of photosynthesis (**Figure 7**). Additionally, the Brunt-Väisälä frequency was significantly associated with hypolimnion DIC (**Table 3** and **Figure 9 e**). These induced the upper layer NEP was positive from spring to summer, and lower layer NEP dramatically decreased from summer to autumn due to the weak stratification (**Figure 11**). Thus, the lower layer DIC produced was vertically transferred easily to the upper layer in autumn, resulting in the highest CO_2 emissions in YYL (**Table 4** and **Figure 11**). Since ecological production was the lowest in winter due to the low water temperature, the absolute value of NEP in the upper layer was smaller in winter than in autumn (**Figure 6 a** and **Figure 11**).

In general, the residence time is determined by stratification and inflow. The residence times from spring to summer were longer than autumn and winter due to the stable stratification. Although the rainfall intensity is higher in summer and autumn than in spring and winter, the inflow returns to the base flow immediately after the typhoons cease. Tsai et al. (2011) found that typhoons (precipitation) caused vertical mixing of the water column for up to 7–10 days after the typhoons. Hence, we assumed that the inflow was constant between seasons and thus expected there to be

no direct influence of precipitation on residence time at the seasonal timescale

We categorized the seasonal pattern of thermal stratification and vertical profiles of DIC in YYL (**Figure 21**). The strength of thermal stratification is expected to be the critical physical process controlling the vertical distribution of DIC. Although bottom layer (hypolimnion) DIC is very high due to the release of sediments from the lake bottom, strong stratification inhibits the vertical mixing of bottom DIC into the water surface layer (epilimnion). We investigated DIC and water temperature vertical profiles for 13 years in YYL. The results showed that the stratification is most intense from spring to summer, forming an apparent three-layer system. In contrast, the water column is weakly stratified in winter, and river flow intrudes in a layer adjacent to the water surface.

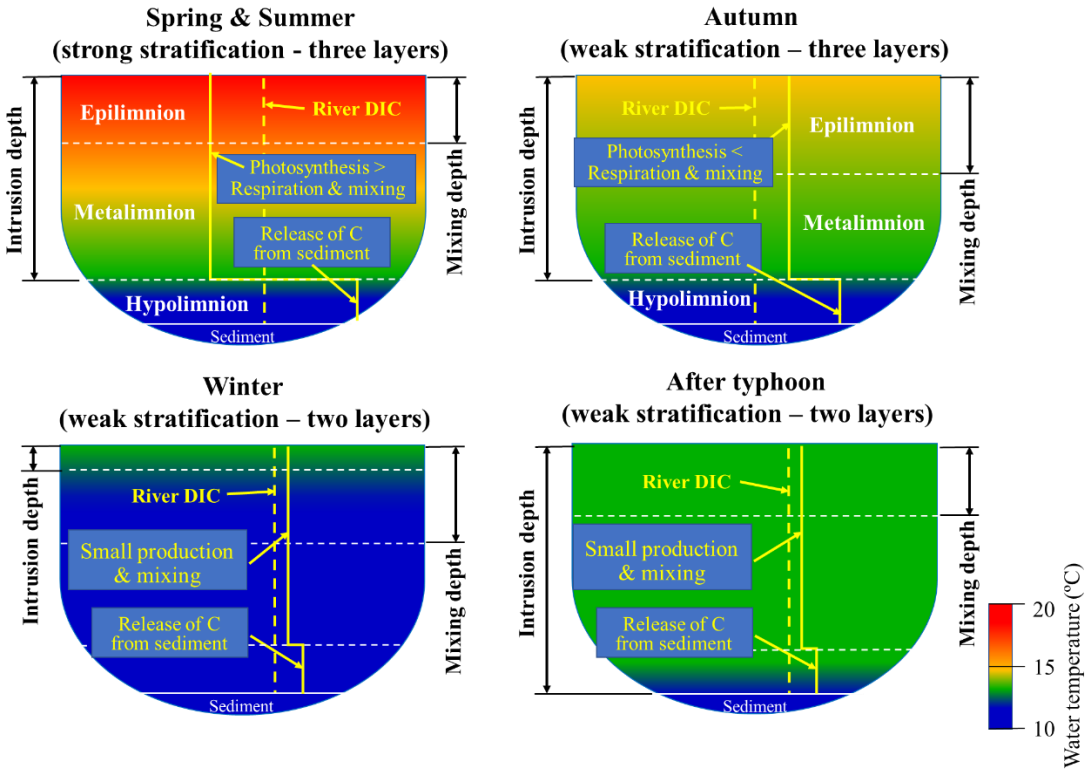

Figure 21. Schematic diagrams of stratification and DIC_R in **(a)** spring and summer, **(b)** autumn, **(c)** winter, and **(d)** after typhoons. The horizontal white-dash lines represent the thermocline, the vertical yellow lines represent the DIC_L, and the vertical yellow-dash lines represent DIC_R.

Kimura et al. (2012) showed that wind shear might be a vital factor inducing turbulent mixing in YYL. We compared the numerical simulations with and without wind stress and found that inflow is one of the main factors controlling residence time. However, we found that wind shear was not a key driver of vertical mixing on a seasonal scale because the wind speed was low during sampling dates. The average wind speeds were 0.70 ± 0.33, 1.15 ± 0.8, 1.11 ± 0.76, and 1.07 ± 0.51 m s^{-1} in spring, summer, autumn, and winter, respectively. Therefore, although the averages and standard deviations of wind speed from summer to autumn were higher than those in spring and winter, the residence times were mainly controlled by the intrusion depth of river flow, not wind speeds.

As a result, stratification in spring and summer is more substantial than in autumn and winter (**Figure 8 b**). In summer and spring, since the river water temperature is similar to that of the metalimnion and is higher than in the hypolimnion, river inflows were constrained in the metalimnion (**Figure 22 a–b**). Thus, the river intrusion cannot penetrate the hypolimnion due to strong stratification. In this case, only partial vertical mixing occurs between the metalimnion and epilimnion. In contrast, river water temperature is similar to that of the metalimnion or epilimnion (upper layer), and river inflows intrude into the upper layer in autumn and winter (**Figure 22 c–d**). Even though the intrusion occurs adjacent to the water surface or metalimnion, whole-lake mixing occurs because stratification is weak and vertical mixing is less suppressed. Therefore, autumn and winter have a shorter residence time than spring and summer, and stratification plays a key role in controlling the water renewal within lakes. This role can be evaluated precisely using a three-dimensional numerical simulation; this simulation method is more accurate for estimating residence time than using the total volume of a lake and river inflow. Consequently, it takes longer to renew hypolimnion water with river inflows.

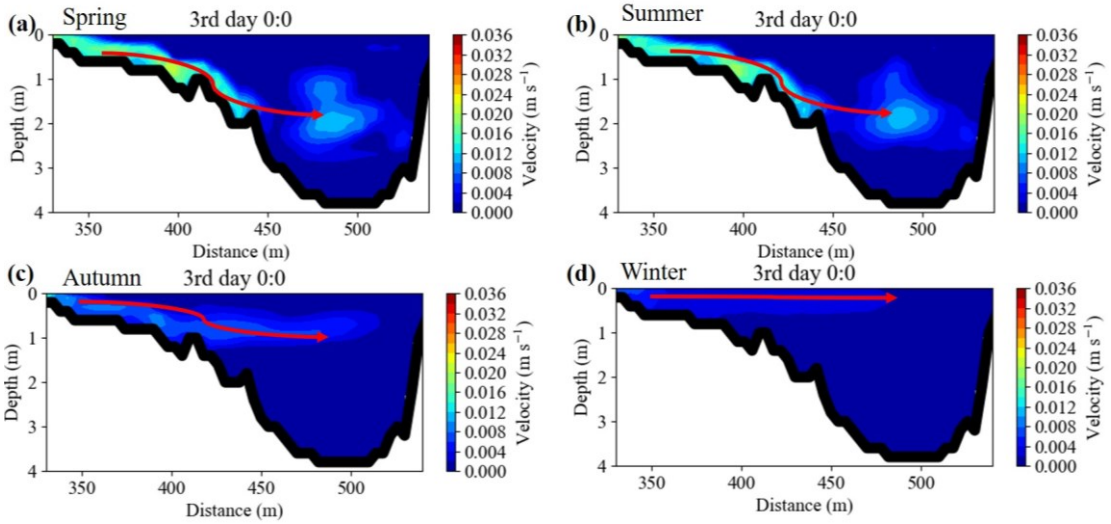

Figure 22. Vertical distribution of horizontal velocities on day 3 (00:00 a.m.) in (a) spring, (b) summer, (c) autumn, and (d) winter. The horizontal coordinate shows the distance from the northernmost end of YYL (m); the vertical coordinate shows the depth (m) from the water surface to the bottom. Contour shows the horizontal velocity (m s^{-1}).

Some previous studies demonstrated that thermal stratification was a significant driver of $pCO2$ and CO_2 fluxes (Åberg et al., 2010; Vachon and del Giorgio, 2014; Andersen et al., 2019). Our results (**Table 4**) showed that CO_2 emissions ranged from 131.2 to 207.4 mg CO_2 m^{-2} d^{-1}in YYL, which were confirmed to be similar to other shallow temperate lakes in previous studies (Aufdenkampe et al., 2011; Raymond et al., 2013). Notably, the mean F_{CO2} was lowest in summer because of the strong stratification (**Table 4**). Mean F_{CO2} was highest in autumn due to the supply of DIC from the lower to the upper layer under weak stratification (**Figure 5 c** and **Figure 7 c**). The significant standard deviation (SD) of DIC from summer to autumn was associated with a large SD in F_{CO2} due to high-frequency typhoons (**Table 6**). There were ten typhoon events in our dataset in summer and autumn (**Table 6**). Although the strength and frequency of typhoons differed between summer and autumn (**Table 6**), our results showed that the vertical profile of DIC and water temperature reflected a weak stratification after all typhoons (**Figure 5 b–f**). Each typhoon event led to considerable precipitation and river discharge events relative to the annual precipitation, so the stratification became weak after each typhoon (**Figure 5 e–f**). Kimura et al. (2012) applied the lake number (Robertson and Imberger, 1994, L_N) to quantify the vertical mixing in YYL and suggested that the water column was well-mixed ($L_N < 1$) during typhoons and the winter. Wind shear and convective mixing play a significant role in diurnal heat flux in lakes (Imberger, 1985). When typhoons mixed the water column, the heat flux from the air into the lake decreased dramatically in YYL (Kimura et al., 2014). Additionally, Czikowsky et al. (2018) demonstrated that the duration of well-mixed conditions due to storms was around 1 to 2 days in Lake Pleasant, which resulted in a 50% decrease in heat flux compared with the strongly stratified period. Previous studies suggested that storm events may impact CO_2 fluxes (Vachon and del Giorgio, 2014; Liu et al., 2016; Tonetta et al., 2017). Due to seasonal cooling-induced mixing, CO_2 emissions across the air-water interface are larger than storm-induced mixing (Czikowsky et al., 2018). Precipitation and storm events played a particularly vital role when they flushed large terrestrial DIC concentrations into the lake, releasing CO_2 and CH_4 (Hope et al., 2004; Vachon and del Giorgio, 2014; Bartosiewicz et al., 2015; Tonetta et al., 2017). Consequently, we suggest that both extensive loading of allochthonous C from the surrounding forest and storm events seasonally influence CO_2 emissions from shallow lakes (Sobek et al., 2003; Hope et al., 2004; Tsai et al., 2008; Shade et al., 2010; Chiu et al., 2020). Thus, we discussed the effects of typhoon disturbance on the C fluxes in the next section.

Table 6. Characteristics of precipitation and wind speed of summer and autumn typhoons from 2004 to 2017.

Typhoon Name	Date	Sampling date	Total precipitation (mm)	Maximum daily precipitation (mm)	Maximum wind speed ($m\ s^{-1}$)	Ranking
Summer typhoons (Total 56 typhoon events)						
201513SOUDELOR	7-9 Aug. 2015	-	355.5	304.0	49.7	3rd/81
200708SEPAT	16-19 Aug.2007	22-24 Aug.2007	266.2	129.6	27.8	16th/81
200417AERE	23-26 Aug.2004	31 Aug. 2004	283.9	232	34.1	4th/81
200509MATSA	3-6 Aug. 2005	9 Aug. 2005	227.4	127	31.2	18th/81
200505HAITANG	16-20 Jul. 2005	20 Jul.2005	248.7	120.5	36.8	20th /81
Autumn typhoons (Total 25 typhoon events)						
200813SINLAKU	12-15 Sep.2008	20 Sep. 2008	552	355.5	44.7	2nd /81
201013MEGI	21-23 Oct. 2010	25 Oct. 2010	501.9	356.5	16.6	1st /81
200513TALIM	1 Sep. 2005	5 Sep. 2005	149	149	39.5	13th /81
200712WIPHA	17-18 Sep. 2007	20 Sep. 2007	85.3	59.5	16.3	33th /81

The data come from the typhoon database of the Central Weather Bureau in Taiwan. The meteorological station is located in Yilan CWBT station (24°76'39" N, 121°75'65" E).

The ranking uses maximum daily precipitation of typhoons events. 201513SOUDELOR was the best ranking in summer.

4.2. Effects of typhoon disturbances on C flux in shallow subtropical lakes with different nutrient levels.

Overall, typhoon-induced mixing is one of the vital processes determining the seasonal patterns of water quality (DIC, DOC, and Chl. *a*) and their effect on C flux and NEP in shallow subtropical lakes. Typhoon disturbances and external C loading via rivers control the vertical distribution of C in lakes, resulting in that NEP decreasing during- and post-typhoon periods (**Figure 15**). The numerical simulations showed that the mean $\boldsymbol{t_r}$ was 5.30 and 22.3 days in YYL and TFL, respectively, according to base flow, meaning that the hydraulic retention between TFL and YYL is significantly different (**Table 5**). Thus, the magnitude of $\boldsymbol{t_r}$ may indicate that YYL (oligotrophic) and TFL (mesotrophic) had different regimes of ecosystem resilience as well.

4.2.1. Hydraulic retention effect on C flux

The strength of stratification varied considerably, indicating that a model can be applied in not only a stratified lake but also a well-mixed lake (**Figure 12 b** and **Figure 13 b**). Our two-layer model covers vertical flux between the upper and lower layers with entrainment velocities and the intrusion of river inflow into both the upper and lower layers. Therefore, a two-layer model in this study has a significant advantage in analyzing a weakly stratified lake, even a one-layer system, by giving large entrainment velocity and inflow into the lower layer in Equation (13). Note that the total water depth was greater than the thermistor chain (3.50 m) in TFL, and water temperature under 3.50 m in the hypolimnion was not measured, which suggests that the stratification strength estimated from **Figure 12 b** is weaker than the actual one. Additionally, the Wedderburn number and Lake number were confirmed to be large enough not to cause upwelling and turnover on normal days in TFL, even though wind speed is larger on TFL than YYL, so the stronger wind does not mean the occurrence of a weak stratification (Imberger, 1985; Shintani et al., 2010). The Wedderburn number is the parameter showing the magnitude of the upwelling scale inversely. Also, the Lake number is the parameter to predict the modal-type response, such as turnover in a whole lake (Robertson and Imberger, 1994).

We followed the NEP equation by equation (6) based on Nakayama et al. (2020a). Nakayama assumed that the water column was well-mixed and considered a target domain to be one box. However, section 4.1 demonstrated the importance of stratification on vertical mixing in YYL. According to previous studies, a two-layer assumption is acceptable for water quality analysis (Maruya et al., 2010; Nakayama and Imberger, 2010; Sato et al., 2012). The longer the residence time, the more

chemical transformations among DIC, DOC, and phytoplankton growth, which result in a high correlation among $pCO2$, DOC, and Chl. *a* due to photosynthesis and respiration (Carpenter et al., 1998; Sobek et al., 2003; Sobek et al., 2005; Dodds and Whiles, 2019) and mineralization (Aarnos et al., 2018; Allesson et al., 2020; Allesson et al., 2021). In addition, the residence time is a function of the total lake volume and river inflow. Our analysis of Typhoon Megi also showed that TFL had a longer $\boldsymbol{t_r}$ than YYL, even during a strong typhoon. We found that the significant point is whether outflow matches inflow in a shallow or small lake, as it takes more than one week for phytoplankton and planktic bacteria to grow after storm events (Padisák, 1993; Shade et al., 2011; Jennings et al., 2012; Chiu et al., 2020). The SEM analysis results also support our hypothesis (**Figure 17**) that Chl. *a* is one of the significant factors controlling $\boldsymbol{F_{CO2}}$. Therefore, it is necessary to clarify the physical processes needed to estimate $\boldsymbol{F_{CO2}}$ in a lake, such as hydraulic retention considering the photosynthesis effect due to phytoplankton (Nakayama et al., 2020b).The theoretical residence time, $\boldsymbol{t_r}'$ (equation (15)), tends to overestimate the actual $\boldsymbol{t_r}$ obtained using Fantom, as **Table 5** shows. For example, the simulated $\boldsymbol{t_r}$ was 39.0 d during a post-typhoon period in TFL, but the $\boldsymbol{t_r}'$ estimated by river inflow is 58.6 d. The $\boldsymbol{t_r}'$ overestimates by around 5.5–191% if the stratification is ignored in the whole lake based on a three-dimensions numerical model. Thus, we recommended that residence time be computed using a three-dimensional hydrological model. Although the NEP obtained by equation (6) uses epilimnion DIC and $\boldsymbol{F_{CO2}}$, equation (13) revealed that equation (6) indeed includes DIC flux from the lake bottom within the entire lake. Therefore, equation (6) is applicable enough to estimate NEP in an entire lake, even a stratified one.

Moreover, it is possible to predict future discharge and residence time changes under projected precipitation variations by using the general circulation model. Consequently, Equation (6) is promising to predict the long-term DIC variation in a subtropical shallow lake under the circumstance of climate change. Also, we can forecast the effect of global warming on C flux in a lake if the long-term meteorological dataset is available, for example, from 1990 to 2010. Even a dataset from 2000 to 2020 may assist in investigating the climate change effect on C flux in a lake.

4.2.2. Comparison of the F_{CO2} between lakes during storm events

We select to compare the F_{CO2} in the two lakes from this study with previous studies of shallow lakes during storms from tropical to temperate climate zones (**Table 7**). Overall, F_{CO2} increased during the post-storm period. F_{CO2} increased by 48–694% during the post-storm period (**Table 7**). It was demonstrated that the fall overturn is a vital process for mixing the water column, resulting in F_{CO2} increase after summer storms (Vachon and del Giorgio, 2014; Czikowsky et al., 2018). Our study showed that the post-storm period had the most considerable SD, 323 mg C m^{-2} d^{-1}, due to the intense precipitation (maximum rainfall was 678 mm $time^{-1}$ for the 2016 Typhoon Megi, **Figure 19 i–j**), strong winds (maximum U_{10} was 30 m s^{-1} for the 2016 Typhoon Megi, **Figure 19 g–h**), and short residence time (t_r') (**Table 7**). Zwart et al. (2017) suggested that the t_r' was not only related to the water renewal rates (hydraulic retention) but also negatively associated with terrestrial DOC (tDOC) during extreme rainstorms which may induce the increase in F_{CO2} during the post-storm period (**Table 5**). Chiu et al. (2020) found substantial colored dissolved organic matter (CDOM) and terrestrial dissolved organic matter (tDOM) loads into YYL and TFL, resulting in a dramatic increase in F_{CO2} after strong typhoons. The previous studies investigated storm events with a maximum rainfall of about 50 mm (**Table 7**), which is less than the subtropical storm event from Kossin et al. (2013).

The ecological respiration contributed 10–50% of the C flux in lakes from autotrophic organisms (Vachon et al., 2017). Our results showed that Chl. *a* is one of the significant factors controlling DIC during the pre- and post-typhoon periods in TFL (**Figure 17 b–c**). The Chl. *a* rapidly turned back to its original level until the next day during Typhoon Megi (**Figure 19 f**). Additionally, the DOC and total phosphorus (TP) are critical factors determining the trophic state and primary production in shallow lakes (Hanson et al., 2003; Tsai et al., 2008). In previous studies, TP was associated with algae biomass in TFL (Tsai et al., 2016; Chiu et al., 2020). Therefore, it may enhance the positive NEP from pre- to post-typhoon periods in a shallow mesotrophic lake (TFL) (**Figure 15**; **Table 7**). Conversely, the YYL depends on river discharge and allochthonous and autochthonous DOC load (Tsai et al., 2008; Chiu et al., 2020). Additionally, the planktic bacteria composition changes during typhoon events in YYL (Shade et al., 2010; Shade et al., 2011), impacting ecological respiration. Thus, hydraulic retention and typhoon disturbance are revealed to play a significant role in C flux patterns in an oligotrophic and mesotrophic lake.

Lake and watershed morphometries may be a key to predicting the CO_2 flux in lakes after storm events (Klug et al., 2012; Vachon and del Giorgio, 2014). For example, Klug et al. (2012) revealed that the ratio of Watershed Area (WA) and Lake

Volume (LV) (WA:LV) is correlated with typhoon disturbance: high WA:LV lakes are more sensitive to storms than the low WA:LV. In general, high WA:LV lakes tend to have higher lake water renewal rates during storm events (Klug et al., 2012; Vachon and del Giorgio, 2014). den Heyer and Kalff (1998) found that the higher the WA:LA, the shorter the $\boldsymbol{t_r}$, resulting in lower mineralization rates. In contrast, CO_2 dynamics with low WA:LV depend highly on internal production unless a strong typhoon comes (**Table 7**). Thus, the different responses of $\boldsymbol{F_{CO2}}$during storms depend on lake and watershed morphometries, such as $\boldsymbol{t_r}$ and storm intensity (den Heyer and Kalff, 1998; Klug et al., 2012; Vachon and del Giorgio, 2014; Zwart et al., 2017). In addition, our study revealed that $\boldsymbol{t_r}$ and typhoons are also vital factors impacting $\boldsymbol{F_{CO2}}$ in both lakes.

Table 7. Comparison of the F_{CO2} (mg C m^{-2} d^{-1}) between different shallow lakes (average water depth < 15 m) during post-storm events.

Lake Site	Location	Climate zone	Trophic State	Lake Area (ha)	Average Depth (m)	WA: LV*	Average t_r' (d)	Average F_{CO2} (SD)	Average F_{CO2} Post-storm (SD)	Storm Rainfall (mm $time^{-1}$)	Max. U_{10} (m s^{-1})	Reference
Nhecolândia, Brazil	15°-22°S, 55°-60°W	Tropical	Oligo. (Black)	0.087-0.093	~ 0.5	-	-	102.5	-	-	-	Barbiero et al. (2018)
			Meso. or Eutrophic (Green)	0.285-0.053		-	-	-229	~ -110	150	-	
Yuang-Yang, Taiwan	24.58° N, 121.40° E	Subtropical	Oligo. (humic)	3.6	4.4	3.37	10.4	145 (100)	210.5 (323)	330-678	8-15	This study
Tsui-Fong, Taiwan	24.52° N, 121.60° E	Subtropical	Meso.	8.0-25	4.8	4.2-15.5	31.9	-165.1 (55.2)	-96.5 (223)	330-678	10-30	This study
Pleasant, USA	43.48° N, 74.38° W	Temperate	Oligo.	600	8.0	-	-	276	342	-	8.0	Czikowsky et al., (2018)
Croche, Canada	45.99° N, 74.00° W	Temperate	Oligo.	6.3	6.0	0.95	170	88.7 (36.8)	616 (209)	30-50	4.0	Vachon and del Giorgio (2014)
Simoncouche, Canada	48.23° N, 71.25° W	Temperate	Oligo.	86.1	2.1	14.6	50	107.8 (65.7)	458.1 (181)	20-30	4.0	Vachon and del Giorgio (2014)

* shows the watershed area to lake volume ratio

4.2.3. C fluxes in shallow subtropical lakes

On the global scale, despite some previous studies showing the carbon emission in freshwater ecosystems, the small lakes were usually ignored that occupied around 1.25-1.75×10^6 km^2 of total lakes area (Downing et al. 2006; Verpoorter et al., 2014). In other words, these were underestimated around 7-33% of the total lakes (Cole et al. 2007; Raymond et al. 2013), if the average of $\boldsymbol{F_{CO2}}$ was 150 mg C m^{-2} d^{-1} in small lakes (**Table 7**), the small lakes released approximately 68.5-95.8 Tg C yr^{-1} to atmosphere. However, the magnitudes of $\boldsymbol{F_{CO2}}$ varied with different trophic lakes and regions (**Table 7**). Thus, we suggested that knowing the trophic states can be more accurate to estimate the global $\boldsymbol{F_{CO2}}$ in small lakes.

The DIC is the most critical parameter for $\boldsymbol{F_{CO2}}$ (**Figure 16**–**Figure 18**) and NEP (Bade et al., 2004). Significantly, the absolute value of $\boldsymbol{F_{CO2}}$ is 96–537% of NEP in YYL and 42–70% in TFL (**Figure 12 f**; **Figure 13 f**; **Figure 15**). Our results showed that $\boldsymbol{F_{CO2}}$ > NEP in two lakes revealed that most C was degassed to the atmosphere from the sediment or the river inputs. CO_2 or the other forms of C could be brought into the lake, contributing to the DIC level during rainy seasons by groundwater or surface flow (Vachon and del Giorgio, 2014; Chiu et al., 2020). Since NEP > 0 though $\boldsymbol{F_{CO2}}$ for the entire lake should be the same as NEP under no significant stratification. Therefore, the net ecosystem exchange (NEE) for the two-layer model is also following Equation (12), which assumes the organic matters production and respiration are predominant, but the other fluxes are negligible as following

$$\mathrm{NEE} = \frac{C_U Q_{in} \mathrm{DIC}_R - C_U Q_{out} \mathrm{DIC}_U - A_L F_{CO2}}{V_{total}} = \frac{V_U \alpha_{PU} Chl_U + V_L \alpha_{PL} Chl_L - A_B D_B}{V_{total}} \quad (16)$$

By using t_r',

$$\mathrm{NEE} = \frac{C_U(\mathrm{DIC}_R - \mathrm{DIC}_U)}{t_r'} - \frac{A_L}{V_{total}} F_{CO2} = \frac{V_U \alpha_{PU} Chl_U + V_L \alpha_{PL} Chl_L - A_B D_B}{V_{total}} \quad (17)$$

If the lake is not stratified, NEE should be the same as NEP for the entire lake. However, since t_r' overestimates the actual residence time (t_r, section 4.2.1), inducing NEE is smaller than NEP in a stratified lake. Thus, $\boldsymbol{F_{CO2}}$ for the entire lake tends to be smaller than NEP in a stratified lake when organic matters production and respiration are predominant in the ecosystem.

The SEM analysis results showed that mineralization might be essential for DIC and $\boldsymbol{F_{CO2}}$ (**Figure 8–9**). den Heyer and Kalff (1998) showed that organic matter and C mineralization at the water surface were three times higher than sediment C emission. On the other hand, our results showed that photo-mineralization was not associated with DIC (**Figure 16** and **Figure 17**) because the contribution of C emission may be < 10% in lakes (Tranvik et al., 2009; Vachon et al., 2017). In contrast to linear regression, the SEM analysis showed that the correlation among $pCO2$, DOC, and Chl. *a* was higher in TFL than YYL, suggesting that the SEM analysis is more suitable for analyzing the correlation paths than the one-to-one linear regression analysis.

The wind speed is one of the most significant parameters influencing $\boldsymbol{F_{CO2}}$ (**Table 1**). Moreover, Czikowsky et al. (2018) showed that wind speed is negatively correlated with $\boldsymbol{F_{CO2}}$ whenU_{10} < 4.0 m s^{-1} in a stratified temperate lake, similar to our results in TFL (**Figure 17** and **Figure 19 g**). However, the wind speed in YYL is not associated with $\boldsymbol{F_{CO2}}$ because wind speed in this lake was low—0.11 to 2.72 m s^{-1} (

Figure 18 h).

This study revealed that the hydraulic retention effect is critical for estimating NEP accurately in a stratified lake. Vertical mixing is a crucial physical process that decides the seasonal dynamics of C flux in shallow subtropical lakes (Chiu et al., 2020). However, the other processes may affect C flux in lakes, such as C burial and sedimentation (Cole et al., 2007; Mendonça et al., 2017; Bartosiewicz et al., 2019) demonstrated that organic C burial in sediment was 38.4–101 mg C m^{-2} d^{-1}, contributing approximately 20–40% of $\boldsymbol{F_{CO2}}$ in global lakes (Cole et al., 2007; Raymond et al., 2013). C burial primarily has a dramatic effect in strong thermal stratified lakes (Bartosiewicz et al., 2019) because the CDOC and CDOM rapidly increase via terrestrial DOC (tDOC) after extreme storm events (Read and Rose, 2013; Chiu et al., 2020). Our results show that the CDOM became diluted by 30–50% after Typhoon Megi (**Figure 19 e–f**). CDOM and tDOM are vital drivers that regulate metabolism and C flux in lakes (Staehr et al., 2010; Lapierre et al., 2013; Chiu et al., 2020), resulting in the NEP dramatically decreasing during strong typhoons (**Figure 15** and **Figure 19**). Additionally, the particulate organic C (POC) and DOC comprise 10–50% of total C fluxes in the lake ecosystem (Hope et al., 1994; Tranvik et al., 2009; Hanson et al., 2015). Moreover, the allochthonous and autochthonous C mostly come from tDOC and terrestrial POC (Tranvik et al., 2009; Hanson et al., 2015). The external C load contributes 20–50% of the C flux into the lakes (Vachon et al., 2017).

As a future scope, we suggest exploring the organic C load, mineralization rates, and C burial in sediment during typhoons to clarify total C fluxes' fate in shallow subtropical lakes. It could help us understand the total C fluxes' internal resilience and modulation under extreme weather events in a lake ecosystem. To clarify the

contributions of C fluxes in a future study, we suggested that a stable isotope analysis is needed to clarify the allochthonous and autochthonous C loading in YYL and TFL.

5. Conclusion

In this study, a conceptual equation is developed by the interval of DIC concentration between the lake and river inflow, considering hydraulic retention time (residence time) can be used to estimate the NEP as follows:

$$\mathrm{NEP} = \frac{(\mathrm{DIC}_R - \mathrm{DIC}_L)}{t_r} - \frac{A_L}{V_{total}} F_{CO2}$$

where DIC_R is the average DIC in river flows, DIC_L is the average vertical profile of DIC in a lake, t_r is the residence time, A_L is the lake surface area, V_{total} is the total lake volume, and F_{CO2} is the CO_2 emission across the air-water interface. Indeed, the thermal stratification and hydraulic retention effects are critical processes affecting C fluxes in shallow subtropical lakes. A three-dimensional numerical model helps to consider thermal stratification and hydraulic retention effects accuracy and can also calculate the NEP within whole-lake. In YYL, the thermal stratification was associated with the vertical distribution of DIC and seasonal NEP. We found that the stratification inhibits the vertical mixing of DIC between the upper and lower layers, resulting in the high concentration of DIC in the hypolimnion. In contrast, the vertical mixing is enhanced due to typhoons or turnover from autumn to winter, following the vertically uniform DIC profile. In YYL, primary production and ecological respiration are low, finding that the CO_2 emission across water surface into the atmosphere was positive values all year round. NEP in YYL decreased by 950 mg C m^3 d^{-1} from summer to autumn because the lower layer DIC produced was vertically transferred easily to the upper layer in autumn. In addition, NEP in YYL decreased by 107 % in the typhoon periods because inflow rapidly refreshes the lake water (t_r was 4.4 days). In contrast, the NEP in TFL decreased by 82.3% in the typhoon period because of the relatively long t_r of 39 days. Therefore, typhoon-induced mixing was a critical physical factor in deciding carbon flux in two lakes with different trophic levels. However, although the typhoon-induced mixing was a critical physical process to impact the seasonal C fluxes in shallow subtropical lakes, the plankton and bacterial growth rate and sediment C might also control the C fluxes in YYL and TFL. We also found that CO_2 emission across water surfaces into the atmosphere is critical to consider the shallow subtropical lakes. In general, the absolute values of $\boldsymbol{F_{CO2}}$were higher than NEP in YYL and TFL. The $\boldsymbol{F_{CO2}}$ could contribute around half to five times of NEP due to the allochthonous and autochthonous C loading during typhoon periods. Thus, clarifying these physical and biochemical processes can help us know C fluxes' fates in shallow subtropical lakes under extreme weather conditions and climate change.

Acknowledgments

First, I greatly thank professor K Nakayama for giving me helpful comments and supporting me during my doctoral progress. In addition, I thank professor T Shintani in Tokyo Metropolitan University for developing the three-dimensional hydrodynamic model (Fantom). Next, I also appreciate Dr. CY Chiu in Academia Sinica (Taiwan) and professor JW Tsai in China Medical University (Taiwan) for investigating data in research sites and some critical comments in this study. I thank BS Lin, YL Chou, YS Hsueh, JY Liu, YX Lan, ZY Wu, YJ Miao, and LC Jiang in Academia Sinica for assisting with water sample collection and chemical analysis.

References

Aarnos, H., Gélinas, Y., Kasurinen, V., Gu, Y., Puupponen, V.-M., and Vähätalo, A. V., Photochemical Mineralization of Terrigenous DOC to Dissolved Inorganic Carbon in Ocean. *Global Biogeochem. Cycles* **32**:**2**, 250–266 (2018). doi: 10.1002/2017GB005698.

Åberg, J., Jansson, M., and Jonsson, A., Importance of water temperature and thermal stratification dynamics for temporal variation of surface water CO_2 in a boreal lake. *J. Geophys. Res.* **115**:**G2**, G02024 (2010). doi: 10.1029/2009JG001085.

Adcroft, A., Hill, C., and Marshall, J., Representation of Topography by Shaved Cells in a Height Coordinate Ocean Model. *Mon. Wea. Rev.* **125**:**9**, 2293–2315 (1997). doi: 10.1175/1520-0493(1997)125<2293:ROTBSC>2.0.CO;2.

Allesson, L., Andersen, T., Dörsch, P., Eiler, A., Wei, J., and Hessen, D. O., Phosphorus Availability Promotes Bacterial DOC-Mineralization, but Not Cumulative CO2-Production. *Front. Microbiol.* **11**, 569879 (2020). doi: 10.3389/fmicb.2020.569879.

Allesson, L., Koehler, B., Thrane, J.-E., Andersen, T., and Hessen, D. O., The role of photomineralization for CO_2 emissions in boreal lakes along a gradient of dissolved organic matter. *Limnol Oceanogr* **66**:**1**, 158–170 (2021). doi: 10.1002/lno.11594.

Andersen, M. R., Kragh, T., Martinsen, K. T., Kristensen, E., and Sand-Jensen, K., The carbon pump supports high primary production in a shallow lake. *Aquat Sci* **81**:**2**, 1–11 (2019). doi: 10.1007/s00027-019-0622-7.

Aufdenkampe, A. K., Mayorga, E., Raymond, P. A., Melack, J. M., Doney, S. C., Alin, S. R., Aalto, R. E., and Yoo, K., Riverine coupling of biogeochemical cycles between land, oceans, and atmosphere. *Front. Ecol. Environ.* **9**:**1**, 53–60 (2011). doi: 10.1890/100014.

Bade, D. L., Carpenter, S. R., Cole, J. J., Hanson, P. C., and Hesslein, R. H., Controls of δ^{13}C-DIC in lakes: Geochemistry, lake metabolism, and morphometry. *Limnol. Oceanogr.* **49**:**4**, 1160–1172 (2004). doi: 10.4319/lo.2004.49.4.1160.

Bartosiewicz, M., Laurion, I., and MacIntyre, S., Greenhouse gas emission and storage in a small shallow lake. *Hydrobiologia* **757**:**1**, 101–115 (2015). doi: 10.1007/s10750-015-2240-2.

Bartosiewicz, M., Przytulska, A., Lapierre, J.-F., Laurion, I., Lehmann, M. F., and Maranger, R., Hot tops, cold bottoms: Synergistic climate warming and shielding

effects increase carbon burial in lakes. *Limnol Oceanogr* **4**:**5**, 132–144 (2019). doi: 10.1002/lol2.10117.

Belanger, T. V., and Korzun, E. A., Critique of Floating-Dome Technique for Estimating Reaeration Rates. *Journal of Environmental Engineering* **117**:**1**, 144–150 (1991). doi: 10.1061/(ASCE)0733-9372(1991)117:1(144).

Boehrer, B., and Schultze, M., Stratification of lakes. *Rev. Geophys.* **46**:**2** (2008). doi: 10.1029/2006RG000210.

Cai, W.-J., and Wang, Y., The chemistry, fluxes, and sources of carbon dioxide in the estuarine waters of the Satilla and Altamaha Rivers, Georgia. *Limnol Oceanogr* **43**:**4**, 657–668 (1998). doi: 10.4319/lo.1998.43.4.0657.

Carpenter, S. R., Cole, J. J., Kitchell, J. F., and Pace, M. L., Impact of dissolved organic carbon, phosphorus, and grazing on phytoplankton biomass and production in experimental lakes. *Limnol Oceanogr* **43**:**1**, 73–80 (1998). doi: 10.4319/lo.1998.43.1.0073.

Chang, S.-C., Wang, C.-P., Feng, C.-M., Rees, R., Hell, U., and Matzner, E., Soil fluxes of mineral elements and dissolved organic matter following manipulation of leaf litter input in a Taiwan Chamaecyparis forest. *Forest Ecology and Management* **242**:**2-3**, 133–141 (2007). doi: 10.1016/j.foreco.2007.01.025.

Chiu, C.-Y., Jones, J. R., Rusak, J. A., Lin, H.-C., Nakayama, K., Kratz, T. K., Liu, W.-C., Tang, S.-L., and Tsai, J.-W., Terrestrial loads of dissolved organic matter drive inter-annual carbon flux in subtropical lakes during times of drought. *The Science of the total environment* **717**, 137052 (2020). doi: 10.1016/j.scitotenv.2020.137052.

Cole, J. J., and Caraco, N. F., Atmospheric exchange of carbon dioxide in a low-wind oligotrophic lake measured by the addition of SF 6. *Limnol. Oceanogr.* **43**:**4**, 647–656 (1998). doi: 10.4319/lo.1998.43.4.0647.

Cole, J. J., Caraco, N. F., Kling, G. W., and Kratz, T. K., Carbon dioxide supersaturation in the surface waters of lakes. *Science* **265**:**5178**, 1568–1570 (1994). doi: 10.1126/science.265.5178.1568.

Cole, J. J., Prairie, Y. T., Caraco, N. F., McDowell, W. H., Tranvik, L. J., Striegl, R. G., Duarte, C. M., Kortelainen, P. L., Downing, J. A., Middelburg, J. J., and Melack, J. M., Plumbing the Global Carbon Cycle: Integrating Inland Waters into the Terrestrial Carbon Budget. *Ecosystems* **10**:**1**, 172–185 (2007). doi: 10.1007/s10021-006-9013-8.

Czikowsky, M. J., MacIntyre, S., Tedford, E. W., Vidal, J., and Miller, S. D., Effects of Wind and Buoyancy on Carbon Dioxide Distribution and Air-Water Flux of a Stratified Temperate Lake. *J. Geophys. Res.* **123**:**8**, 2305–2322 (2018). doi: 10.1029/2017JG004209.

del Giorgio, P. A., Cole, J. J., Caraco, N. F., and Peters, R. H., Linking planktonic biomass and metabolism to net gas fluxes in northern temperate lakes. *Ecology* **80**:**4**, 1422–1431 (1999). doi: 10.1890/0012-9658(1999)080[1422:LPBAMT]2.0.CO;2.

den Heyer, C., and Kalff, J., Organic matter mineralization rates in sediments: A within- and among-lake study. *Limnol. Oceanogr.* **43**:**4**, 695–705 (1998). doi: 10.4319/lo.1998.43.4.0695.

Dodds, W. K., and Whiles, M. R., Freshwater ecology, *Concepts and environmental applications of limnology*, Academic Press, an imprint of Elsevier, Amsterdam (Netherlands), Boston (Mass.), Heidelberg (Germany), 1 online resource (2019). ISBN: 9780128132562.

Doubek, J. P., Anneville, O., Dur, G., Lewandowska, A. M., Patil, V. P., Rusak, J. A., Salmaso, N., Seltmann, C. T., Straile, D., Urrutia-Cordero, P., Venail, P., Adrian, R., Alfonso, M. B., DeGasperi, C. L., de Eyto, E., Feuchtmayr, H., Gaiser, E. E., Girdner, S. F., Graham, J. L., Grossart, H.-P., Hejzlar, J., Jacquet, S., Kirillin, G., Llames, M. E., Matsuzaki, S.-I. S., Nodine, E. R., Piccolo, M. C., Pierson, D. C., Rimmer, A., Rudstam, L. G., Sadro, S., Swain, H. M., Thackeray, S. J., Thiery, W., Verburg, P., Zohary, T., and Stockwell, J. D., The extent and variability of storm-induced temperature changes in lakes measured with long-term and high-frequency data. *Limnol. Oceanogr.* **66**:**5**, 1979–1992 (2021). doi: 10.1002/lno.11739.

Downing, J. A., Prairie, Y. T., Cole, J. J., Duarte, C. M., Tranvik, L. J., Striegl, R. G., McDowell, W. H., Kortelainen, P. L., Caraco, N. F., Melack, J. M., and Middelburg, J. J., The global abundance and size distribution of lakes, ponds, and impoundments. *Limnol. Oceanogr.* **51**:**5**, 2388–2397 (2006). doi: 10.4319/lo.2006.51.5.2388.

Duarte, C. M., and Cebrián, J., The fate of marine autotrophic production. *Limnol. Oceanogr.* **41**:**8**, 1758–1766 (1996). doi: 10.4319/lo.1996.41.8.1758.

Duarte, C. M., and Krause-Jensen, D., Export from Seagrass Meadows Contributes to Marine Carbon Sequestration. *Front. Mar. Sci.* **4** (2017). doi: 10.3389/fmars.2017.00013.

Einsele, G., Atmospheric carbon burial in modern lake basins and its significance for the global carbon budget. *Global and Planetary Change* **30**:**3-4**, 167–195 (2001). doi: 10.1016/S0921-8181(01)00105-9.

Groeneveld, M., Tranvik, L., Natchimuthu, S., and Koehler, B., Photochemical mineralisation in a boreal brown water lake: considerable temporal variability and minor contribution to carbon dioxide production. *Biogeosciences* **13**:**13**, 3931–3943 (2016). doi: 10.5194/bg-13-3931-2016.

Gudasz, C., Bastviken, D., Steger, K., Premke, K., Sobek, S., and Tranvik, L. J., Temperature-controlled organic carbon mineralization in lake sediments. *Nature* **466**:**7305**, 478–481 (2010). doi: 10.1038/nature09186.

Hanson, P. C., Bade, D. L., Carpenter, S. R., and Kratz, T. K., Lake metabolism: Relationships with dissolved organic carbon and phosphorus. *Limnol Oceanogr* **48**:**3**, 1112–1119 (2003). doi: 10.4319/lo.2003.48.3.1112.

Hanson, P. C., Pace, M. L., Carpenter, S. R., Cole, J. J., and Stanley, E. H., Integrating Landscape Carbon Cycling: Research Needs for Resolving Organic Carbon Budgets of Lakes. *Ecosystems* **18**:**3**, 363–375 (2015). doi: 10.1007/s10021-014-9826-9.

Holgerson, M. A., and Raymond, P. A., Large contribution to inland water CO_2 and CH_4 emissions from very small ponds. *Nat. Geosci.* **9**:**3**, 222–226 (2016). doi: 10.1038/ngeo2654.

Hope, D., Billett, M. F., and Cresser, M. S., A review of the export of carbon in river water: Fluxes and processes. *Environmental Pollution* **84**:**3**, 301–324 (1994). doi: 10.1016/0269-7491(94)90142-2.

Hope, D., Kratz, T. K., and Riera, J. L., Relationship between and Dissolved Organic Carbon in Northern Wisconsin Lakes. *J. environ. qual.* **25**:**6**, 1442–1445 (1996). doi: 10.2134/jeq1996.00472425002500060039x.

Hope, D., Palmer, S. M., Billett, M. F., and Dawson, J. J. C., Variations in dissolved CO2 and CH4 in a first-order stream and catchment: an investigation of soil-stream linkages. *Hydrol. Process.* **18**:**17**, 3255–3275 (2004). doi: 10.1002/hyp.5657.

Igolkina, A. A., and Meshcheryakov, G., semopy: A Python Package for Structural Equation Modeling. *Structural Equation Modeling: A Multidisciplinary Journal* **27**:**6**, 952–963 (2020). doi: 10.1080/10705511.2019.1704289.

Imberger, J., The diurnal mixed layer. *Limnol. Oceanogr.* **30**:**4**, 737–770 (1985). doi:

10.4319/lo.1985.30.4.0737.

Imboden, D. M., and Wüest, A., Physics and chemistry of lakes, *Mixing Mechanisms in Lakes*, Springer Berlin Heidelberg (1995). doi: 10.1007/978-3-642-85132-2_4.

Intergovernmental Panel on Climate Change (IPCC), Carbon and Other Biogeochemical Cycles, *Climate Change 2013 – The Physical Science Basis: Working Group I Contribution to the Fifth Assessment Report of the Intergovernmental Panel on Climate Change*, Cambridge University Press, Cambridge, 465-570 (2014). doi: 10.1017/CBO9781107415324.015.

Jähne, B., Münnich, K. O., Bösinger, R., Dutzi, A., Huber, W., and Libner, P., On the parameters influencing air-water gas exchange. *J. Geophys. Res.* **92**:**C2**, 1937 (1987). doi: 10.1029/JC092iC02p01937.

Jennings, E., Jones, S. E., Arvola, L., Staehr, P. A., Gaiser, E. E., Jones, I. D., Weathers, K. C., Weyhenmeyer, G. A., Chiu, C.-Y., and de Eyto, E., Effects of weather-related episodic events in lakes: an analysis based on high-frequency data. *Freshwater Biology* **57**:**3**, 589–601 (2012). doi: 10.1111/j.1365-2427.2011.02729.x.

Jones, S. E., Kratz, T. K., Chiu, C.-Y., and McMahon, K. D., Influence of typhoons on annual CO_2 flux from a subtropical, humic lake. *Global Change Biology* **15**:**1**, 243–254 (2009). doi: 10.1111/j.1365-2486.2008.01723.x.

Kimura, N., Liu, W.-C., Chiu, C.-Y., and Kratz, T., The influences of typhoon-induced mixing in a shallow lake. *Lakes & Reservoirs: Research & Management* **17**:**3**, 171–183 (2012). doi: 10.1111/j.1440-1770.2012.00509.x.

Kimura, N., Liu, W.-C., Chiu, C.-Y., and Kratz, T. K., Assessing the effects of severe rainstorm-induced mixing on a subtropical, subalpine lake. *Environ Monit Assess* **186**:**5**, 3091–3114 (2014). doi: 10.1007/s10661-013-3603-7.

Klug, J. L., Richardson, D. C., Ewing, H. A., Hargreaves, B. R., Samal, N. R., Vachon, D., Pierson, D. C., Lindsey, A. M., O'Donnell, D. M., Effler, S. W., and Weathers, K. C., Ecosystem effects of a tropical cyclone on a network of lakes in northeastern North America. *Environmental science & technology* **46**:**21**, 11693–11701 (2012). doi: 10.1021/es302063v.

Kortelainen, P. L., Rantakari, M., Huttunen, J. T., Mattsson, T., Alm, J., Juutinen, S., Larmola, T., Silvola, J., and Martikainen, P. J., Sediment respiration and lake trophic state are important predictors of large CO 2 evasion from small boreal lakes. *Global Change Biology* **12**:**8**, 1554–1567 (2006). doi: 10.1111/j.1365-2486.2006.01167.x.

Kossin, J. P., Olander, T. L., and Knapp, K. R., Trend Analysis with a New Global Record of Tropical Cyclone Intensity. *Journal of Climate* **26**:**24**, 9960–9976 (2013). doi: 10.1175/JCLI-D-13-00262.1.

Kraemer, B. M., Anneville, O., Chandra, S., Dix, M., Kuusisto, E., Livingstone, D. M., Rimmer, A., Schladow, S. G., Silow, E., Sitoki, L. M., Tamatamah, R., Vadeboncoeur, Y., and McIntyre, P. B., Morphometry and average temperature affect lake stratification responses to climate change. *Geophys. Res. Lett.* **42**:**12**, 4981–4988 (2015). doi: 10.1002/2015GL064097.

Lai, I.-L., Chang, S.-C., Lin, P.-H., Chou, C.-H., and Wu, J.-T., Climatic Characteristics of the Subtropical Mountainous Cloud Forest at the Yuanyang Lake Long-Term Climatic Characteristics of the Subtropical Mountainous Cloud Forest at the Yuanyang Lake Long-Term Ecological Research Site, Taiwan. *Taiwania* **51**:**4**, 317–329 (2006). doi: 10.6165/tai.2006.51(4).317.

Laniak, G. F., Olchin, G., Goodall, J., Voinov, A., Hill, M., Glynn, P., Whelan, G., Geller, G., Quinn, N., Blind, M., Peckham, S., Reaney, S., Gaber, N., Kennedy, R., and Hughes, A., Integrated environmental modeling: A vision and roadmap for the future. *Environmental Modelling & Software* **39**, 3–23 (2013). doi: 10.1016/j.envsoft.2012.09.006.

Lapierre, J.-F., Guillemette, F., Berggren, M., and del Giorgio, P. A., Increases in terrestrially derived carbon stimulate organic carbon processing and CO_2 emissions in boreal aquatic ecosystems. *Nature communications* **4**, 2972 (2013). doi: 10.1038/ncomms3972.

Lauerwald, R., Laruelle, G. G., Hartmann, J., Ciais, P., and Regnier, P. A., Spatial patterns in CO_2 evasion from the global river network. *Global Biogeochem. Cycles* **29**:**5**, 534–554 (2015). doi: 10.1002/2014GB004941.

Liu, H., Zhang, Q., Katul, G. G., Cole, J. J., Chapin, F. S., and MacIntyre, S., Large CO 2 effluxes at night and during synoptic weather events significantly contribute to CO 2 emissions from a reservoir. *Environ. Res. Lett.* **11**:**6**, 64001 (2016). doi: 10.1088/1748-9326/11/6/064001.

MacIntyre, S., Vertical mixing in a shallow, eutrophic lake: Possible consequences for the light climate of phytoplankton. *Limnol. Oceanogr.* **38**:**4**, 798–817 (1993). doi: 10.4319/lo.1993.38.4.0798.

MacIntyre, S., Bastviken, D., Arneborg, L., Crowe, A. T., Karlsson, J., Andersson, A., Gålfalk, M., Rutgersson, A., Podgrajsek, E., and Melack, J. M., Turbulence in a small boreal lake: Consequences for air-water gas exchange. *Limnol. Oceanogr.*

66:**3**, 827–854 (2021). doi: 10.1002/lno.11645.

MacIntyre, S., Eugster, W., and Kling, G. W., The Critical Importance of Buoyancy Flux for Gas Flux Across the Air-Water Interface. *Geophysical Monograph Series* **127**, 135–139 (2002). doi: 10.1029/GM127p0135.

Macreadie, P. I., Anton, A., Raven, J. A., Beaumont, N., Connolly, R. M., Friess, D. A., Kelleway, J. J., Kennedy, H., Kuwae, T., Lavery, P. S., Lovelock, C. E., Smale, D. A., Apostolaki, E. T., Atwood, T. B., Baldock, J., Bianchi, T. S., Chmura, G. L., Eyre, B. D., Fourqurean, J. W., Hall-Spencer, J. M., Huxham, M., Hendriks, I. E., Krause-Jensen, D., Laffoley, D., Luisetti, T., Marbà, N., Masque, P., McGlathery, K. J., Megonigal, J. P., Murdiyarso, D., Russell, B. D., Santos, R., Serrano, O., Silliman, B. R., Watanabe, K., and Duarte, C. M., The future of Blue Carbon science. *Nat Commun* **10**:**1**, 3998 (2019). doi: 10.1038/s41467-019-11693-w.

Maruya, Y., Nakayama, K., Shintani, T., and Yonemoto, M., Evaluation of entrainment velocity induced by wind stress in a two-layer system. *Hydrological Research Letters* **4**, 70–74 (2010). doi: 10.3178/hrl.4.70.

Mendonça, R., Müller, R. A., Clow, D., Verpoorter, C., Raymond, P., Tranvik, L. J., and Sobek, S., Organic carbon burial in global lakes and reservoirs. *Nat Commun* **8**:**1**, 1694 (2017). doi: 10.1038/s41467-017-01789-6.

Nakamoto, A., Nakayama, K., Shintani, T., Maruya, Y., Komai, K., Ishida, T., and Makiguchi, Y., Adaptive management in Kushiro Wetland in the context of salt wedge intrusion due to sea level rise. *Hydrological Research Letters* **7**:**1**, 1–5 (2013). doi: 10.3178/hrl.7.1.

Nakayama, K., and Imberger, J., Residual circulation due to internal waves shoaling on a slope. *Limnol Oceanogr* **55**:**3**, 1009–1023 (2010). doi: 10.4319/lo.2010.55.3.1009.

Nakayama, K., Komai, K., Tada, K., Lin, H.-C., Yajima, H., Yano, S., Hipsey, M. R., and Tsai, J.-W., Modeling dissolved inorganic carbon considering submerged aquatic vegetation. *Ecological Modelling* **431**, 109188 (2020a). doi: 10.1016/j.ecolmodel.2020.109188.

Nakayama, K., Shintani, T., Kokubo, K., Kakinuma, T., Maruya, Y., Komai, K., and Okada, T., Residual currents over a uniform slope due to breaking of internal waves in a two-layer system. *J. Geophys. Res.* **117**:**C10**, n/a-n/a (2012). doi: 10.1029/2012JC008155.

Nakayama, K., Shintani, T., Komai, K., Nakagawa, Y., Tsai, J. W., Sasaki, D., Tada, K., Moki, H., Kuwae, T., Watanabe, K., and Hipsey, M. R., Integration of

Submerged Aquatic Vegetation Motion Within Hydrodynamic Models. *Water Resour. Res.* **56**:**8**, e2020WR027369 (2020b). doi: 10.1029/2020WR027369.

Nakayama, K., Shintani, T., Shimizu, K., Okada, T., Hinata, H., and Komai, K., Horizontal and residual circulations driven by wind stress curl in Tokyo Bay. *J. Geophys. Res. Oceans* **119**:**3**, 1977–1992 (2014). doi: 10.1002/2013JC009396.

Nellemann, C., Blue carbon, *The role of healthy oceans in binding carbon : a rapid response assessment*, GRID-Arendal, Arendal [Norway], 78 (2009). ISBN: 9788277010601.

Ojala, A., Bellido, J. L., Tulonen, T., Kankaala, P., and Huotari, J., Carbon gas fluxes from a brown-water and a clear-water lake in the boreal zone during a summer with extreme rain events. *Limnol. Oceanogr.* **56**:**1**, 61–76 (2011). doi: 10.4319/lo.2011.56.1.0061.

Ortega, A., Geraldi, N. R., Alam, I., Kamau, A. A., Acinas, S. G., Logares, R., Gasol, J. M., Massana, R., Krause-Jensen, D., and Duarte, C. M., Important contribution of macroalgae to oceanic carbon sequestration. *Nat. Geosci.* **12**:**9**, 748–754 (2019). doi: 10.1038/s41561-019-0421-8.

Padisák, J., The influence of different disturbance frequencies on the species richness, diversity and equitability of phytoplankton in shallow lakes. *Hydrobiologia* **249**:**1-3**, 135–156 (1993). doi: 10.1007/BF00008850.

Plummer, L., and Busenberg, E., The solubilities of calcite, aragonite and vaterite in CO_2-H_2O solutions between 0 and 90°C, and an evaluation of the aqueous model for the system $CaCO_3$-CO_2-H_2O. *Geochimica et Cosmochimica Acta* **46**:**6**, 1011–1040 (1982). doi: 10.1016/0016-7037(82)90056-4.

Raymond, P. A., Caraco, N. F., and Cole, J. J., Carbon Dioxide Concentration and Atmospheric Flux in the Hudson River. *Estuaries* **20**:**2**, 381 (1997). doi: 10.2307/1352351.

Raymond, P. A., Hartmann, J., Lauerwald, R., Sobek, S., McDonald, C., Hoover, M., Butman, D., Striegl, R. G., Mayorga, E., Humborg, C., Kortelainen, P. L., Dürr, H., Meybeck, M., Ciais, P., and Guth, P., Global carbon dioxide emissions from inland waters. *Nature* **503**:**7476**, 355–359 (2013). doi: 10.1038/nature12760.

Read, J. S., Hamilton, D. P., Desai, A. R., Rose, K. C., MacIntyre, S., Lenters, J. D., Smyth, R. L., Hanson, P. C., Cole, J. J., Staehr, P. A., Rusak, J. A., Pierson, D. C., Brookes, J. D., Laas, A., and Wu, C. H., Lake-size dependency of wind shear and convection as controls on gas exchange. *Geophys. Res. Lett.* **39**:**9**, n/a-n/a (2012). doi: 10.1029/2012GL051886.

Read, J. S., and Rose, K. C., Physical responses of small temperate lakes to variation in dissolved organic carbon concentrations. *Limnol Oceanogr* **58**:**3**, 921–931 (2013). doi: 10.4319/lo.2013.58.3.0921.

Robertson, D. M., and Imberger, J., Lake Number, a Quantitative Indicator of Mixing Used to Estimate Changes in Dissolved Oxygen. *Int. Revue ges. Hydrobiol. Hydrogr.* **79**:**2**, 159–176 (1994). doi: 10.1002/iroh.19940790202.

Sato, C., Nakayama, K., and Furukawa, K., Contributions of wind and river effects on DO concentration in Tokyo Bay. *Estuarine, Coastal and Shelf Science* **109**, 91–97 (2012). doi: 10.1016/j.ecss.2012.05.023.

Scully, N. M., McQueen, D. J., and Lean, D. R. S., Hydrogen peroxide formation: The interaction of ultraviolet radiation and dissolved organic carbon in lake waters along a 43-75°N gradient. *Limnol Oceanogr* **41**:**3**, 540–548 (1996). doi: 10.4319/lo.1996.41.3.0540.

Shade, A., Chiu, C.-Y., and McMahon, K. D., Seasonal and episodic lake mixing stimulate differential planktonic bacterial dynamics. *Microb Ecol* **59**:**3**, 546–554 (2010). doi: 10.1007/s00248-009-9589-6.

Shade, A., Read, J. S., Welkie, D. G., Kratz, T. K., Wu, C. H., and McMahon, K. D., Resistance, resilience and recovery: aquatic bacterial dynamics after water column disturbance. *Environmental microbiology* **13**:**10**, 2752–2767 (2011). doi: 10.1111/j.1462-2920.2011.02546.x.

Smith, S. V., Physical, chemical and biological characteristics* of CO_2 gas flux across the air-water interface. *Plant Cell Environ* **8**:**6**, 387–398 (1985). doi: 10.1111/j.1365-3040.1985.tb01674.x.

Sobek, S., Algesten, G., Bergström, A.-K., Jansson, M., and Tranvik, L. J., The catchment and climate regulation of pCO_2 in boreal lakes. *Global Change Biology* **9**:**4**, 630–641 (2003). doi: 10.1046/j.1365-2486.2003.00619.x.

Sobek, S., Tranvik, L. J., and Cole, J. J., Temperature independence of carbon dioxide supersaturation in global lakes. *Global Biogeochem. Cycles* **19**:**2**, n/a-n/a (2005). doi: 10.1029/2004GB002264.

Staehr, P. A., and Sand-Jensen, K., Temporal dynamics and regulation of lake metabolism. *Limnol Oceanogr* **52**:**1**, 108–120 (2007). doi: 10.4319/lo.2007.52.1.0108.

Striegl, R. G., and Michmerhuizen, C. M., Hydrologic influence on methane and carbon dioxide dynamics at two north-central Minnesota lakes. *Limnol Oceanogr*

43:**7**, 1519–1529 (1998). doi: 10.4319/lo.1998.43.7.1519.

Tonetta, D., Staehr, P. A., and Petrucio, M. M., Changes in CO_2 dynamics related to rainfall and water level variations in a subtropical lake. *Hydrobiologia* **794**:**1**, 109–123 (2017). doi: 10.1007/s10750-017-3085-7.

Tranvik, L. J., Availability of dissolved organic carbon for planktonic bacteria in oligotrophic lakes of differing humic content. *Microb Ecol* **16**:**3**, 311–322 (1988). doi: 10.1007/BF02011702.

Tranvik, L. J., Downing, J. A., Cotner, J. B., Loiselle, S. A., Striegl, R. G., Ballatore, T. J., Dillon, P., Finlay, K., Fortino, K., Knoll, L. B., Kortelainen, P. L., Kutser, T., Larsen, S., Laurion, I., Leech, D. M., McCallister, S. L., McKnight, D. M., Melack, J. M., Overholt, E., Porter, J. A., Prairie, Y., Renwick, W. H., Roland, F., Sherman, B. S., Schindler, D. W., Sobek, S., Tremblay, A., Vanni, M. J., Verschoor, A. M., Wachenfeldt, E. von, and Weyhenmeyer, G. A., Lakes and reservoirs as regulators of carbon cycling and climate. *Limnol. Oceanogr.* **54**:**6part2**, 2298–2314 (2009). doi: 10.4319/lo.2009.54.6_part_2.2298.

Tsai, J.-W., Kratz, T. K., Hanson, P. C., Kimura, N., Liu, W.-C., Lin, F.-P., Chou, H.-M., Wu, J.-T., and Chiu, C.-Y., Metabolic changes and the resistance and resilience of a subtropical heterotrophic lake to typhoon disturbance. *Can. J. Fish. Aquat. Sci.* **68**:**5**, 768–780 (2011). doi: 10.1139/f2011-024.

Tsai, J.-W., Kratz, T. K., Hanson, P. C., Wu, J.-T., Chang, W. Y. B., Arzberger, P. W., Lin, B.-S., Lin, F.-P., Chou, H.-M., and Chiu, C.-Y., Seasonal dynamics, typhoons and the regulation of lake metabolism in a subtropical humic lake. *Freshwater Biology* **53**:**10**, 1929–1941 (2008). doi: 10.1111/j.1365-2427.2008.02017.x.

Tsai, J.-W., Kratz, T. K., Rusak, J. A., Shih, W.-Y., Liu, W.-C., Tang, S.-L., and Chiu, C.-Y., Absence of winter and spring monsoon changes water level and rapidly shifts metabolism in a subtropical lake. *Inland Waters* **6**:**3**, 436–448 (2016). doi: 10.1080/IW-6.3.844.

Vachon, D., and del Giorgio, P. A., Whole-Lake CO_2 Dynamics in Response to Storm Events in Two Morphologically Different Lakes. *Ecosystems* **17**:**8**, 1338–1353 (2014). doi: 10.1007/s10021-014-9799-8.

Vachon, D., Solomon, C. T., and del Giorgio, P. A., Reconstructing the seasonal dynamics and relative contribution of the major processes sustaining CO 2 emissions in northern lakes. *Limnol Oceanogr* **62**:**2**, 706–722 (2017). doi: 10.1002/lno.10454.

Verpoorter, C., Kutser, T., Seekell, D. A., and Tranvik, L. J., A global inventory of lakes based on high-resolution satellite imagery. *Geophys. Res. Lett.* **41**:**18**, 6396–6402 (2014). doi: 10.1002/2014GL060641.

von Rohden, C., and Ilmberger, J., Tracer experiment with sulfur hexafluoride to quantify the vertical transport in a meromictic pit lake. *Aquat. sci.* **63**:**4**, 417–431 (2001). doi: 10.1007/s00027-001-8042-9.

Wang, W., Roulet, N. T., Kim, Y., Strachan, I. B., Del Giorgio, P., Prairie, Y. T., and Tremblay, A., Modelling CO2 emissions from water surface of a boreal hydroelectric reservoir. *The Science of the total environment* **612**, 392–404 (2018). doi: 10.1016/j.scitotenv.2017.08.203.

Wanninkhof, R., Relationship between wind speed and gas exchange over the ocean. *J. Geophys. Res.* **97**:**C5**, 7373 (1992). doi: 10.1029/92JC00188.

Williamson, C. E., Morris, D. P., Pace, M. L., and Olson, O. G., Dissolved organic carbon and nutrients as regulators of lake ecosystems: Resurrection of a more integrated paradigm. *Limnol Oceanogr* **44**:**3part2**, 795–803 (1999). doi: 10.4319/lo.1999.44.3_part_2.0795.

Winslow, L. A., Read, J. S., Hansen, G. J. A., and Hanson, P. C., Small lakes show muted climate change signal in deepwater temperatures. *Geophys. Res. Lett.* **42**:**2**, 355–361 (2015). doi: 10.1002/2014GL062325.

Woolway, R. I., Kraemer, B. M., Lenters, J. D., Merchant, C. J., O'Reilly, C. M., and Sharma, S., Global lake responses to climate change. *Nat. Rev. Earth Environ.* **1**:**8**, 388–403 (2020). doi: 10.1038/s43017-020-0067-5.

Woolway, R. I., Simpson, J. H., Spiby, D., Feuchtmayr, H., Powell, B., and Maberly, S. C., Physical and chemical impacts of a major storm on a temperate lake: a taste of things to come? *Climatic Change* **151**:**2**, 333–347 (2018). doi: 10.1007/s10584-018-2302-3.

Wu, J.-T., Chang, S.-C., Wang, Y.-S., Wang, Y.-F., and Hsu, M.-K., Characteristics of the acidic environment of the Yuanyang Lake (Taiwan). *Bot. Bull. Acad. Sin.* **42**, 17–22 (2001).

Zwart, J. A., Sebestyen, S. D., Solomon, C. T., and Jones, S. E., The Influence of Hydrologic Residence Time on Lake Carbon Cycling Dynamics Following Extreme Precipitation Events. *Ecosystems* **20**:**5**, 1000–1014 (2017). doi: 10.1007/s10021-016-0088-6.

Supplement

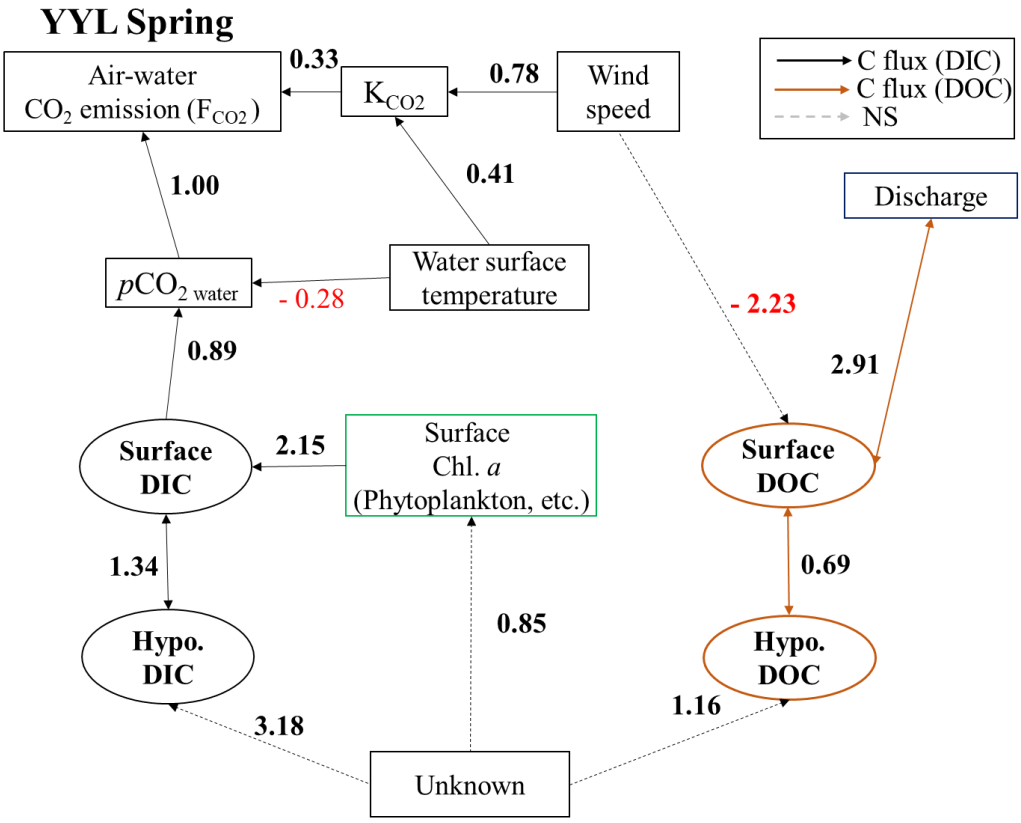

Supplementary figure 1. SEM analysis showing DIC fluxes (black arrows) and DOC fluxes (brown arrows) during spring in YYL. The coefficient values are calculated from the Wishart likelihood function. The value of a coefficient indicates the relative influence of the path. The path coefficients (black and brown arrows) show statistical significance (p-value < 0.05). Standardized RMSE is less than 0.10; AGFI is more than 0.95.

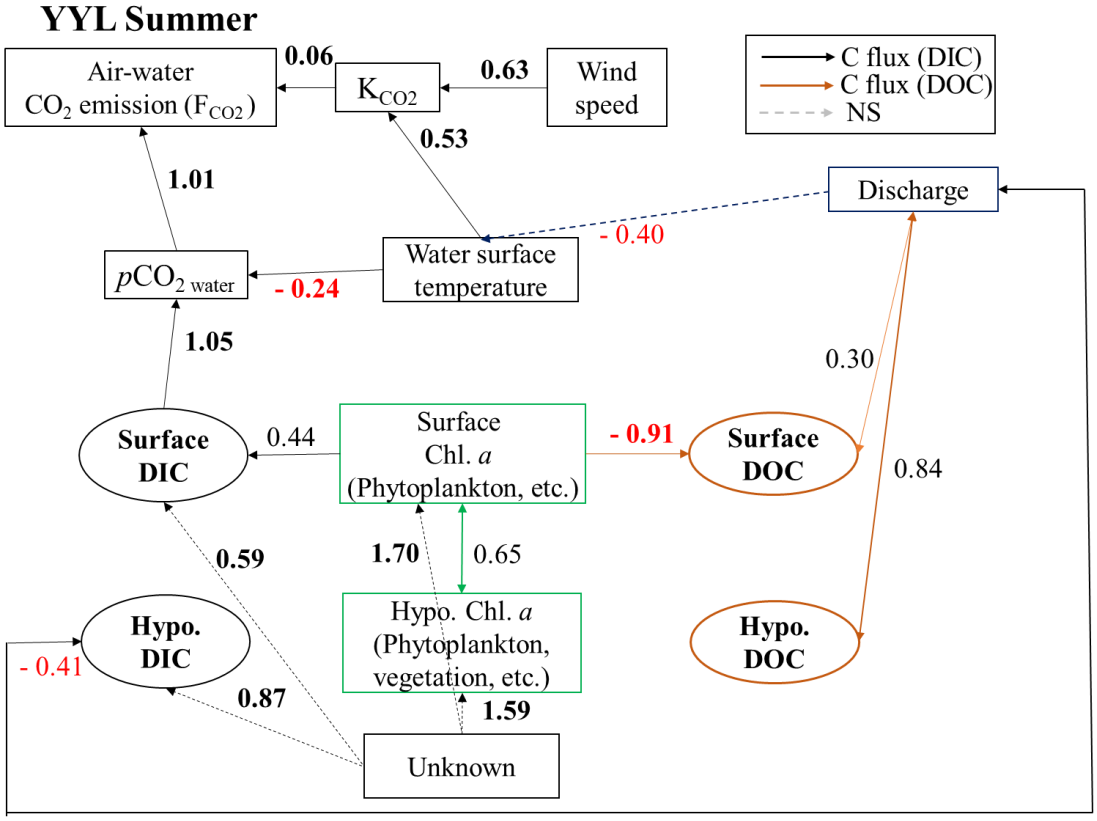

Supplementary figure 2. SEM analysis showing DIC fluxes (black arrows) and DOC fluxes (brown arrows) during summer in YYL. The coefficient values are calculated from the Wishart likelihood function. The value of a coefficient indicates the relative influence of the path. The path coefficients (black and brown arrows) show statistical significance (p-value < 0.05). Standardized RMSE is less than 0.10; AGFI is more than 0.95.

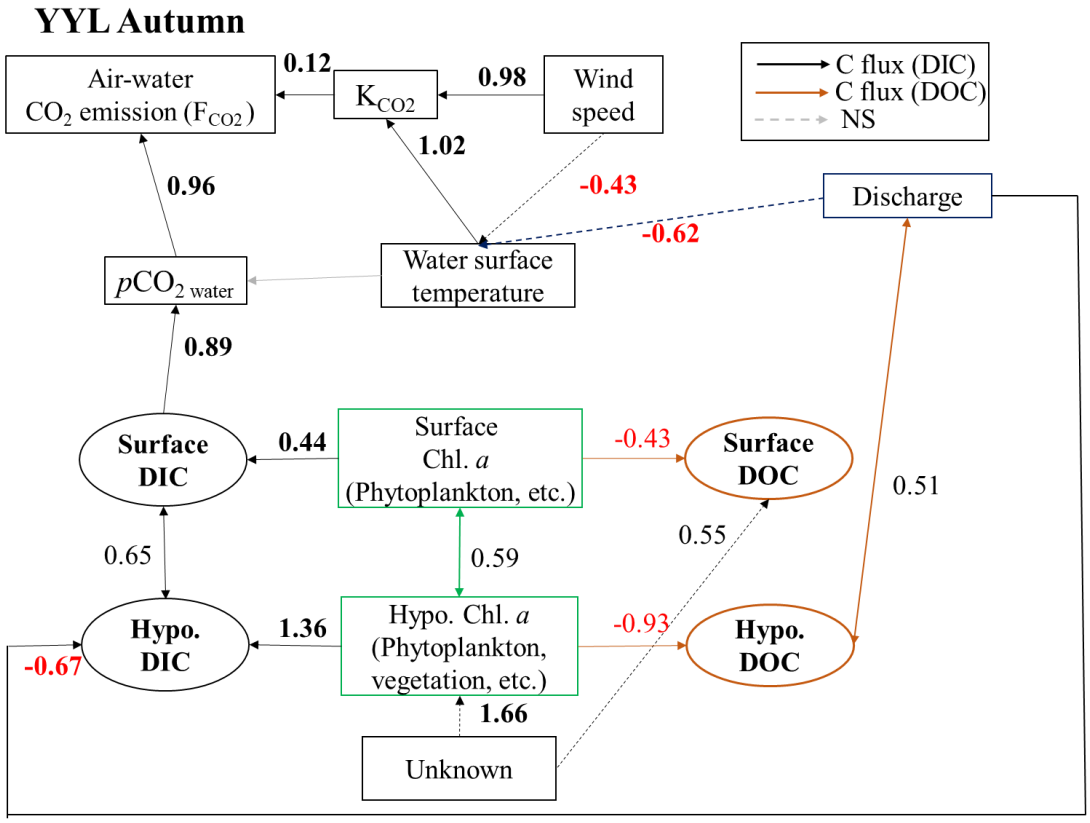

Supplementary figure 3. SEM analysis showing DIC fluxes (black arrows) and DOC fluxes (brown arrows) during autumn in YYL. The coefficient values are calculated from the Wishart likelihood function. The value of a coefficient indicates the relative influence of the path. The path coefficients (black and brown arrows) show statistical significance (p-value < 0.05). Standardized RMSE is less than 0.10; AGFI is more than 0.95.

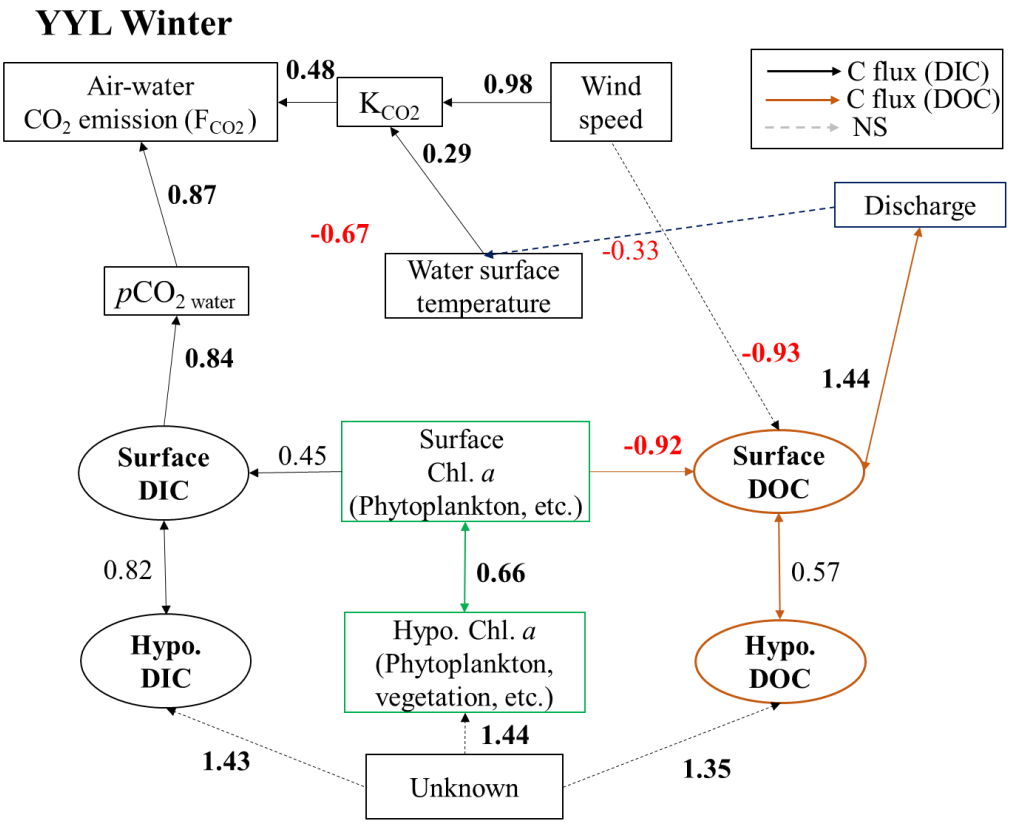

Supplementary figure 4. SEM analysis showing DIC fluxes (black arrows) and DOC fluxes (brown arrows) during winter in YYL. The coefficient values are calculated from the Wishart likelihood function. The value of a coefficient indicates the relative influence of the path. The path coefficients (black and brown arrows) show statistical significance (p-value < 0.05). Standardized RMSE is less than 0.10; AGFI is more than 0.95.

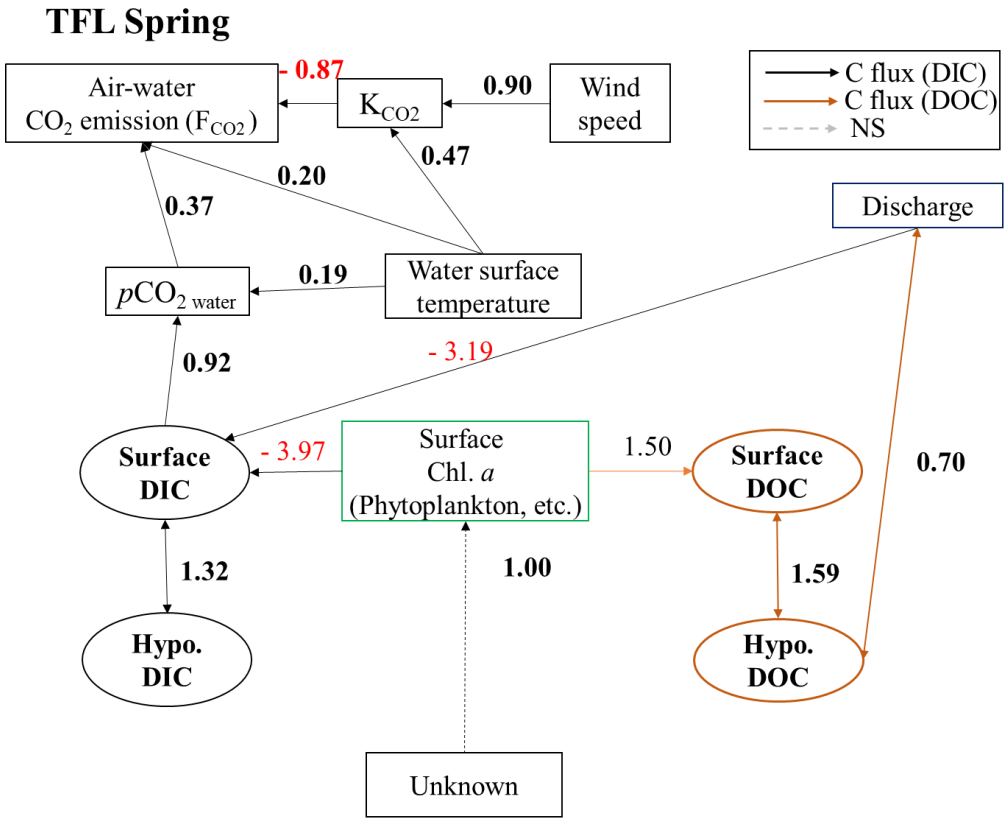

Supplementary figure 5. SEM analysis showing DIC fluxes (black arrows) and DOC fluxes (brown arrows) during spring in TFL. The coefficient values are calculated from the Wishart likelihood function. The value of a coefficient indicates the relative influence of the path. The path coefficients (black and brown arrows) show statistical significance (p-value < 0.05). Standardized RMSE is less than 0.10; AGFI is more than 0.95.

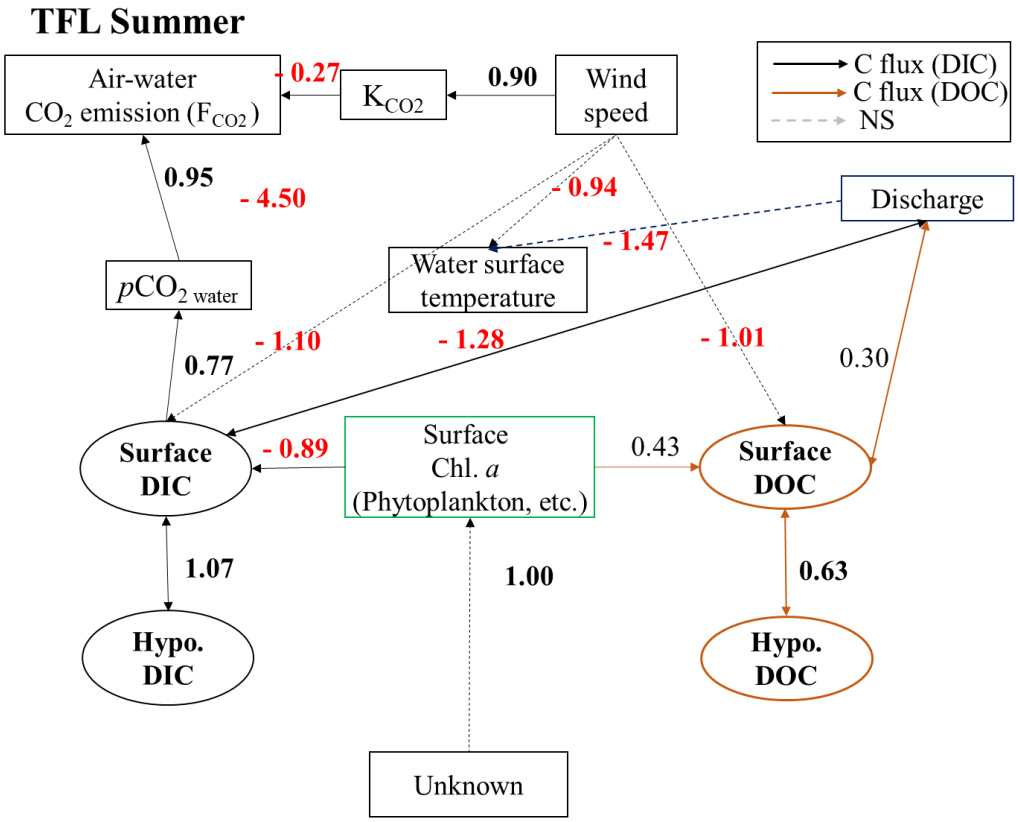

Supplementary figure 6. SEM analysis showing DIC fluxes (black arrows) and DOC fluxes (brown arrows) during summer in TFL. The coefficient values are calculated from the Wishart likelihood function. The value of a coefficient indicates the relative influence of the path. The path coefficients (black and brown arrows) show statistical significance (p-value < 0.05). Standardized RMSE is less than 0.10; AGFI is more than 0.95.

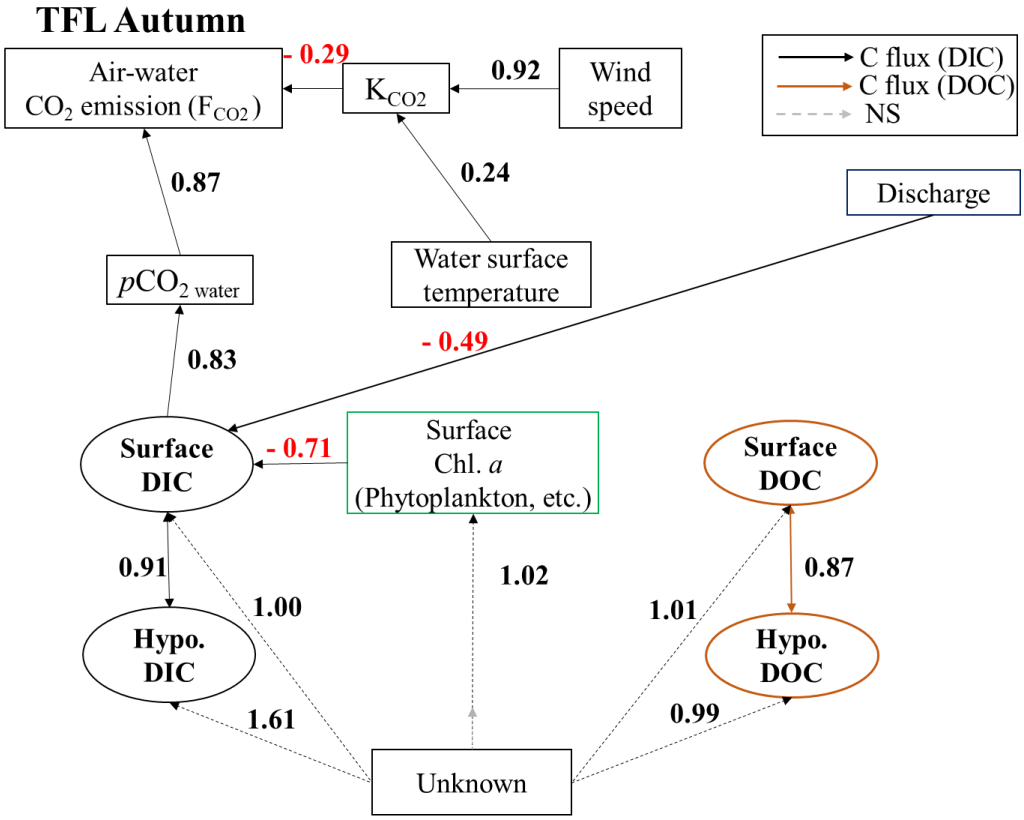

Supplementary figure 7. SEM analysis showing DIC fluxes (black arrows) and DOC fluxes (brown arrows) during autumn in TFL. The coefficient values are calculated from the Wishart likelihood function. The value of a coefficient indicates the relative influence of the path. The path coefficients (black and brown arrows) show statistical significance (p-value < 0.05). Standardized RMSE is 0.353; AGFI is 0.753.

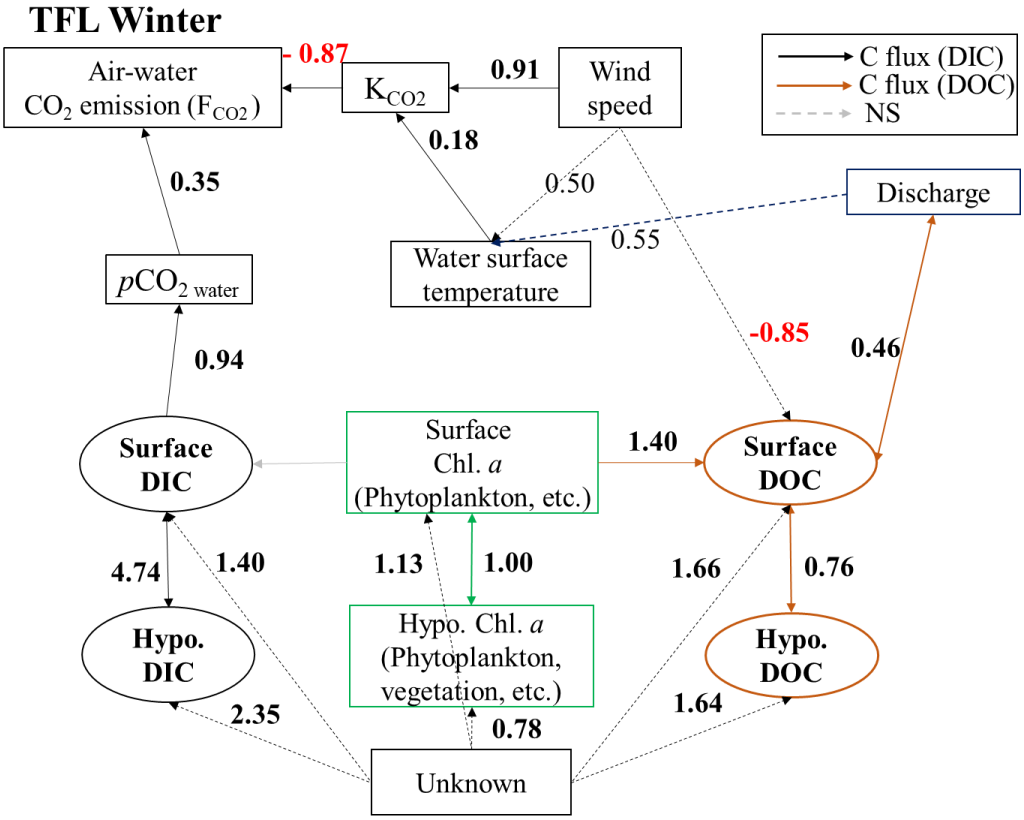

Supplementary figure 8. SEM analysis showing DIC fluxes (black arrows) and DOC fluxes (brown arrows) during winter in TFL. The coefficient values are calculated from the Wishart likelihood function. The value of a coefficient indicates the relative influence of the path. The path coefficients (black and brown arrows) show statistical significance (p-value < 0.05). Standardized RMSE is 0.142; AGFI is 0.946.

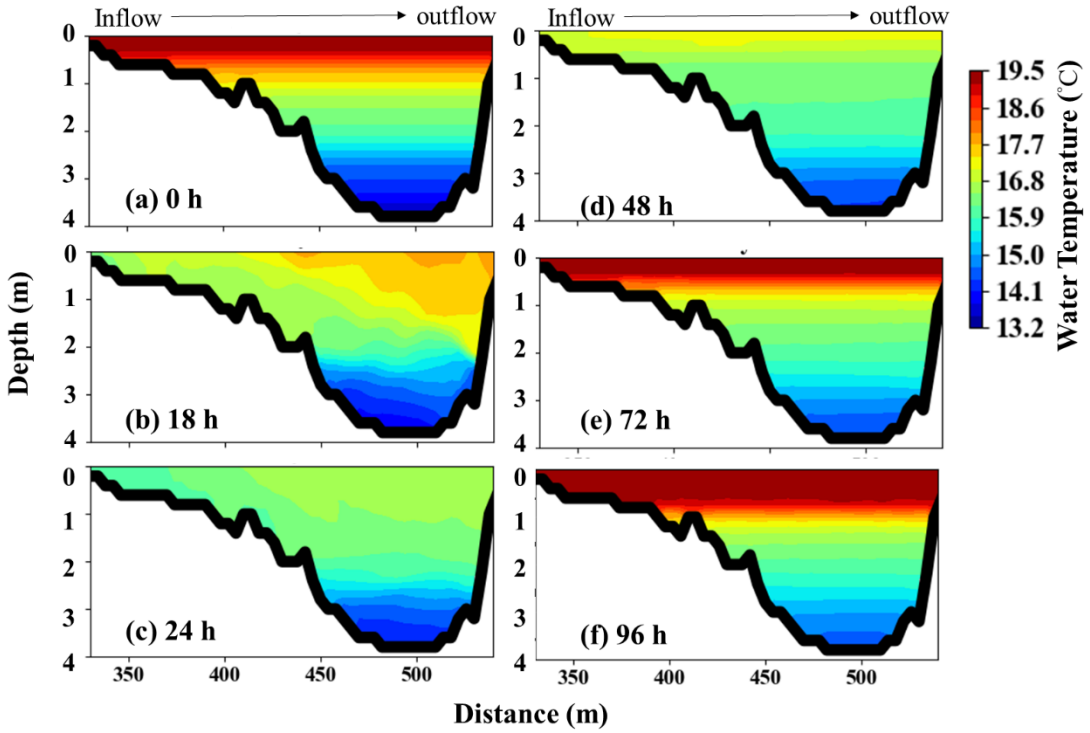

Supplementary figure 9. Vertical distribution of the water temperature during Typhoon Dujuan (2015) in YYL. (a) 28th Sep., 00:00 a.m.; (b) 28th Sep., 6:00 p.m.; (c) 29th Sep., 00:00 a.m. (d) 30th Sep., 00:00 a.m. (e) 1st Oct., 00:00 a.m. (f) 2nd Oct., 00:00 a.m. The horizontal coordinate shows the distance from the northernmost point (m); the vertical coordinate shows the depth (m).

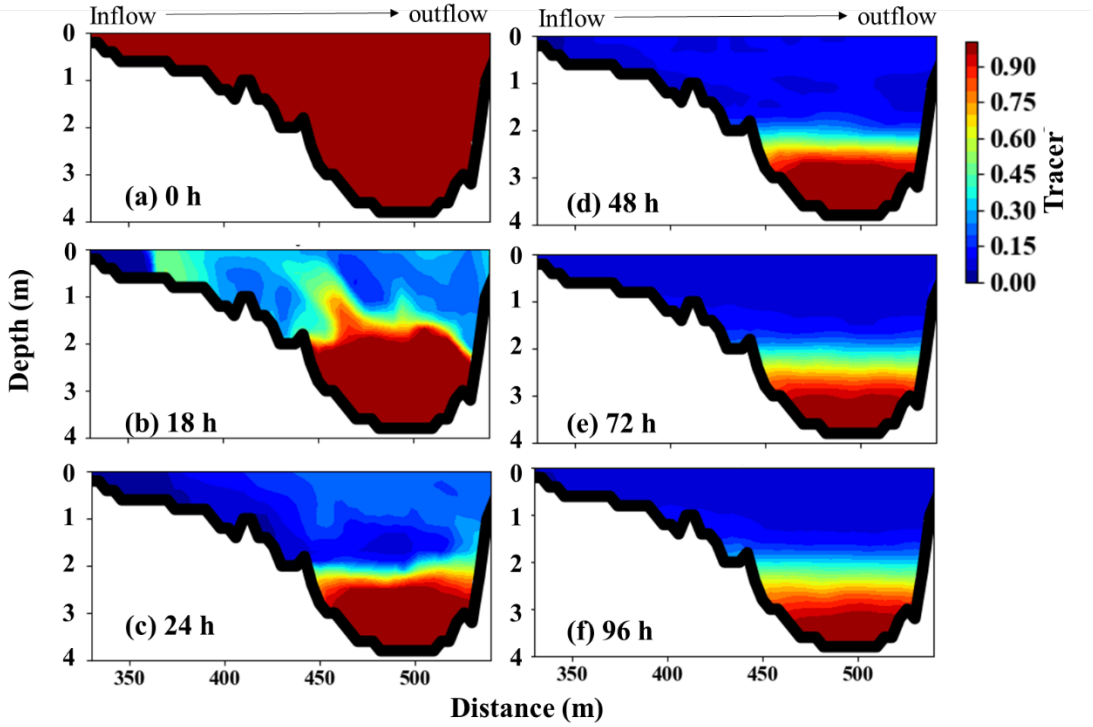

Supplementary figure 10. Vertical distribution of the tracer during Typhoon Dujuan (2015) in YYL. (a) 28th Sep., 00:00 a.m.; (b) 28th Sep., 6:00 p.m.; (c) 29th Sep., 00:00 a.m. The red arrow shows the intrusion river. (d) 30th Sep., 00:00 a.m. (e) 1st Oct., 00:00 a.m. (f) 2nd Oct., 00:00 a.m. The horizontal coordinate shows the distance from the northernmost point (m); the vertical coordinate shows the depth (m). The residence time is around 2.2 days.

Doctoral Dissertation, Kobe University

Effects of thermal stratification and hydraulic retention on carbon flux in shallow subtropical lakes, 81 pages

Submitted on January, 20, 2022.

The date of publication is printed in cover of repository version published in Kobe University Repository Kernel.